UNDERSTANDING THE FACTORS AFFECTING THE MECHANICAL PROPERTIES OF MARINE COMPOSITES

By:

KEVIN DANIEL BEAVERS

A thesis submitted in partial fulfillment of
the requirements for the degree of

Master of Science in Mechanical Engineering

WASHINGTON STATE UNIVERSITY
School of Engineering and Computer Science

May 2009

To the Faculty of Washington State University:

The members of the Committee appointed to examine the thesis of KEVIN D. BEAVERS find it satisfactory and recommend that it be accepted.

_____
Dae-Wook (Dave) Kim, Ph.D., Chair

_____
Xiaolin (Linda) Chen, Ph.D.

_____
Wei Xue, Ph.D.

ACKNOWLEDGMENT

The author wishes to acknowledge Professor Dae-Wook (Dave) Kim, PhD for his hours of guidance, insight, and support; Christensen Yachts Inc. for their trust and commitment; Troy Dunmire for his expertise and patience in effort to make this research possible; Daniel Hennigan for his assistance with this research; University of Portland engineering faculty that made it possible for me to pursue this degree; WSUV engineering faculty for allowing me to learn about my personal ability and how to become a better engineer.

UNDERSTANDING THE FACTORS AFFECTING THE

MECHANICAL PROPERTIES OF MARINE COMPOSITES

Abstract

By Kevin Daniel Beavers, MS
Washington State University
May 2009

Chair: Dae-Wook (Dave) Kim

In order to meet the American Bureau of Shipping (ABS) requirements for speed and weight in the marine vessels, advanced composite materials such as glass fiber reinforced plastics (GFRP) must be incorporated into the hull structure, which is the major component of the vessel. Composite hull design and fabrication are cost and skill intensive techniques. Quality control requires frequent hull design/manufacturing validation tests and continuous process improvement based on objective tests and analysis results. In this study, an investigation of the factors that affect the mechanical properties of marine composites is presented. In particular, the effect of composite fabrication process, material systems, and test methods on mechanical properties of GFRP composite materials was experimentally investigated. For sample fabrication, hand lay-up (HL), vacuum infusion (VI), and hybrid processes were used. For mechanical property testing, tensile, compressive, and ignition loss testing was performed. Results showed that vacuum pressure implemented during composite fabrication did have an effect on mechanical properties. As the vacuum pressure increased, more voids were extracted from the material system, leading to improved properties. Increasing layers of fiber within composite panels did not have significant effect on measured properties. Even though the panels experienced more load before failure, the area also increased giving no improvement in comparison. The panel type was influenced by fabrication method. HL, hybrid (HL+VI), and VI processes showed some increase in properties as fabrication method trended towards the VI procedure. The two standard compressive test methods, ASTM

D695 and ASTM D695M, were compared. While the ASTM D 695M testing procedure gave better ultimate strengths, the ASTM D 695 testing procedure indicated better moduli. Finally, it was found that by deviating the end surface of a compressive test specimen negatively influences the outcomes in compressive properties.

TABLE OF CONTENTS

LIST OF TABLES

LIST OF FIGURES

Dedication

This thesis is dedicated to four very important people in my life. First, to my family Debra, Dan and Erin, who have believed in me when even I did not. Their years of love and support will never be matched and for that I am forever grateful. Finally, to my very good friend Juan Christen. The outcomes of this research would not exist if it weren't for his kind heart and guidance. No better man could have entered my life and I will never forget what you have done for me. Thank you all.

CHAPTER ONE

INTRODUCTION

Polymer composite materials offer high strength-to-weight and stiffness-to-weight ratios that are appealing to the marine industry. Integration of these materials can be seen as far back as the Second World War where composites found their way into the construction of small personnel boats for the US Navy. Immediate popularity grew when it was found that composites offer stiff, strong, durable, and easy to repair properties [1]. Since then, increasing efforts are being made to incorporate these materials into the design of various components and structures of yacht and naval craft.

(a)

(b)

(c)

Fig. 1-1 (a) Yacht Example (Courtesy of Christensen Yacht Inc.), (b) High-Speed Combatant Craft Example, (c) Composite Hull Design

In order to build these crafts, design and optimization of laminated composite material systems must be accomplished for the hull structures. In addition, composite hull fabrication, which is a cost intensive technique as well as a high-risk process, must be controlled to meet the demanding design specifications. Therefore, there is a strong need for conducting composite material testing and failure analysis for advanced marine composite material systems to improve marine vessel hull design and manufacturing.

Even though it is understood that composite materials offer enhanced mechanical properties, the factors affecting these properties are not fully understood. Like any acquired mechanical property, certain testing procedures apply. The American Bureau of Shipping (ABS) requires three different testing procedures that should be implemented for the acquisition of all mechanical properties for marine hull applications. Static tension testing was administered in compliance with ASTM D3039 [2]. Static compression testing was accomplished using two different testing procedures. ASTM D695 [3] and ASTM D695M [4] were implemented as the two compression testing procedures. Finally, ignition loss testing used to gather information about the fiber and matrix makeup of each tested material was done in accordance with ASTM D2584 [5].

This study purposes to characterize various influences that may or may not affect the resultant mechanical properties of various laminates. In all, 8 different material systems were implemented for the scope of this research. They either incorporated different manufacturing methods, different layup sequences, or different material components. By incorporating a wide range of materials, many comparisons can be made between resultant mechanical properties. These comparisons include the influences from different manufacturing procedures, influences from different testing methods, influences between similar materials with different layup sequences, and influences from altered test specimen geometries. This work may lead to a better understanding of how composite fabrication method, testing procedure, and test specimen fabrication can affect the outcomes of mechanical properties.

This thesis is composed of six chapters. The first chapter, the Introduction, provides some general information about some of the topics that will be discussed in this report. The Literature Review, chapter 2, provides additional depth about topics significant to the direction of this report and provides details as to past and present research in relevant areas. The Objectives chapter, chapter 3, concisely explains the reason for this research and the goals that were established at the onset of this study. Chapter 4 informs the reader of the procedures and equipment used during all experimental analysis in this work. Next, chapter 5 presents the

results obtained from the experimental work and also provides a discussion of these results. Finally, chapter 6 establishes conclusions from this study.

CHAPTER TWO

LITERATURE SURVEY

2.1 Fiber Reinforced Polymer (FRP) Composite Fabrication Processes

Fabrication processes for fiber reinforced polymer composites have long been of interest for a wide variety of applications. Certain applications impose specific fabrication methods, but the idea is the same in all cases; imbed fiber reinforcements within a matrix media. This section describes the major manufacturing processes for which FRP composites are formed.

2.1.1 Hand Lay-Up (HL)

In the nautical sector, where large products are involved and where there is no massive series production, hand lay-up (HL) is by large the most widely used manufacturing technique [6]. In a typical HL process, the resin and fibers are placed manually. Entrapped air is expelled with squeegees or rollers, and, if necessary, multiple layers are built up. Hardening is done at ambient conditions but may be sped up by additional heating processes [7]. A schematic of this method is shown below in Figure 2.1-1.

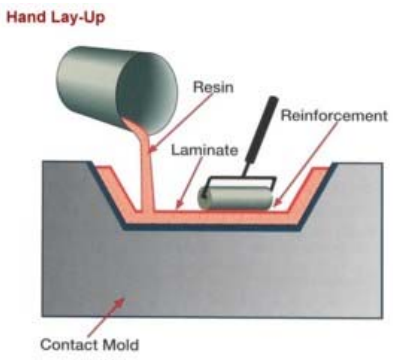

Fig 2.1-1: Hand Lay-Up Schematic

2.1.2 Vacuum Infusion (VI)

Vacuum infusion (VI) is a low cost process, particularly suitable for low volume production of large parts. The process offers many advantages such as an emission free work environment, improved part quality, superior mechanical properties, etc., over manual processes such as HL [8]. In the VI process, porous reinforcement is laid on top of a rigid mould. Injection and vent lines can be a part of the mould bottom half or can be attached after placing the reinforcement. Then, the mould is sealed with a flexible plastic sheet, which acts as the mould top half. The air inside is evacuated once the vacuum pump starts. This pump pulls the air from inside the sealed mould, thus creating a negative pressure which is also the resin driving force [9]. Once the reinforcement is completely infused, resin is allowed to cure before extracting the finished part. A schematic of this process is shown below in Figure 2.1-2.

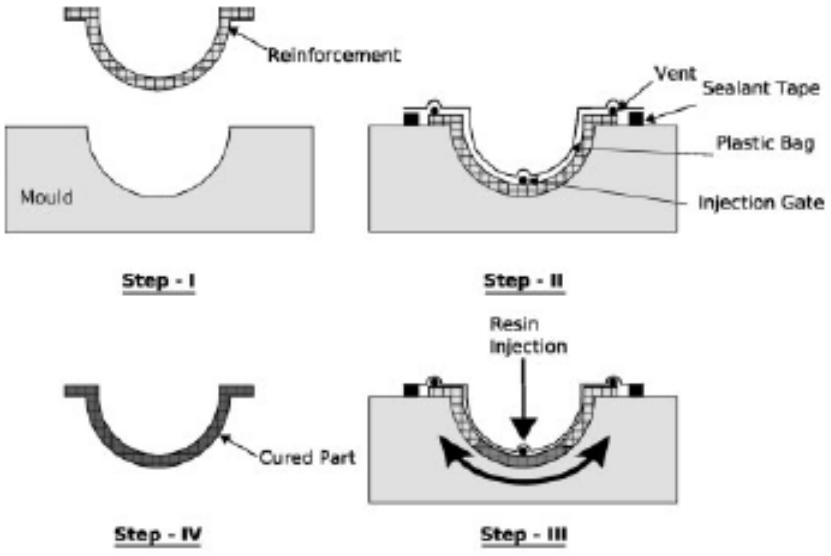

Fig 2.1-2: General Steps of the VI Process [2]

2.1.3 Resin Transfer Moulding (RTM)

Resin transfer moulding (RTM) is an injection technique, similar to that of VI, where resin is drawn into a mould via the influence of vacuum pressure. The defining difference between VI and RTM is that the fully enclosing, two rigid moulds used in RTM are replaced with a one part rigid mould sealed with a vacuum bag for the VI process [10]. Basically, VI requires only a single, primary mould to lay reinforcement upon, and is covered only by a vacuum bag, while the RTM process insists a secondary mould to encase the entire lay-up.

Reinforcement is laid on the base mould with a layer of removable, flow-enhancement medium, used to reduce fill time, along with peel ply to facilitate disposal. Resin inlets and outlets are placed and the vacuum bag is sealed to the base mould using a sealant tape. Air is extracted from the cavity to compact the material between the vacuum bag and the top mould, and to subject resin to a pressure differential. As a result, resin flows through the compacted cavity. A schematic of this process is shown below in Figure 2.1-3.

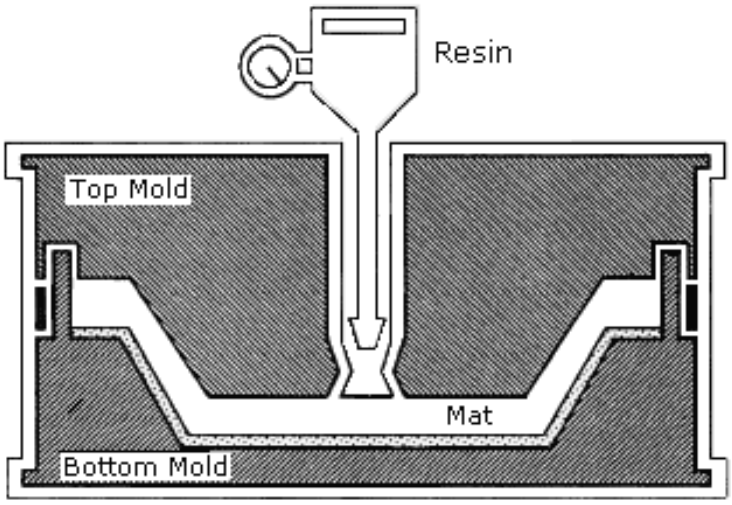

Fig 2.1-3: Schematic of the RTM Setup

2.2 Failure Mechanisms of FRP Composites

Physical, chemical, and/ or mechanical induced defects that result in partial degradation or complete failure of a product are the mechanisms that attribute to overall failure [11]. It is important to understand, upon the specified loading condition, how composite structures eventually fail. This section describes the failure mechanisms by which fiber reinforced polymer composites lose their structural integrity.

2.2.1 Failure in Tension

In theory, fiber reinforced composite lamina in tension are assumed to have fibers with equal strength and failure occurs suddenly after the beginning of initial fiber failure. However, in practice, all fibers are not of equal strength and are statistical in nature [11]. Therefore, it is expected that some fibers will fail at low stress levels. Although this means that the remaining intact fibers will then carry some of the additional load that the premature fibers once held, they may not fail simultaneously.

Fiber Breakage

When a fiber is pulled to the point of failure, the normal stress at each of its broken ends becomes zero. However, over the remaining surface area of the fiber, the stress builds back up by effect of shear at the fiber/matrix interface [12]. Additionally, the stress states in the region close to the broken ends contain:

1) Stress concentrations at the void created by the broken fiber [12]
2) Shear stress concentrations at the matrix interface near the broken fiber ends [12]
3) An increase in normal stress in the adjacent fibers [12] (Figure 2.2-1)

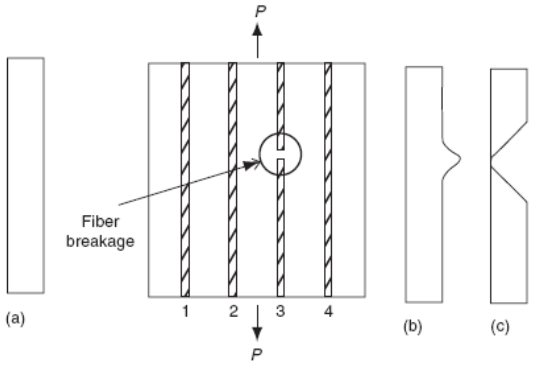

Fig 2.2-1: Longitudinal Stress Distributions (a) In Unidirectional Continuous Fibers Before the Failure of Fiber 3, (b) In Fibers 2 and 4 After the Failure of Fiber 3, (c) In Fiber 3 After it Fails. [12]

From these local magnifications in stress, possibilities of further failure may exist. These possibilities include [12]:

Broken Fiber Debonding

Partial or total debonding of broken fibers from the surrounding matrix is due to high interfacial shear stresses at its ends. As a result, the effectiveness of the fiber is reduced either completely or over a substantial length. See Figure 2.2-2.

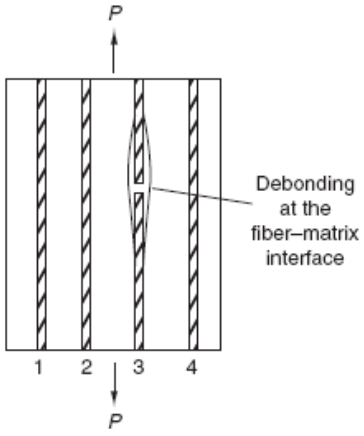

Fig 2.2-2: Debonding at the Fiber/Matrix Interface from Fiber Breakage [12]

Matrix Cracking

Initiation of a crack in the matrix is due to high stress concentrations at a void caused by the broken fiber ends. See Figure 2.2-3.

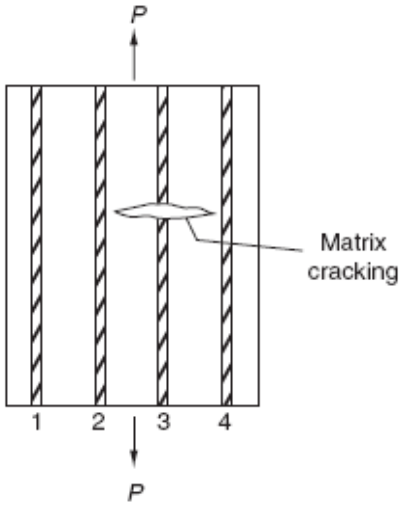

Fig 2.2-3: Matrix Cracking Due to Fiber Breakage [12]

Micro-Yielding

Plastic deformation (micro-yielding) in the matrix is a common occurrence for composite materials, particularly if the matrix is ductile.

Failure of Adjacent Fibers

Failure of other fibers in the vicinity of the first fiber break is due to high average normal stresses and local stress concentrations. Each fiber break creates additional stress concentrations in the matrix as well as in other fibers. Eventually, many of these fibers break and the

surrounding matrix micro-cracks may join to form a long micro-crack in the lamina. See Figure 2.2-4.

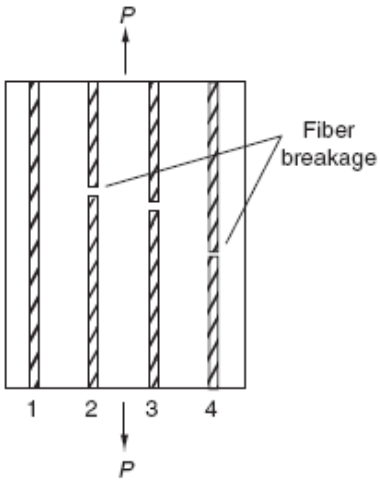

Fig 2.2-4: Additional Fiber Failures Due to the Initial Fiber Break [12]

High fiber strength and low interfacial strength promote debonding over fiber tensile failure. With increasing load, fibers continue to break randomly at various locations in the lamina. Because of the statistical distribution of surface flaws, the fiber failure may not always occur in the same plane as a crack. Therefore, the opening of a matrix crack may cause broken fibers to pull out from the surrounding matrix, which is resisted by the friction at the fiber/matrix interface. If the interfacial strength is high or the broken fiber lengths are great, the fiber pullout is preceded by either debonding or fiber failure even behind the crack front. Thus, broken fibers act as a bridge between the two faces of the matrix crack [12].

2.2.2 Compressive Mechanisms

It is well established that the compressive strength in FRP composites is generally lower than the tensile strength. This relative weakness in compression is often the limiting factor in the application of composite materials [13]. Since the microstructure of FRP composites is tailored, it is expected that the failure mechanisms will be related to microstructural details, such as the mechanical properties of the constituents, the quality of adhesion between the fiber and matrix, fiber volume fraction, orientation of the reinforcement, and even the geometry of the fibers themselves [14].

Micro-Buckling

Micro-buckling has been the most widely studied failure mode for composites made of strong reinforcing fibers and matrices due to the fact that it is easily visualized and physically intuitive [14]. It is partially dependent on the initial imperfections of a composite which results from manufacturing associated defects, such as fiber misalignment or waviness, residual stresses (possibly caused by matrix shrinkage during curing), and porosity (presence of voids) [14]. Two elastic micro-buckling modes associated with fibers in an elastic matrix under compressive loading have been recognized. These modes are known as extensional (Figure 2.2-5) and shear (Figure 2.2-6).

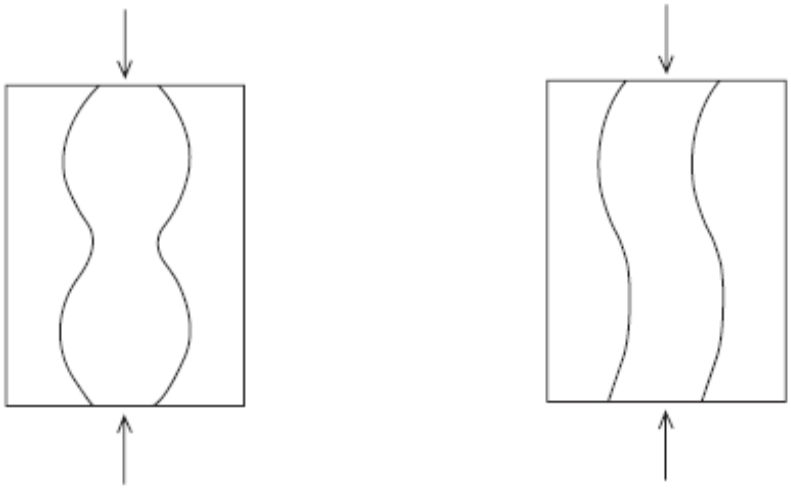

Fig 2.2-5: (Left) Extensional Micro-Buckling Mode [12]

Fig 2.2-6: (Right) Shear Micro-Buckling Mode [12]

The extensional mode of micro-buckling occurs at low fiber volume fractions ($v_f < 0.2$) and creates an extensional strain in the matrix because of out-of-phase buckling of fibers. The shear mode of micro-buckling occurs at high fiber volume fractions and creates a shear strain in the matrix because of in-phase buckling of fibers. Since most fiber-reinforced composites contain fiber volume fractions greater than 30%, the shear mode is more common than the extensional mode [12].

Kinking

Kinking is an important failure mode in longitudinal compression which occurs in highly localized areas of fiber [12]. In many fibrous composites with softening matrices, the localization of the compressive failure leads to fiber kinking, eventually fracturing fibers [15]. Kinking is sometimes considered to be a final consequence of micro-buckling, but is also considered to be a

separate failure mechanism. It has been shown to not only depend on matrix stiffness, but also on fiber misalignment, fiber strength, and matrix yield behavior in shear [12, 14].

Fiber bundles in these areas rotate or tilt by an additional angle from their initial configuration to form kink bands, and the surrounding matrix undergoes large shearing deformations. Failure patterns appear in the form shown in Figure 2.2-7.

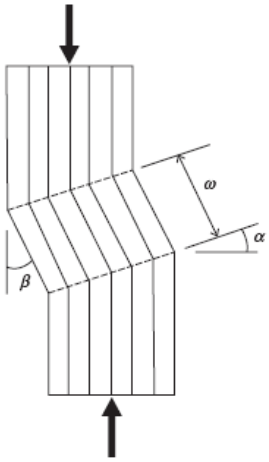

Fig 2.2-7: Kink Band Geometry: α = Kink Band Angle, β = Fiber Tilt Angle, and ω = Kink Band Width [12]

This kink band geometry is characterized by the kink band width, ω, the inclination angle of the kinked fibers with respect to the loading direction, α, and the orientation angle of the kink band boundary with respect to the transverse loading direction, β [16]. As can be seen from the microscope photo in Figure 2.2-8, these kink bands follow the mathematical model fairly accurately.

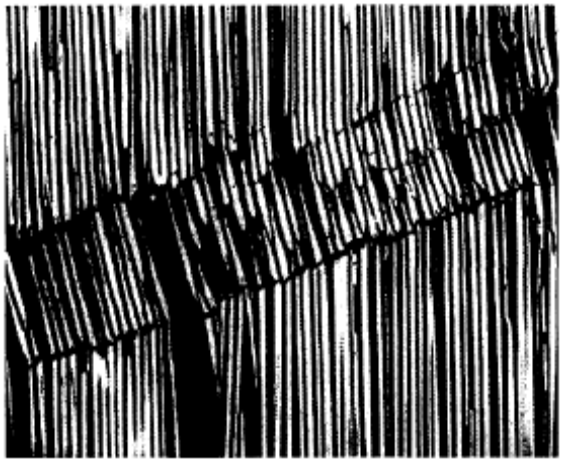

Fig 2.2-8: Illustration of Kink Band with Changing Plane [16]

Fiber Failure

Fiber failure is expected to dominate the behavior for fibers that are weak in compression (Kevlar, Organic Fibers, etc.) and is generally neglected as a mode of failure for fibers that are strong under the same loading (Carbon, Glass, Boron, etc.). This mode of failure is most influenced by the properties of the fibers themselves such as stiffness, size, and strength [14].

Longitudinal Cracking

For strong fibers with brittle matrices or weak interfaces, the failure is expected to take the form of longitudinal cracking, either in the matrix or at the interface. Thus, longitudinal cracking is generally controlled by the fracture toughness of the matrix or interface, and may be strongly affected by the mismatch between Poisson's Ratio of the fibers and matrix [14]. It must be noted that longitudinal cracking seen in unidirectional laminates finds its counterpart in general laminates in the form of delamination failure [14]. Delamination, also known as splitting, is the separation of layers within a laminate causing a severely weakened structure. It seems that

delamination is the most likely form of failure found in composites, usually caused by the same reasons for cracking, and also from weak fiber/matrix adhesion [14].

2.3 Mechanical Properties of FRP Composites

2.3.1 Construction of a Laminate

A laminate is constructed by stacking multiple laminas (single fiber sheets of composite) in the thickness (z) direction. The sequence in which these laminas are stacked upon one another has a significant effect on mechanical properties on the entire laminate. The following are specified types of laminates based on stacking sequence [12]:

1) *Unidirectional Laminate*: In unidirectional laminates, the fiber direction is oriented at the same angle in all laminas. See Figure 2.3-1.

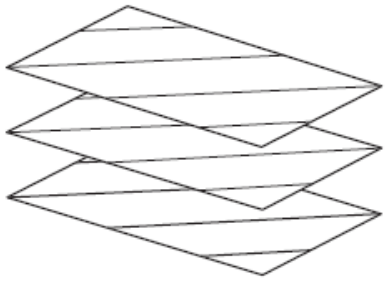

Fig 2.3-1: Unidirectional Laminate [θ] [12]

2) *Angle-Ply Laminates*: In angle-ply laminates, the fiber orientation alternates in layers from +θ to -θ. This does not include an alternation between 0 and 90 degrees. See Figure 2.3-2.

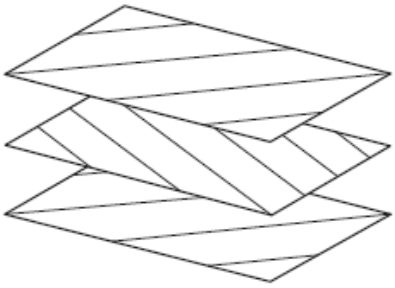

Fig 2.3-2: Angle-Ply Laminate [+θ/-θ]s [12]

3) *Cross-Ply Laminates*: In a cross-ply laminate, fiber orientations only alternate between 0 and 90 degrees for a sequence of layers. See Figure 2.3-3.

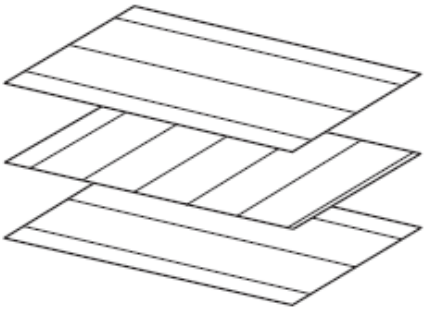

Fig 2.3-3: Cross-Ply Laminate [0/90]s [12]

4) *Symmetric Laminate*: For a symmetric laminate, the ply orientation is symmetric about the centerline of the laminate; that is, for each ply above the midplane, there is an identical ply (in thickness, material, and fiber orientation) at an equal distance below the midplane. An example of this stacking sequence can be [90/45/0/45/90]s. The subscript “s” denotes symmetry about the midplane.

5) *Antisymmetric Laminate*: In antisymmetric laminates, the ply orientation is antisymmetric about the centerline of the laminate; that is, for each ply of fiber orientation angle θ above the midplane, there is ply of fiber orientation -θ with identical material and thickness at an equal distance below the midplane.

6) *Unsymmetric Laminate*: For unsymmetric laminates, the ply orientation has no symmetry or anitsymmetry.

7) *Quasi-Isotropic Laminate*: These laminates are made from three or more laminas of identical thickness and material with equal angles between each adjacent lamina.

2.3.2 Tensile Properties

Unidirectional Laminates

For unidirectional polymer matrix laminates containing fibers parallel to the tensile loading direction (i.e., $\theta = 0$), the tensile stress–strain curve is linear up to the point of failure. These specimens fail by tensile rupture of fibers, which is followed or accompanied by longitudinal splitting (debonding along the fiber/matrix interface). For off- axis specimens with $0 < \theta < 90$, the tensile stress–strain curves may exhibit nonlinearity. For $\theta = 90$ specimens in which the fibers are 90 degrees to the tensile loading direction, tensile rupture of the matrix or the fiber/matrix interface causes the ultimate failure. For intermediate angles, failure may occur by a combination of fiber/matrix interfacial shear failure, matrix shear failure, and matrix tensile rupture [12].

Both tensile strength and modulus for unidirectional specimens depend strongly on the fiber orientation angle θ. The maximum tensile strength and modulus are at $\theta = 0$ degrees. With increasing fiber orientation angle, both tensile strength and modulus are reduced. The maximum reduction is observed near $\theta = 0$ degree orientations. Typical unidirectional laminate stress-strain curves can be seen in Figure 2.3-4 for various $\theta = 0$ degree composite types [12].

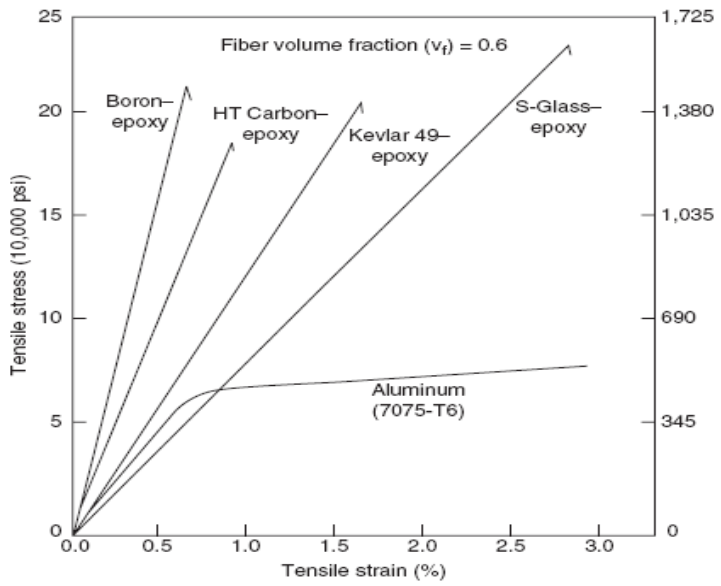

Fig 2.3-4: Tensile Stress-Strain Curves for Various θ = 0 Degree Laminates [12]

Cross-Ply Laminates

The tensile stress–strain curve for a cross-ply laminate tested at θ = 0 direction is slightly nonlinear. However, it is commonly approximated as a bilinear curve. The point at which the two linear sections intersect is called the knee and represents the failure of 90 degree plies. Ultimate failure of the laminate occurs at the fracture strain of 0 degree plies. The change in slope of the stress–strain curve at the knee can be reasonably predicted by assuming that all 90 degree plies have failed at the knee and can no longer contribute to the laminate modulus. A comparison between θ = 0, θ = 90, and plies alternating between 0 and 90 degrees can be seen in Figure 2.3-5 [12].

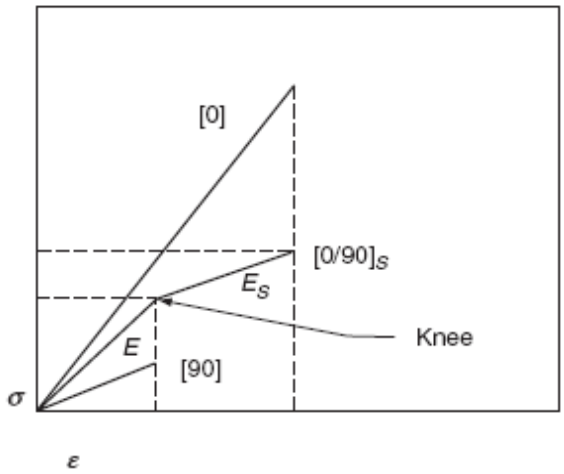

Fig 2.3-5: Stress-Strain Curves for Unidirectional [0], Transverse [90], and Cross-Ply [0/90]s laminates, [12]

Multi-Directional Laminates

Tensile stress–strain curves for laminates containing different fiber orientations in different laminas are in general nonlinear. For the purposes of analysis, these curves are approximated by a number of linear portions that have different slopes. When these linear portions are extended, a number of knees, similar to that observed in a cross-ply laminate, can be identified. The first knee in these diagrams is called the First Ply Failure (FPF) point. Many laminates retain a significant load-carrying capacity beyond the FPF point, but for some laminates with high notch sensitivity (the extent to which the sensitivity of a material to fracture is increased by the presence of a surface inhomogeneity such as a notch, a sudden change in section, a crack, or a scratch. Low notch sensitivity is usually associated with ductile materials and high notch sensitivity with brittle materials), failure occurs just after FPF. Furthermore, cracks appearing at the FPF point may increase the possibility of environmental damage (such as moisture pickup) as well as fatigue failure. For all these reasons, the FPF point has special importance in many laminate designs [12].

Angle-ply laminates containing [+/- θ] layups exhibit two kinds of stress–strain nonlinearity. At values of θ closer to 0 degrees, a stiffening effect is observed so that the modulus increases with increasing load. At larger values of θ, a softening effect is observed so that the modulus decreases with the increasing load. The stiffening effect is attributed to the longitudinal tensile stresses in various plies, whereas the softening effect is attributed to the shear stresses. Stiffening laminates do not exhibit residual strain on unloading. Softening laminates, on the other hand, exhibit a residual strain on unloading and a hysteresis loop on reloading. However, the slope of the stress–strain curve during reloading does not change from the slope of the original stress–strain curve. The tensile failure mode and the tensile strength of a multidirectional laminate containing laminas of different fiber orientations depend strongly on the lamina stacking sequence [12].

Woven Fabric Laminates

The principal advantage of using woven fabric laminates is that they provide properties that are more balanced in the 0 and 90 degree directions than unidirectional laminates. Although multilayered laminates can also be designed to produce balanced properties, the fabrication (lay-up) time for woven fabric laminates is less than that of a multilayered laminate. However, the tensile strength and modulus of woven fabric laminates are, in general, lower than those of multilayered laminates. The principal reason for their lower tensile properties is the presence of fiber undulation in woven fabrics as the fiber yarns in the fill direction cross over and under the fiber yarns in the warp direction to create an interlocked structure. Under tensile loading, these crimped fibers tend to straighten out, which creates high stresses in the matrix. As a result, micro-cracks are formed in the matrix at relatively low loads. This is also evidenced by the appearance of one or more knees in the stress–strain diagrams of woven fabric laminates. Another factor to consider is that the fibers in woven fabrics are subjected to additional mechanical handling during the weaving process, which tends to reduce their tensile strength.

Tensile properties of woven fabric laminates can be controlled by varying the yarn characteristics and the fabric style. The yarn characteristics include the number of fiber ends, amount of twist in the yarn, and relative number of yarns in the warp and fill directions [12].

2.3.3 Compressive Properties

Based on the available compressive test data for fiber reinforced composites, the following observations have been made for laminates with 0 degree fiber orientations [12]:

1) Unlike ductile metals, the compressive modulus of a 0 degree laminate is not the same as the tensile modulus.

2) Unlike tensile stress-strain curves which may be linear, compressive stress-strain curves may not be linear.

3) The longitudinal compressive strength of a 0 degree laminate may depend on the fiber type, fiber diameter-to-length ratio, fiber volume fraction, matrix strength, fiber straightness, fiber alignment and fiber/matrix interfacial shear strength.

4) Among the commercially used fibers, carbon and glass fiber reinforced composites exhibit slightly lower compressive strengths than their respective tensile values.

2.4 Variables Affecting the Compressive Properties of FRP Composites

The compressive properties of fiber reinforced composites are poor in comparison to their tensile properties. Composite compressive strength is matrix dominated and hence does not withstand loads seen from tension testing [17]. However, variables that affect the performance of composites in compression are noted and discussed in this section.

2.4.1 Imperfection Influences

Fiber Orientation

The direction in which reinforcing fibers are oriented with respect to the loading direction is an important factor in compressive testing. It has been stated that fiber misalignment has the greatest detrimental effect on mechanical properties, particularly under tensile and compressive loading [18]. This misalignment tends to be due to the waviness of fibers once embedded in a matrix material. Waviness occurs as a consequence of lamination residual stresses built up during resin curing [19]. It has been shown that even well-made fiber composite laminates contain a significant degree of misalignment and with the increasing use of thick composite structures under compressive loading; this effect becomes an important issue [20].

For unidirectional specimens with graded waviness, interlaminar shear failure was found to be the dominant failure mode. These interlaminar shear stresses may cause local delamination in a composite having low matrix strength, and, therefore, reduce the local transverse support of the fibers. After delamination initiates, the layers, especially the ones with the highest degree of waviness, are more susceptible to buckling than the original laminate because of their smaller thickness. This buckling will eventually lead to final failure [19].

To understand the effect of fiber misalignment on unidirectional composite compressive strength, the fibers are assumed to be parallel, and orientated at an angle to the loading direction. See Figure 2.4-1.

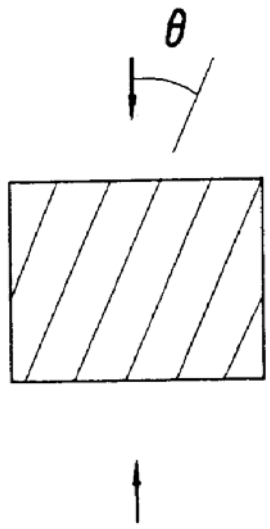

Fig 2.4-1: Fiber Misalignment with Respect to Loading Direction, [21]

This misalignment reduces the strength of fiber reinforced composites strongly past certain angles of θ. It has been reported that initial fiber misalignment of the order of 1.5 to 2 degrees offset from the loading direction significantly reduces the compressive strength [22]. From the compressive strength predictions in Figure 2.4-2, it can be seen that after about 5 degrees of offset from the load axis, compressive strengths are already greatly reduced [21].

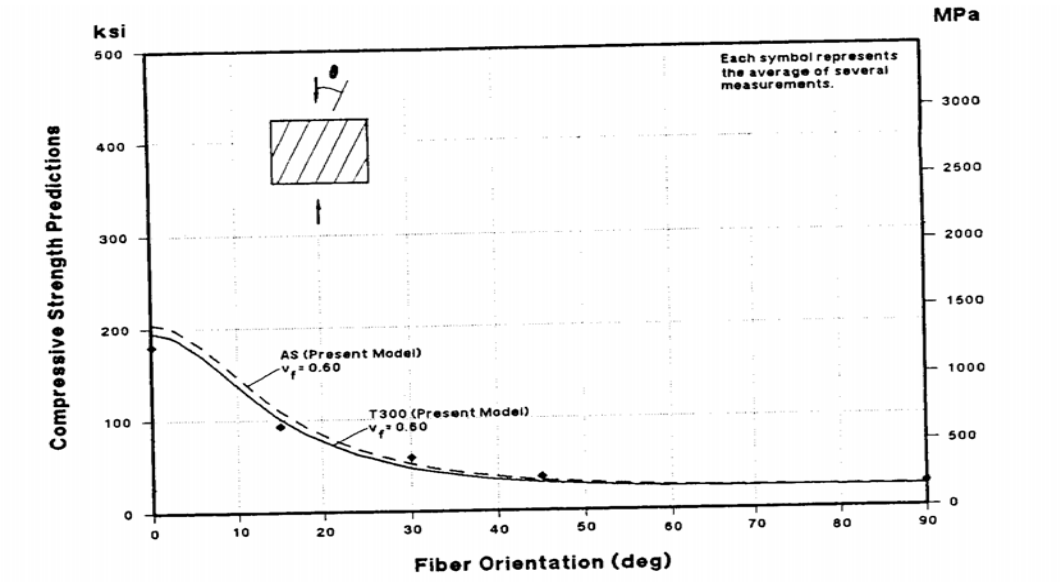

Fig 2.4-2: Fiber Orientation vs. Predicted Compressive Strength [21]

Fiber/Matrix Interface

Many combinations of fiber and matrix materials exist, and achieving good adhesion between the two plays an important role in mechanical testing. The main role of the matrix is usually to transfer the load between fibers, but the resin may also protect fibers, prevent fluid ingress, ensure required electrical properties and maintain the geometry of the component [23]. During compression, the function of the fiber/matrix interface (also known as the interphase region) is to provide lateral support to the reinforcing fiber. If this support is weak, also shall be the material.

The strength of the interface determines how much of the applied stress can be transferred to the load-bearing fibers, and this interfacial strength is largely determined by the degree to which the fibers and matrix are intimately contacted and the level of adhesion at those contact points [24]. In composites reinforced with inorganic fibers, interfacial adhesion is often divided into three categories [24]:

1) *Chemical Adhesion* due to the formation of chemical bonds at the interface. These bonds may be formed by direct reaction between the matrix and fiber or may be due to the inclusion of molecular species designed to react with both fiber and matrix to form a chemical bridge between the two.
2) *Physical Adhesion* due to the decrease in the free energy of a system when two surfaces of surface tension γ_m and γ_f come together to form an interface with interfacial tension γ_{mf}.
3) *Mechanical Adhesion*, which refers to microscopic mechanical interlocking over substantial portions of the interface. This will be affected by the surface roughness of the fiber and the wetting ability of the matrix.

A weak interface can be the result of voids, poor fiber wet out, poor interfacial adhesion, and/or incompatible fiber/matrix chemistry at the interface [21]. Lo and Chim represented this by a normalized mathematical model with artificial material property values. The interface was assumed to be weak (E = 10,000 psi) and the interface volume was allowed to grow in volume fraction [21]. Figure 2.4-3 represents the composite interface model used to simulate the calculations and Figure 2.4-4 shows the results.

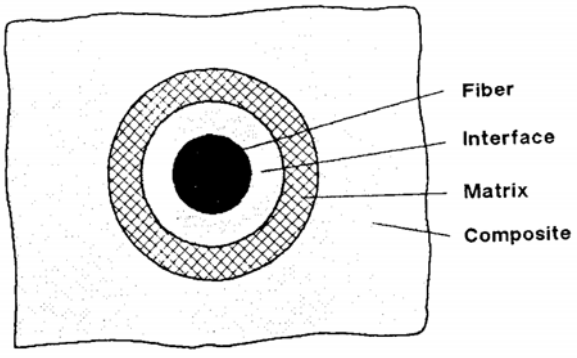

Fig 2.4-3: Composite Interface Model [21]

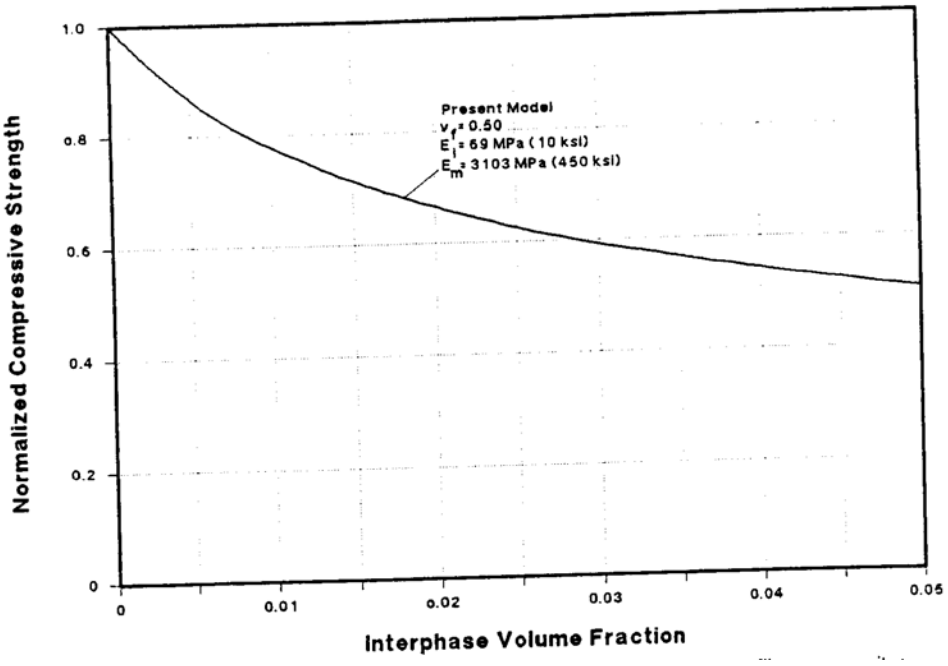

Fig 2.4-4: Normalized Compressive Strength vs. Interphase Volume Fraction [21]

As can be seen from their model, when this weak interface grows to about 5% of the total volume of the composite, the normalized compressive strength is reduced by nearly 50%. Hence, the importance of the size and stiffness of the interphase region in composite compression strength is illustrated.

Void Volume Content

Voids are often found in composite materials produced by commercially available manufacturing processes. They form in the matrix from mechanically entrapped air or moisture, solvents or polymerization by-products [25]. They are essentially defects that weaken the structure of the composite. When the voids are trapped at the fiber/matrix interface, a weak interphase region will occur [21]. This will lead to a reduction in compressive strength. When the

voids are dispersed in the resin matrix, the effective stiffness properties of the matrix are reduced. Hence, voids act as a porous cavity where failure is likely to initiate. As can be seen from Figure 2.4-5, the effect of void content on compressive structural performance has a negative effect.

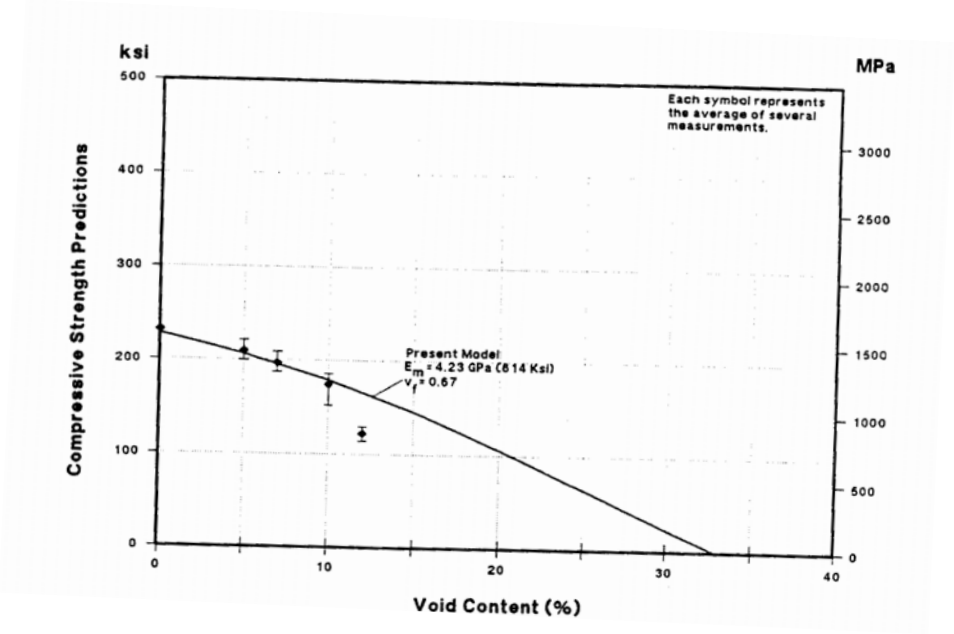

Fig 2.4-5: Compressive Strength Predictions vs. Void Content [21]

2.4.2 Material Influences

Resin Stiffness

For those composites whose failure mode from compression is micro-buckling, the use of a stiffer resin matrix will lead to an increase in composite compression strength [21]. However, this increase does not trend at the same rate over increasing resin modulus. From Figure 2.4-6, the rate at which this increase happens in compressive strength eventually levels and no significant advantage can be seen from using very high resin modulus. However, if a resin becomes too stiff or brittle, small imperfections in the composite are likely to initiate longitudinal cracks and the structure can be severely weakened [14].

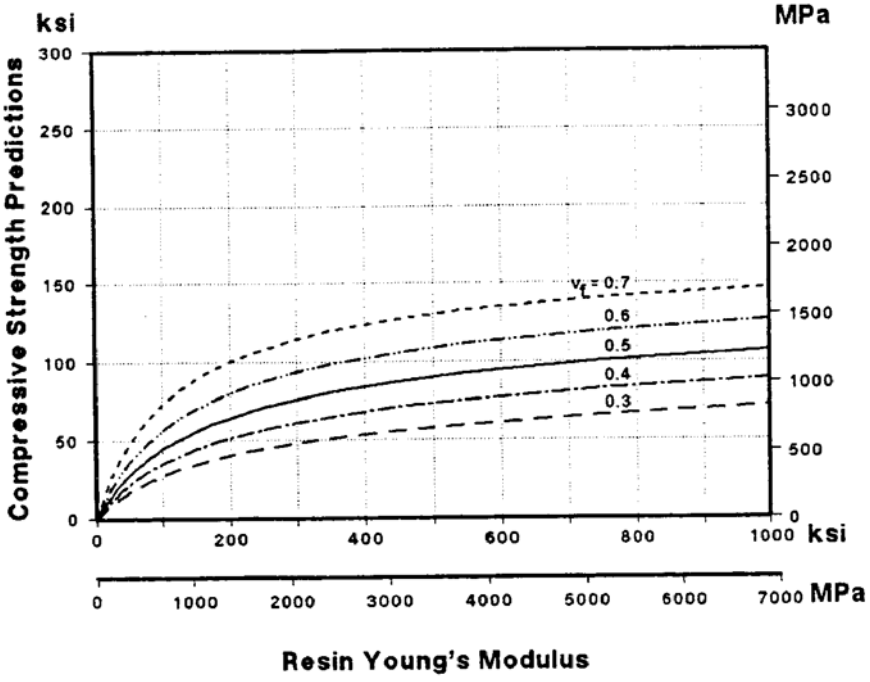

Fig 2.4-6: Compressive Strength Predictions vs. Resin Young's Modulus [21]

Fiber Diameter

In many cases, it has been reported that by increasing reinforcing fiber diameter, an increase in compressive strength will occur [12, 26, 27]. However, thicker fibers appear to be brittle and cannot be implemented well by conventional composite processing methods. The reason for this is due to a major difficulty in protecting the fibers from damage during composite fabrication and achieving good adhesion between the fibers and matrix [26]. If care is taken during fabrication, increasing the fiber diameter and changing the matrix to a more rigid material has been shown to yield 25-30% increases in compressive strength for glass reinforced plastic (GRP) materials [26].

This can be explained, first, by the higher rigidity of thicker fibers which improves the unidirectional orientation of the fibers within the composite. This improved orientation refers to more highly aligned fibers within the composite as well as reduced waviness. Secondly, the resistance to longitudinal cracking is determined, mainly, by the matrix fracture energy. This fracture energy is known to increase with the size of the matrix inelastic deformation zone. In a composite, this deformation zone can be restricted by the distance between neighboring fibers. As an increase in fiber diameter leads to an increase in this distance, it can be accompanied by an increase in fracture energy. Hence, the composite will be stronger [26]. It has been reported that increasing fiber diameter in GRP composites up to 130 μm will lead to an increase in compressive strength. After that, the compressive strength begins to decrease [27].

2.4.3 Specimen Influences

Edge Quality

The quality of a sample's cut edge has proven to be a major influence on the compressive strength of fiber reinforced composites. Edges containing defects, such as saw abrasions or delaminated layers, has been shown to reduce compressive strength of composite materials. Squires, Netting, and Chambers showed trending results of increasing average edge roughness (Ra) to decreasing compressive strength [22]. It was observed that a specimen containing an average edge roughness of 22 μm Ra experienced 60% of the load capacity that the same specimen containing 4 μm Ra experienced. This is a considerable difference and, by recommendation of the researchers, the average edge roughness should remain below 5 μm Ra.

Specimen Thickness

As thicker advanced composites find their way into structural sections where high compressive loads apply, understanding the behavior of these thicker laminates becomes necessary. Existing test methods have not provided precise compressive properties due to the fact that all problems related to testing become more serious and complicated with thicker composites [28]. As the specimen gets thicker, a higher percentage of the load must be transmitted at the end, thus increasing the chances of premature failure, such as end crushing [28]. However, very thin laminates are just as unattractive. Thinner samples are likely to fail prematurely due to buckling, whereas there is no gain in compressive strength from using thicker samples [22].

Specimen Alignment

The alignment of the fabricated specimen with respect to the loading direction is important in order to retrieve accurate results. Compression tests need to obtain perfect alignment of the specimen with respect to the applied load in order to generate a uniform maximum load in the gage section while preventing overall buckling of the specimen [29]. This is especially true for end loaded compressive tests. Direct end loading induces stress concentrations to accumulate at the sample ends. If the sample-end area is not fully in contact with the compressive platen due to misalignment, higher stresses will accumulate in smaller contact areas and will lead to premature failure at the specimen ends [30].

2.5 Influence of FRP Composite Fabrication Process on Mechanical Properties

As fiber reinforced polymer (FRP) composites become increasingly popular with the aerospace and marine industries, the variation of their fabrication method may insist significance when comparing mechanical properties. This variation can also attribute to post-curing processes which may not always be implemented in the manufacturing of composite laminates. Regardless of this, a review of composite manufacturing processes and their effect on mechanical properties are presented in this section.

Common materials yet different manufacturing techniques may give insight as to how composite fabrication can influence mechanical properties. Two studies were recently done on the compressive properties of carbon fiber composites, yet two different processes were implemented. Shivakumar, Swaminathan, and Sharpe fabricated carbon fiber laminates by way of RTM, while Lee and Soutis manufactured their carbon fiber system with the aid of an autoclave [28, 31]. The results of compressive properties indicate a trade off of superiority for certain values. The autoclave process, curing at 120 C, indicates higher compressive strengths with a max of 658 MPa compared to RTM of only 449 MPa, yet the RTM process yields a higher compressive modulus with a max of 67 GPa compared to autoclaving of only 57 GPa. This indicates that the RTM specimens were stiffer than the autoclave specimens, but the autoclaving technique allowed more load until failure.

Another study was recently done on the repeated impact response of glass reinforced laminates. Belingardi, Cavatorta, and Paolino compared the impact damage between hand lay-up fabrication (HL) and vacuum infusion (VI) [6]. It was determined that HL specimens survived more impacts before perforation initiated; hence, absorbing more total energy. No visual differences were conclusive on the impact damage of each specimen, but the stiffness of the vacuum infusion samples reduce more than hand lay-up after each impact. This trend can be seen over four intervals of initial impact velocity as seen in Figure 2.5-1.

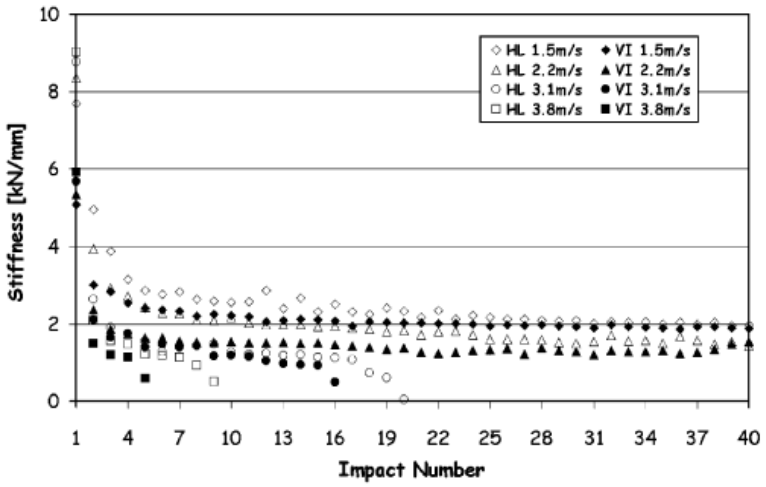

Fig 2.5-1: Repeated Impact Response for HL vs. VI Samples [6]

Other studies have been done on environmental influences, and their effect on mechanical properties of manufactured composites. Regarding marine environments, Karbhari studied E-glass/Vinyl-Ester composites fabricated by vacuum infusion (VI) and their interaction with various aqueous environments [32]. Numerous specimens were fabricated and some were immersed in water over various time intervals and at various water temperatures, while others were not subjected to aqueous interaction or temperature but time was still allowed to pass. Short-beam shear strength properties were taken from all specimens at every interval of time (span of weeks) and/or temperature. The unexposed specimens always increased in shear strength as time progressed, yet the immersed samples did not follow suit. It was shown for the water exposed samples that as immersion time and water temperature increased, shear strength decreased. This was seen in both the warp and fill directions of the tested composite.

In an entirely different study, Mouritz and Mathys based an experiment on post-fire effects on mechanical properties of marine composites [33]. The study is based on the argument that a major problem with using composites in marine craft is that the polymer matrices can ignite within a short time when exposed to a fire. Three different resins were tested (polyester, vinylester, and phenolic), intentionally subjected to an exposed electric radiant heat source.

Results show that despite the fact that phenolic resins are known for fire-resistive properties, they all experienced differences in post-fire mechanical properties.

When increasing exposure time was tested for all resins, polyester and vinlyester resins proved to be very similar in all categories. The phenolic resin excelled in normalized tensile stiffness and flexural modulus while the polyester and vinylester resins outshined the phenolic resin in tensile load and flexural load. Heat exposure time versus mechanical properties is displayed in Figure 2.5-2 a, b, c, d [33].

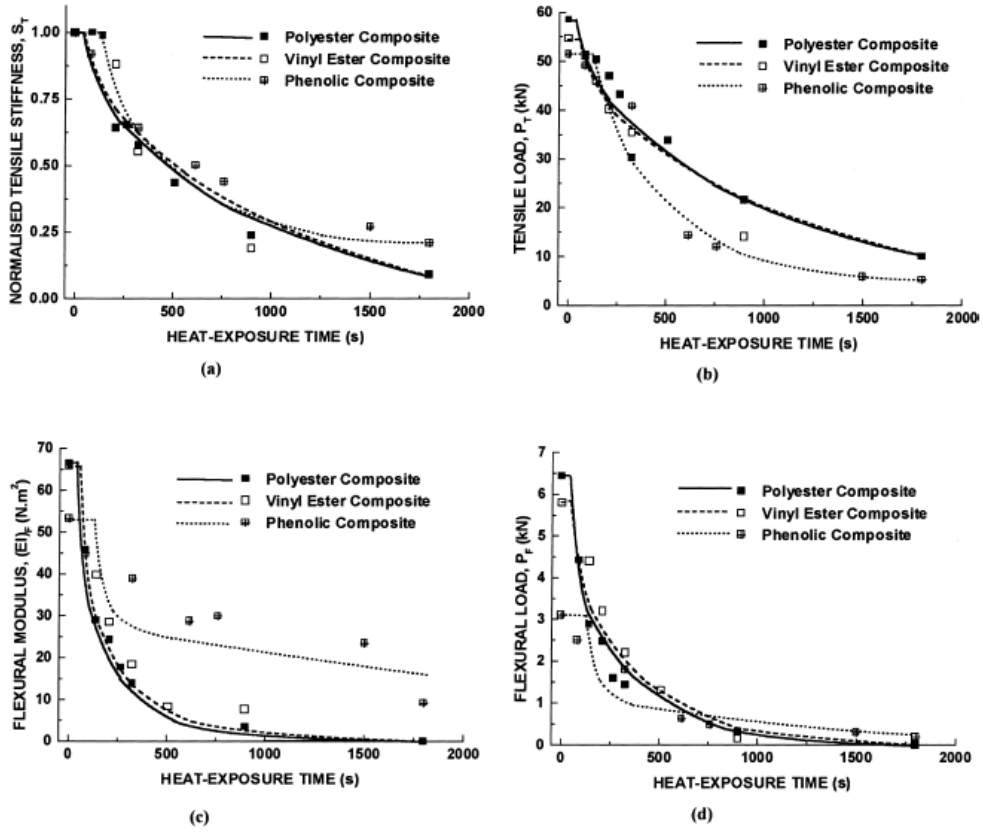

Fig 2.5-2: (a) Tensile Stiffness vs. Heat Exposure Time

(b) Tensile Load vs. Heat Exposure Time

(c) Flexural Modulus vs. Heat Exposure Time

(d) Flexural Load vs. Heat Exposure Time

When increasing heat flux was tested, the polyester resin rarely had supremacy over any other resin except in tensile load when introduced to high heat fluxes. The phenolic resin dominated the flexural modulus at all levels of heat flux but only at low heat fluxes for normalized tensile stiffness and tensile load. Vinylester usually fell in the middle of the two other resin types. Heat flux versus mechanical properties is displayed in Figure 2.5-3 a, b, c, d [33].

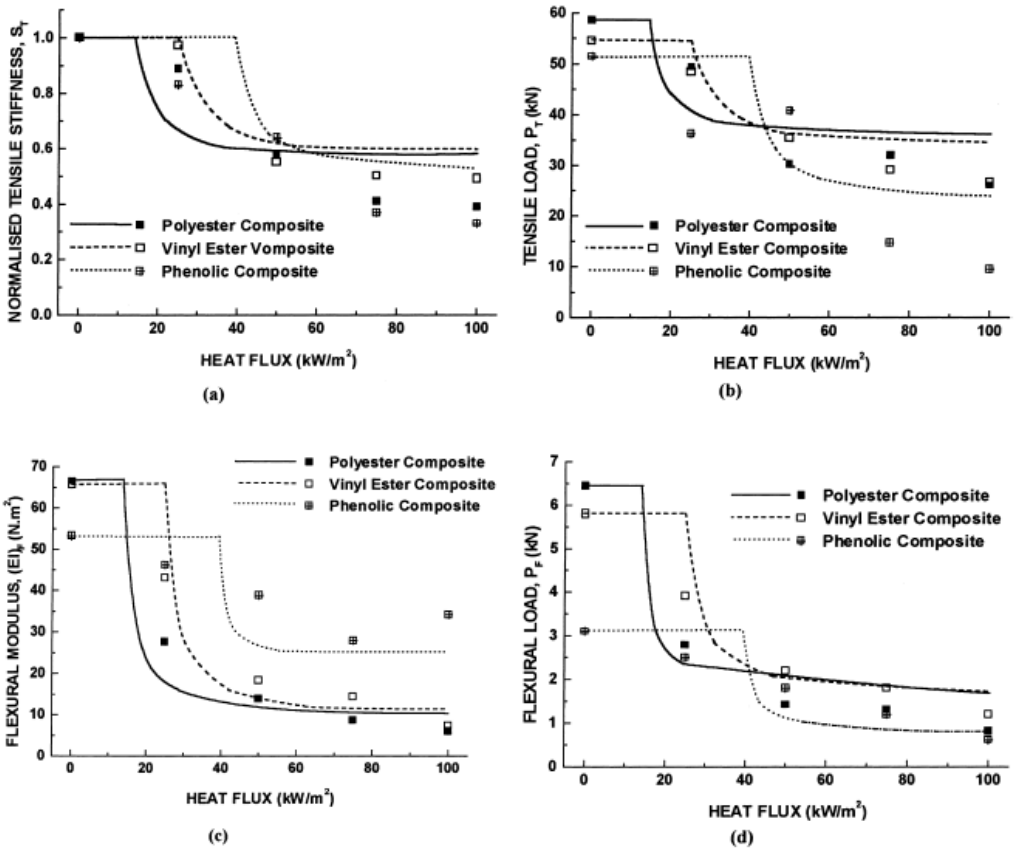

Fig 2.5-3: (a) Tensile Stiffness vs. Heat Flux

(b) Tensile Load vs. Heat Flux

(c) Flexural Modulus vs. Heat Flux

(d) Flexural Load vs. Heat Flux

The results of these properties are attributed to matrix degradation mainly caused by thermal decomposition of the resin that forms a char. It was found that fire induced delamination cracks beneath the char contributed to the reduction in properties of the polyester and vinylester resins more than the phenolic resin. The phenolic resin was more thermally stable and hence charring did not occur until after exposure at a higher heat flux and longer exposure time.

CHAPTER THREE

OBJECTIVES

In the marine industry, composite materials, namely glass fiber reinforced polymers (GFRP), are heavily relied upon to support the structural integrity of major boat and vessel components. Entire ship hulls are being constructed from this material and therefore it is important to understand what factors affect their mechanical performance. In this work, different mechanical testing methods and various manufactured laminates are tested and compared to find trends of mechanical integrity.

The following are the goals of this research:

1) Effect of Fabrication Method on Mechanical Properties
    - Investigate how the applied manufacturing process affects the mechanical properties of GFRP composite, namely hand lay-up vs. vacuum infusion.

2) Effect of Laminate Type and Lay-Up Sequence on Mechanical Properties
    - Investigate how lay-up sequence and laminate type affect the mechanical performance of GFRP composites.

3) Comparison of Different Compressive Testing Methods
    - Compare ASTM D695 and ASTM D695M compressive testing methods and examine the resultant properties of similar GFRP composite materials.

4) Effect of Surface Flatness on Compressive Properties
    - Investigate the compressive performance of specimens prepared with altered surface defects.

CHAPTER FOUR

EXPERIMENTAL DESIGN AND PROCEDURES

4.1 Composite Material Systems

In all, 8 different material systems were used to fabricate glass fiber reinforce polymer (GFRP) composites. Each one utilized either a different fabrication method, lay-up sequence of fibers, or resin type. Two of the eight material systems were manufactured in house at Washington State University Vancouver (WSUV) by the researcher while the others were donated by Christensen Yachts, Inc. The following are the specific material systems used for this study.

Christensen Hand Lay-Up (CHL)

Christensen hand lay-up composites were fabricated at Christensen Yachts, Inc. This lay-up was made in the form of a rectangular panel and was done so by using the hand lay-up technique. Owens Corning CDM 2408 (24 oz/yd^2 biaxial fibers, 8 oz/yd^2 of chopped mat fibers) fiberglass was the fiber used for this lay-up which had a specified dry sheet thickness of 1.498 mm (0.059 in) and an aerial weight of 34.1 oz /yd^2. Reichhold Hydrex 100 Epoxy Vinyl Ester catalyzed with 2 wt% MEKP was the resin implemented for construction which had a defined tensile modulus of 3.5 GPa (510 ksi) and a tensile strength of 86 MPa (12 ksi). Four sheets of this fiber were used in the construction of this laminate. The resulting lay-up sequence of this material is [mat/90/0/mat/90/0/mat/90/0/mat/90/0]. The resulting thickness of these composite panels was found to be 5.664 mm (0.223 in). Fig 4.1-1 shows the microstructure of this material.

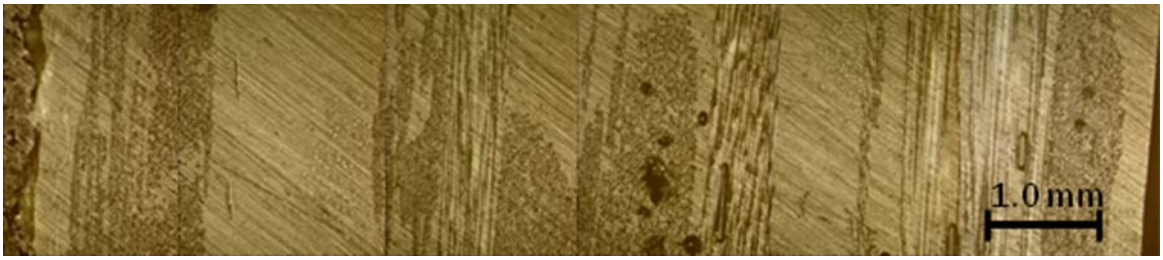

Fig 4.1-1: CHL Microstructure

WSUV Hand Lay-Up (MHL)

WSUV hand lay-up composites were fabricated on site at Washington State University Vancouver. This lay-up was fabricated in the form of a rectangular panel and was done so by using the hand lay-up technique. The fiber implemented for this lay-up was Vectorply E-LTM 3610 (36 oz/yd^2 biaxial fibers, 10 oz/yd^2 of chopped mat fibers) fiberglass, with a specified dry sheet thickness of 1.422 mm (0.056 in) and an aerial weight of 45.42 oz/yd^2. Overall, two sheets of this fiber were used. Derakane Momentum 411-200 Epoxy Vinyl Ester catalyzed with 2 wt% MEKP (methyl ethyl ketone peroxide) was employed as the resin for the construction of this laminate. The resin itself had a defined post-cured density of 1.14 g/cm^3 (0.041 lb/in^3), a tensile modulus of 3.2 GPa (460 ksi), and a tensile strength of 86 MPa (12 ksi). The resulting lay-up sequence of this material is [mat/90/0/mat/90/0]. The resulting thickness of these composite panels was found to be 3.657 mm (0.144 in). This microstructure heavily resembles that of the ILHS material, see Figure 4.1-2.

Inner Laminate Hull Side (ILHS)

ILHS composites were fabricated at Christensen Yachts, Inc. These samples were manufactured in the form of rectangular panels and were done so using by the vacuum infusion process at a vacuum pressure of 28.0 in. Hg (~14 psi). Two sheets of Vectorply E-LTM 3610

fiberglass were infused with Derakane Momentum 411-200 Epoxy Vinyl Ester resin catalyzed with 2 wt% MEKP. The resulting lay-up sequence of this material is [mat/90/0/mat/90/0]. The resulting thickness of these panels was found to be 2.387 mm (0.094 in). Figure 4.1-2 shows the microstructure for this material.

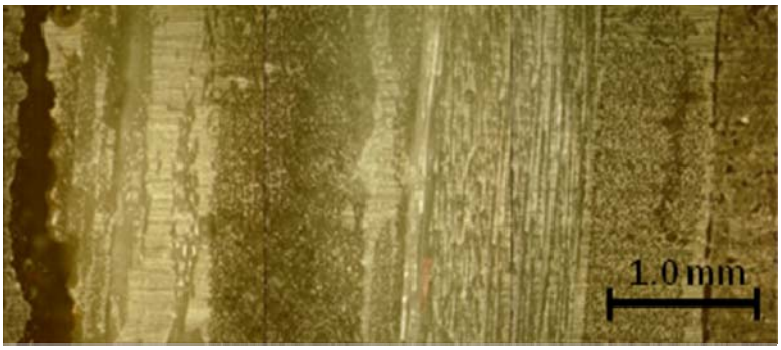

Fig 4.1-2: ILHS Microstructure

Inner Laminate Hull Bottom (ILHB)

ILHB composites were fabricated at Christensen Yachts, Inc. These samples were manufactured in the form of rectangular panels and were done so using the vacuum infusion process at a pressure of 28.0 in. Hg (~14 psi). Three sheets of Vectorply E-LTM 3610 fiberglass were infused with Derakane Momentum 411-200 Epoxy Vinyl Ester resin catalyzed with 2 wt% MEKP. The resulting lay-up sequence of this material is [mat/90/0/mat/90/0/mat/90/0]. The resulting thickness of these panels was found to be 3.353 mm (0.132 in). Fig 4.1-3 shows the microstructure of this material.

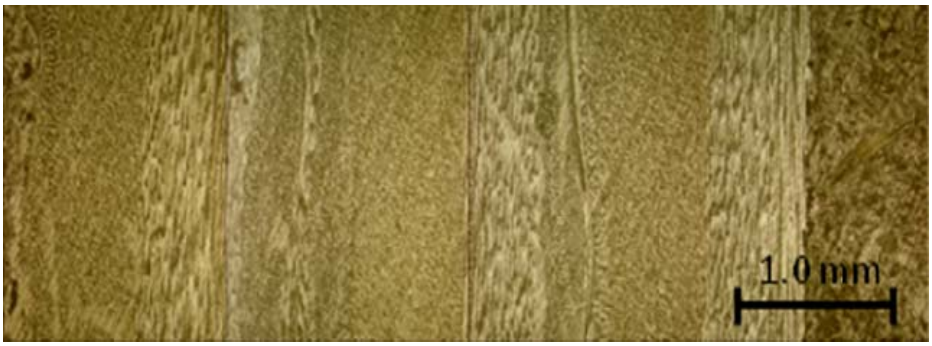

Fig 4.1-3: ILHB Microstructure

4-Layer Inner Laminate Hull Bottom (ILHB2)

ILHB2 composites were fabricated at Christensen Yachts, Inc. These samples were manufactured in the form of rectangular panels and were done so using the vacuum infusion process at a pressure of 28.0 in. Hg (~14 psi). Four sheets of Vectorply E-LTM 3610 fiberglass were infused with Derakane Momentum 411-200 Epoxy Vinyl Ester resin catalyzed with 2 wt% MEKP. The resulting lay-up sequence of this material is [mat/90/0/mat/90/0/mat/90/0/mat/90/0]. The resulting thickness of these panels was found to be 5.080 mm (0.200 in). This microstructure heavily resembles that of the ILHB material with an additional layer of fiber, see Figure 4.1-3.

Outer Laminate Hull Bottom (OLHB)

OLHB composites were fabricated at Christensen Yachts, Inc. These samples were fabricated by combined techniques which implemented both the hand lay-up and vacuum infusion process. Four layers of chopped mat and then one layer of Owens Corning CDM 2408 fiberglass was coated with Reichhold Hydrex 100 Epoxy Vinyl Ester resin catalyzed at 2 wt% MEKP. This sequence of fibers was manufactured using the hand lay-up technique and left to cure overnight. Once the resin was cured, the existing hand lay-up composite had four additional

layers of Vectorply E-LTM 3610 fiberglass stacked on top. Derakane Momentum 411-200 Epoxy Vinyl Ester resin catalyzed at 2 wt% MEKP was then introduced via suction of a vacuum at 28.0 in. Hg (~14 psi). The resin coated the additional layers of fiber and, at the same time, adhesively bonded to the existing hand lay-up laminate. This created a bi-manufactured composite panel. The resulting lay-up sequence of fibers in this material is [mat/90/0/mat/0/90/mat/0/90/mat/0/90/mat/0/90/mat/mat/mat/mat]. The resulting thickness of these panels was found to be 7.798 mm (0.307 in). Figure 4.1-4 shows the microstructure for this material.

Fig 4.1-4: OLHB Microstructure

Outer Laminate Hull Side (OLHS)

OLHS composites were fabricated at Christensen Yachts, Inc. These samples were fabricated by combined techniques of both the hand lay-up and vacuum infusion process. Three layers of chopped mat and then one layer of Owens Corning CDM 2408 fiberglass was coated with Reichhold Hydrex 100 Epoxy Vinyl Ester resin catalyzed at 2 wt% MEKP. This sequence of fibers was manufactured using the hand lay-up technique and left to cure overnight. Once the resin was cured, the existing composite had four additional layers of Vectorply E-LTM 3610 fiberglass stacked on top. Derakane Momentum 411-200 Epoxy Vinyl Ester resin catalyzed at 2 wt% MEKP was then introduced via the suction of a vacuum at 28.0 in. Hg (~14 psi). The resin

coated the additional layers of fiber and, at the same time, adhesively bonded to the existing hand lay-up laminate. This created a bi-manufactured composite panel. The resulting lay-up sequence of this material is [mat/90/0/mat/0/90/mat/0/90/mat/0/90/mat/0/90/mat/mat/mat/]. The resulting thickness of these panels was found to be 7.747 mm (0.305 in). Figure 4.1-5 shows the microstructure for this material.

Fig 4.1-5: OLHS Microstructure

WSUV Vacuum Infusion Medium (VIM)

WSUV vacuum infusion medium laminates were fabricated on site at Washington State University Vancouver. This lay-up was fabricated in the form of a rectangular panel and was done so by using the vacuum infusion process at a vacuum pressure of 20 in. Hg (10 psi). The fiber employed for this lay-up was Vectorply E-LTM 3610 fiberglass, and overall two sheets of this fiber were used. Derakane Momentum 411-200 Epoxy Vinyl Ester catalyzed with 2 wt% MEKP was used as the resin for the construction of this laminate. The resulting lay-up sequence of this material is [mat/90/0/mat/90/0]. The resulting thickness of these composite panels was found to be 2.464 mm (0.097 in). This microstructure heavily resembles that of the ILHS material, see Figure 4.1-2.

4.2 Material Fabrication Processes

4.2.1 Layup Preparation

In order to perform both the hand lay-up (HL) and vacuum infusion (VI) processes, initial preparation procedures were administered in order to manufacture panels from both fabrication methods. The following are the specific procedures taken by the researcher in order to prepare the necessary materials needed for both fabrication processes. It is important to note that the CHL, ILHS, ILHB, ILHB2, OLHS, and OLHB panels were fabricated by Christensen Yachts Inc. All other panels which include MHL and VIM were fabricated by the researcher and encompass the following procedures.

Fiber Preparation

The fiber used for the additional two panels (MHL and VIM) was Vectorply E-LTM 3610 fiberglass. The fiber is oriented in a stitched bonded sheet of three individual layers. The first two layers are longitudinal, biaxial architectures in which the fibers are arranged in straight tows. The first layer is longitudinally oriented at 0 degrees, and the second layer is longitudinally oriented at 90 degrees. The third layer is referred to as chopped mat, which are randomly oriented short strands of chopped fiber. All three layers and stitching material are made from the same fiberglass type, E-Glass, and the two biaxial layers constitute 36 oz/yard^2 of fiber in the sheet while the chopped mat layer constitutes 10 oz/yard^2 of fiber in the sheet. For all manufactured composite panels, sheets of fiber were cut to a 304.8 mm (12 in) by 304.8 mm (12 in) area for laminating.

Resin Preparation

The resin used for the construction of the two panels was Derakane Momentum 411-200 Vinyl Ester Epoxy Resin. This resin was acquired from Christensen Yachts Inc. and has been promoted to have a gel time of 45 minutes (time it takes for curing to begin). For all panels, the resin was catalyzed with methyl ethyl ketone peroxide (MEKP) at 2 wt%. For a single sheet of 304.8 mm (12 in) by 304.8 mm (12 in) Vectorply E-LTM 3610 fiber, approximately 110 grams of resin was found to be the best ratio of resin to fiber sheet area. If numerous sheets are E-LTM 3610 are to be laminated, the recommended amount of resin suggested by the researcher is the number of sheets multiplied by 110 grams of resin. For example, if 2 sheets of fiber are to be laminated, 220 grams of resin must be prepared for laminate construction.

4.2.2 Hand Lay-Up (MHL)

In order to manufacture the MHL composite panel, sheets of fiber needed to be obtained. Two, 304.8 mm (12 in) by 304.8 mm (12 in) sheets of Vectorply E-LTM 3610 fiber were cut using industrial size scissors acquired at WSUV. An illustration of a single sheet of cut fiber can be seen in Figure 4.2-1.

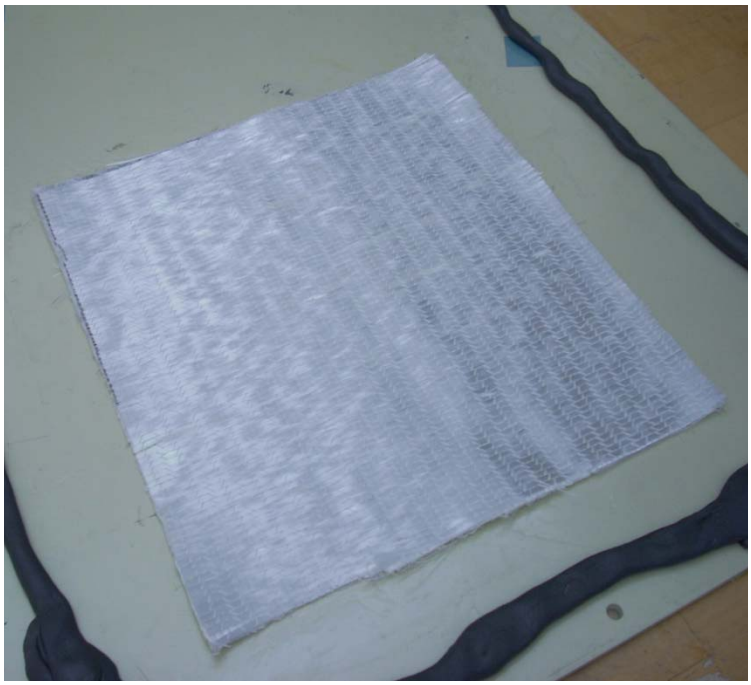

Fig 4.2-1: E-Glass Fiber Sheet, 304.8 mm (12 in) by 304.8 mm (12 in), Laid Upon Anti-Bond Medium

The first sheet of fiber was placed on an anti-bond medium that is made of thermosetting Polyamide 6 and wrapped around a rigid, flat plate of steel to give a solid surface in which to perform the lay-up. This anti-bond medium will ensure that the curing resin won't attach itself to the surface in which the lay-up is performed, which then allows for later removal. Next, the resin was to be prepared for lamination. 220 grams of Derakane Momentum 411-200 Epoxy Vinyl Ester Resin was catalyzed with 2 wt% MEKP in a standard plastic container. Thorough mixing was administered for approximately 2 minutes. A picture of this operation is shown in Figure 4.2-2.

Fig 4.2-2: Epoxy Vinyl Ester Resin Being Catalyzed with 2% MEKP, Thoroughly Mixed

Once the resin was sufficiently catalyzed by thorough mixing, wetting the first layer was the next step. Approximately 110 grams of the catalyzed resin was administered to the first sheet of fiber, which was laid upon the anti-bond medium. The resin was evenly spread throughout the sheet, with care taken not to waste the resin by pouring it elsewhere. Once the resin was administered to the first sheet, a hand roller with a roll diameter of 24.1 mm (0.950 in) and a rolling length of 76.2 mm (3.0 in), was used to spread the resin evenly into the fiber sheet , and more importantly, to wet all the fibers within the sheet. Proper wetting was obtained when the fibers appeared in the color of the resin, and no white streaks of dry fibers were apparent. Illustrations of administering the resin to the first sheet of fiber, and of the hand rolling technique can be seen in Figure 4.2-3 and 4.2-4, respectively.

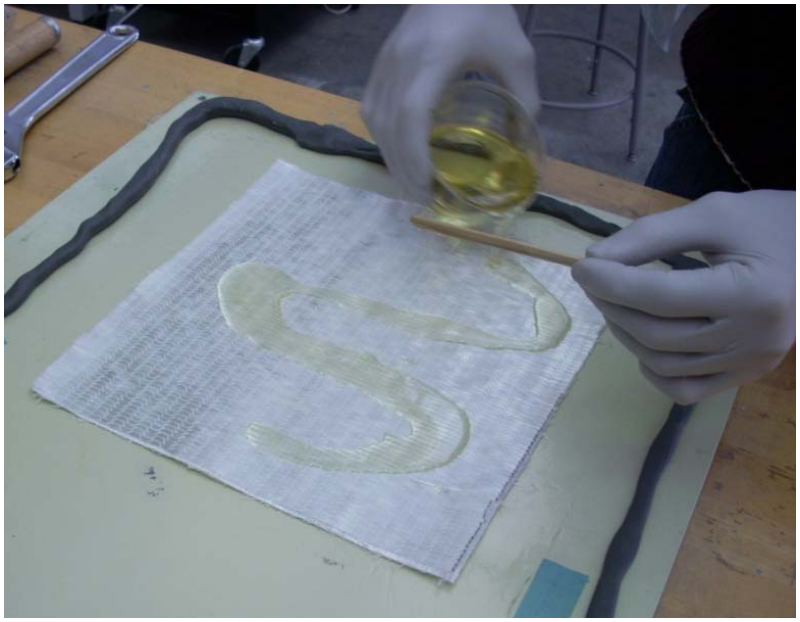

Fig 4.2-3: Administering Resin to the First Sheet of Fiber

Fig 4.2-4: Manual Wetting of Fibers with a Hand Roller

Once the first layer of fibers appeared sufficiently wetted, the next sheet of fiber with the same dimensions was added on top of the first layer. Care was taken to make sure that the top layer of the second sheet matched the fiber direction of the top layer from the first sheet. This way the fibers were oriented in the same direction for each sheet.

Once the second sheet was oriented properly, it was wetted with the remaining 110 grams of resin, and rolled once again to ensure that all the fibers were sufficiently impregnated with resin. A final product of a successful HL panel can be seen in Figure 4.2-5. Once the panel's construction was complete, it was left to cure overnight at ambient conditions.

Fig 4.2-5: Final Product from the HL Process, Two Layers of Fiber Imbedded with Resin

4.2.3 Vacuum Infusion (VIM)

Preparation of panels for the VI process include some of the same steps from the HL process, however, additional procedures are necessary. The most noticeable difference between the HL and VI techniques is the fact that HL panels are left to cure at ambient conditions while VI panels are held under the pressure of a vacuum while curing occurs. The presence of vacuum pressure extracts most voids within the lay-up, depending on vacuum pressure. The following are the procedures used to create the VIM panel.

The first procedure taken to prepare the VIM panel was to line the perimeter of the anti-bond surface with a sealant in order to later create an air-tight seal around the lay-up. The same steel plate wrapped with the Polyamide 6 anti-bond material used in the HL process was lined with a putty material called duct seal. Before and after pictures of this procedure can be seen in Figures 4.2-6 and 4.2-7, respectively.

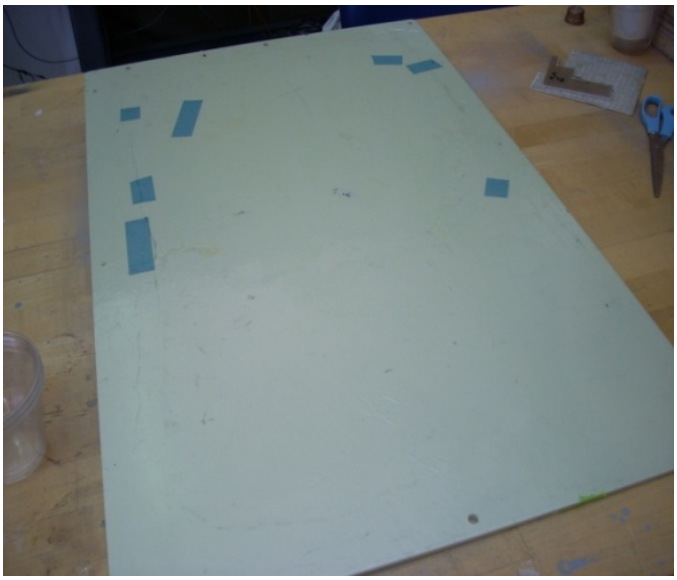

Fig 4.2-6: Covered Steel Plate with Anti-Bond Medium

Fig 4.2-7: Covered Steel Plate with Duct Seal Lined Around the Perimeter

Before additional steps were to be taken, an adequate vacuum was obtained for the use of creating vacuum pressure while performing the proposed lay-up. The vacuum used for this lay-up was a compressed air operated, 28 in. Hg max (~14 psi), vacuum pump equipped with a pressure gage. Compressed air is administered to the inlet valve which then feeds the mechanism in the pump and creates negative pressure at the outlet. A picture of the vacuum used for these panels can be seen in Figure 4.2-8.

Fig 4.2-8: Vacuum Pump Used for VIM Lay-Up

Once the vacuum was obtained, the vacuum's outlet hose was attached at one corner of the steel plate where a high concentration of sealant was administered. The vacuum outlet was also positioned at the opposite end from where the laminate would be constructed. From careful observation, the vacuum outlet should be placed no closer in proximity than 304.8 mm (12 in) from the layup. The high concentration of sealant acted to hold the tubing in place while the lay-up was being held at negative pressure. Tubing attachments can be seen in Figure 4.2-9.

Fig 4.2-9: Vacuum Tubing Held by Sealant at Front Corner of Laminate Surface

The next steps are those described previously for the HL process. For the VIM panel, two 304.8 mm (12 in) by 304.8 mm (12 in) sheets of fiber were cut and 220 grams of resin was thoroughly mixed for approximately 2 minutes and catalyzed with 2 wt% MEKP. The first sheet of fiber was then laid in between the perimeter of the sealant and coated with approximately 110 grams of catalyzed resin. The hand roller was used to spread the resin evenly around the area of the fiber sheet, taking care to impregnate the resin into each individual layer. Once the first sheet was sufficiently wetted with resin, the second sheet was administered on top of the first sheet,

taking care to align the fibers in the same orientation. This second sheet then was coated with the remaining 110 grams of resin and rolled for sufficient wetting.

After all the necessary procedures were taken to prepare the fiber and administer the resin, the lay-up was ready for infusion. From the same anti-bond material that coated the steel plate, a slightly larger than 304.8 mm (12 in) by 304.8 mm (12 in) square piece of material was cut from excess supply. This acts as an intermediate seal from the vacuum so that while the vacuum is administered, resin will only be extracted from the sides of the lay-up and not the entire area. It has been observed that if resin is extracted from the entire area, too much resin will be sucked from the lay-up and the laminate will incur overly voided regions. By extracting resin from only the sides of the lay-up, the resin will be removed at slower rates while being compressed by the pressure of the vacuum. This pressure reduces the void content in the laminate while not allowing too much resin to leave the lay-up. An illustration of the top seal administered to the prepared lay-up can be seen in Figure 4.2-10.

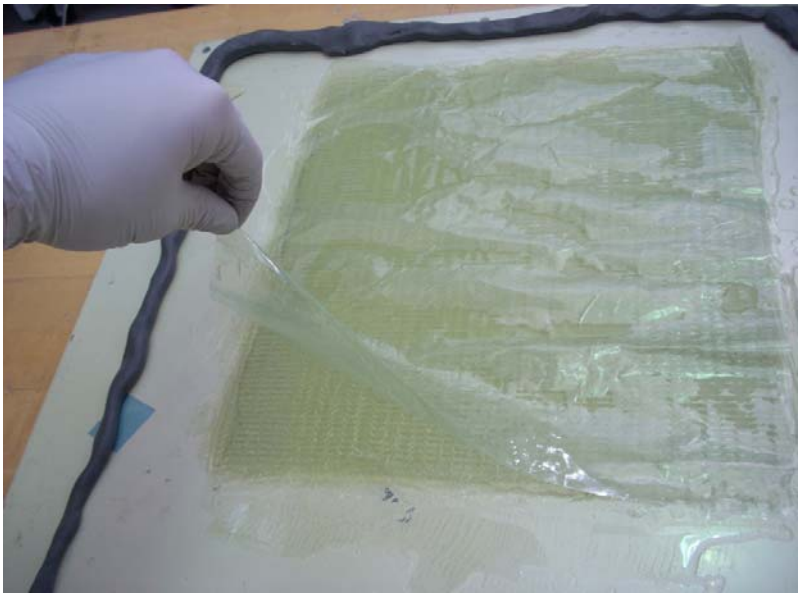

Fig 4.2-10: Top Anti-Bond Seal Being Placed Over Prepared Infusion Laminate

Once the top seal is aligned just over the top area of the lay-up, cheesecloth was arranged over the entire lay-up and back to the vacuum hose. The cheesecloth creates air cavities which allow resin to be extracted from all sides of the lay-up and also absorbs extracted resin before it can be consumed by the vacuum. An illustration of the cheesecloth setup used for the VIM panel can be seen in Figure 4.2-11.

Fig 4.2-11: Cheesecloth Setup for the VI Process

Finally, before the vacuum can be administered to the lay-up, the entire area of the steel plate is covered with a final layer of anti-bond material. The putty sealant around the perimeter of the lay-up surface acts to seal off the lay-up from outside influences. The final layer of anti-bond material going over the lay-up and then sealed off can be seen in Figures 4.2-12 and 4.2-13.

Fig 4.2-12: Final Layer of Anti-Bond Material Going Over Lay-Up

Fig 4.2-13: Final Layer Getting Sealed by Perimeter Putty

Once the lay-up is sealed off, the vacuum can be turned on and left for curing. For the VIM panel, the pressure was set at 20 in. Hg (~10 psi). It should be noted that all vacuum infused panels that came from Christensen Yachts Inc. were fabricated at 28 in. Hg (~14 psi). An illustration of the vacuum taking effect on an infused lay-up can be seen in Figure 4.2-14.

Fig 4.2-14: Vacuum Taking Effect on Prepared Lay-Up

4.3 Test Specimen Configuration

4.3.1 Tensile Configuration

Tensile Geometry

Illustrations of a standard tensile specimen, as well as the dimensional tolerances of that specimen can be seen in Figures 4.3-1 and 4.3-2, respectively.

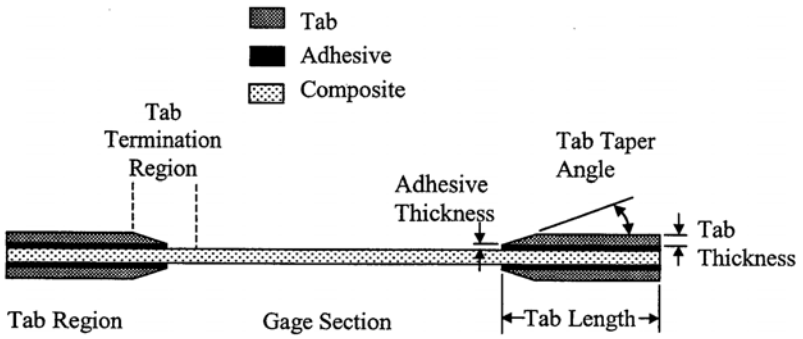

Fig 4.3-1: Typical Tabbed Tensile Composite Test Specimen [34]

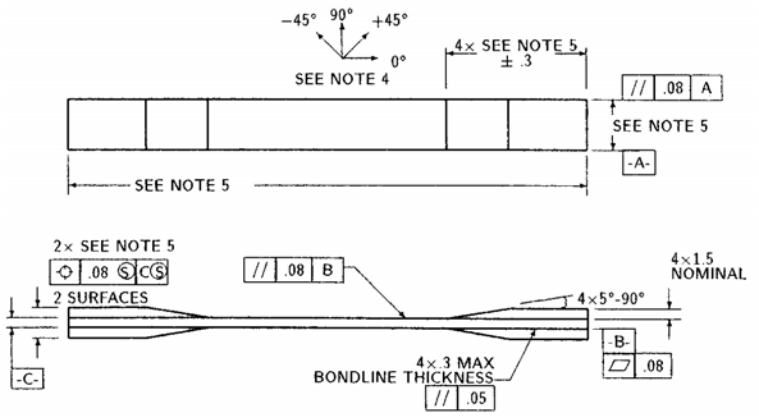

Fig 4.3-2: Dimensional Tolerances of Tensile Specimen [2]

Tensile specimens are straight sided with a constant cross section. Beveled tabs are adhesively bonded at the specimen ends to eliminate grip induced defects and to ensure failure within the specimen gage area. Recommended tensile specimen geometries can be located in Table 4.3-1.

Fiber Orientation	Width, mm [in.]	Overall Length, mm [in.]	Thickness, mm [in.]	Tab Length, mm [in.]	Tab Thickness, mm [in.]	Tab Bevel Angle,°
0° unidirectional	15 [0.5]	250 [10.0]	1.0 [0.040]	56 [2.25]	1.5 [0.062]	7 or 90
90° unidirectional	25 [1.0]	175 [7.0]	2.0 [0.080]	25 [1.0]	1.5 [0.062]	90
balanced and symmetric	25 [1.0]	250 [10.0]	2.5 [0.100]	emery cloth	—	—
random-discontinuous	25 [1.0]	250 [10.0]	2.5 [0.100]	emery cloth	—	—

Table 4.3-1: Recommended Tensile Specimen Geometry [2]

Tensile Tabbing

If tabbing is to be implemented for tensile testing of composite laminates, tabs and tabbing adhesives have a great influence on the measured tensile properties of the material. Tabs are not always required for tensile testing due to the type of testing apparatus. However, tabs are strongly recommended when testing with wedge operated grips where the specimen ends could be damaged by the grips [2]. The following, outlines the tabbing factors that affect composite tensile testing.

1) *Tab Material*: The tabbing material used for testing should be of a compliant strain material. This is done to reduce stress concentrations in the gripped area and thereby promote failure within the gage section. It is not uncommon to use tabs of the same material that is being tested [12].
2) *Tab Adhesive*: Adhesive selection is no less important than the tab material itself. The adhesive must be able to transmit the required load into the test specimen through shear and must be able to withstand the compressive force applied by the grips [34]. Any high-elongation (tough) adhesive system may be used when bonding tabs to the material under test [2].

3) *Tab Thickness*: The tabbing material must be of adequate thickness to protect the specimen from surface damage during gripping. This thickness has no significant effect on tab termination stress concentration. See Figure 4.3-1 for an illustration of the tab termination region. A tab thickness of 1 to 2 mm (0.04 to 0.08 in) is recommended for general use in tensile testing [34].
4) *Tab Length*: A suitable tab length is somewhat determined by the strength of the tab material as well as the adhesive. It also should be suitable to cover the minimum grip length used during testing [34]. A longer tab length serves to slightly reduce the tab termination stress concentrations. According to the standard, a minimum tab length can be estimated by the following equation [2]:

$$L_{min} = \frac{F^{tu} * h}{2 * F^{su}}$$

Where :

L_{min} : Required minimum bonded tab length, mm [in]

F^{tu} : Ultimate tensile strength of the coupon material, MPa [psi]

h : Coupon thickness, mm [in]

F^{su} : Ultimate shear strength of adhesive, coupon material, or tab material (whichever is lowest), MPa [psi]

5) *Tab Taper Angle*: Although a highly tapered tab is desired to minimize tab termination stress concentration, ease of fabrication and maintaining bond-line uniformity must be accounted for. A taper angle serves to feather the tabbed region into the untabbed gage area, minimizing the geometric discontinuity and the corresponding stress concentrations. This is due to the fact that the clamping pressure cannot be exerted onto the beveled region of the tab. Successful tab bevel angles have been reported between 7 and 15 degrees [2, 34].

4.3.2 Compressive Configuration

Compressive Geometry

For both standards, the same testing fixture and procedure apply. However, it is the specimen geometry that distinguishes the two. ASTM D695 requires a “dog-bone” shaped specimen with widened ends to promote failure within the thinner gage area. ASTM D695M (M stands for modified) requires specimens that are machined with a constant rectangular cross-section and then tabbed. A small gage section is revealed in the center of the specimen to promote failure within this region. Figures 4.3-3 and 4.3-4 show the D695 and D695M sample geometries, respectively.

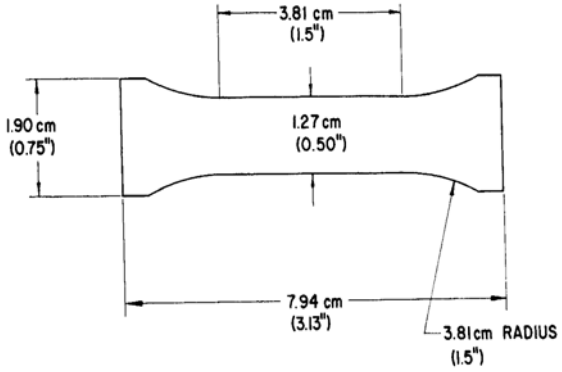

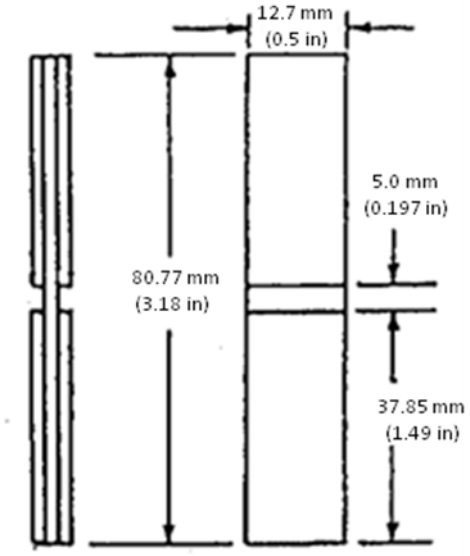

Fig 4.3-3: (left) ASTM D695 Dog-bone Specimen Geometry, cm (in) [3]

Fig 4.3-4: (right) ASTM D695M Front and Side Views of Tabbed Specimen Geometry, mm (in) [4]

Compressive Tabbing (ASTM D695M)

For compressive results obtained through ASTM D695M, the load will be introduced into the specimen through its ends, which are fixed with adhesively bonded tabs. Thus, it is important to discuss the influences tabs may have on a tested composite specimen.

1) *Tab Material*: In general, the tab material must be of adequate strength to transmit the load into the specimen. A lower stiffness tabbing material reduces the stress concentration at the tab termination region. However, overly compliant tab materials produce high shear stress concentrations at the specimen ends due to end loading. It is recommended that glass fabric/epoxy laminated circuit board be used as the tabbing material for compression testing [34].
2) *Tab Adhesive*: Although strength is the primary consideration for tab adhesive selection, the modulus of elasticity has a minor effect on the magnitude of the stress concentration within the composite specimen. Thus, adhesive selection should be based on strength properties, ease of application, cost, and availability before considering elastic modulus [34].
3) *Tab Thickness*: The tabbing material must be of adequate thickness to protect the specimen from surface damage, and to increase surface area at the specimen ends. When a significant amount of the load is administered at the specimen ends, the added cross-sectional area serves to reduce the stress at the end of the composite specimen. A recommended tab thickness for compression testing is approximately 1 to 2 mm (0.04 to 0.08 in) [34].
4) *Tab Length*: The length of tab is determined by the allowed gage length needed to promote failure within that region. It has been recommended that the tab length be at least 40 mm (~ 1.5 in) for most general compressive tests [34].
5) *Tab Taper Angle*: Although a beveled tab is desired to reduce stress concentrations in the tab termination region, tapering the tab increases the unsupported gage length, and

drastically lowers the applied stress at which buckling can occur. It is recommended that an untapered tab (i.e. 90 degree bevel angle) be used for compression testing [34].

Geometrical Tolerance

Great care shall be taken when machining the ends of the specimens to ensure flat, parallel surfaces result. These ends shall be perpendicular to the longitudinal or loading axis to within 0.025 mm (0.001 in) [3]. Both dog-bone and tabbed compression specimens apply. See Figure 4.3-5.

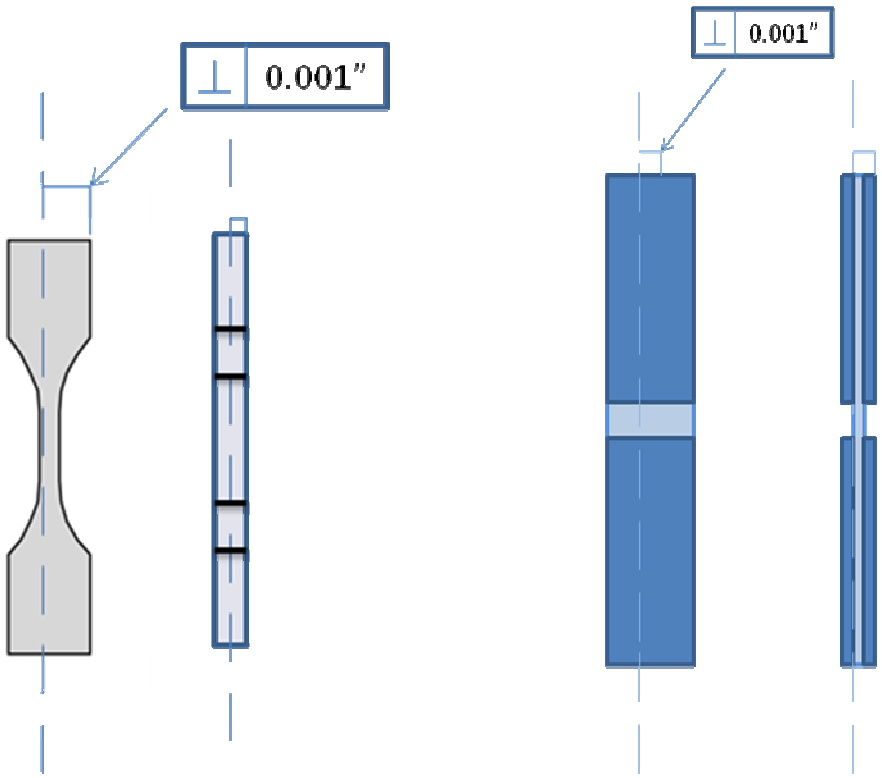

Fig 4.3-5: Perpendicularity Tolerance for Compressive Specimen Ends, “dog-bone” (left), “tabbed” (right)

4.4 Test Specimen Fabrication

For each panel either constructed at WSUV or received from Christensen Yachts Inc., three types of test specimens were fabricated. These types were tensile specimens, compression specimens, and ignition loss test specimens. Tensile coupons were constructed according to ASTM D3039 [2], compression coupons were constructed according to ASTM D695 [3] and ASTM D695M [4], and ignition loss test coupons were constructed according to ASTM D2584 [5]. The following are the specific procedures taken in order to fabricate each type of test coupon based on their corresponding standardized test method.

4.4.1 Tensile and Ignition Loss Test Specimens

To first construct tensile coupons, it was necessary to verify the geometry that needed to be achieved. Based on the parameters outlined in ASTM D3039, the specimens were to be 25.4 mm (1.0 in) wide by 254 mm (10 in) long. Thicknesses varied from each panel depending on the number of fiber layers and manufacturing method. Once the geometry was understood, the first step for construction was to prepare one side of each panel with a straight reference edge. This was done using a Porter Cable Plunge Router that rotated at 22,000 rpm. The router was instrumented with a ¼ inch burr, carbide router bit and a sliding table fence parallel to the direction of cut. An illustration of this can be seen in Figure 4.4-1.

Fig 4.4-1: Panel Being Prepared with a Reference Edge

Once a reference edge was established, strips of each material system were cut slightly larger in width and slightly in length than the final dimensions of the tensile coupon using a Laguna 16” HD Band Saw with a 3/8 inch width, 14 TPI steel band saw blade rotating at 1300 rpm. The band saw table was also instrumented with a sliding table fence, parallel to the direction of cut. The established reference edge began as the side against the fence used for cutting the first strip which left another straight edge used as the reference for the next strip. In all, 5 tensile strips were cut from each panel. An illustration of this can be seen in Figure 4.4-2.

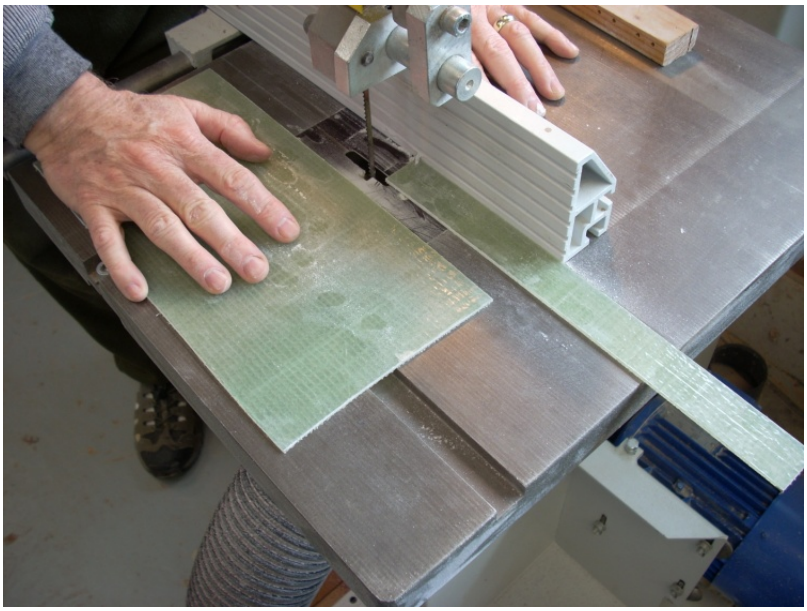

Fig 4.4-2: Tensile Strips Cut Using a Band Saw with a Guided Fence

After 5 strips were cut from each panel, they were again taken back to the router table for finishing. The router fence was adjustable and the ¼ inch carbide burr bit created a very smooth, straight edge which is ideal for specimen fabrication. Each strip was cut from the band saw to a width of approximately 31.8 mm (1.25 in) and a length of approximately 279.4 mm (11.0 in). This gave room for finishing with the router. Both edges of each strip were finished using the carbide burr router bit. Approximately 3.175 mm (0.125 in) of material was removed from each edge to achieve the desired width of 25.4 mm (1.0 in). An illustration of this can be seen in Figure 4.4-3. A light sanding of the routed edges followed using 320 grit sandpaper.

Fig 4.4-3: Tensile Coupon Edges Being Finished on a Router to a Width of 25.4 mm (1.0 in)

Once the correct width was achieved, the extra length of each tensile specimen served a purpose to construct the ignition loss test specimens. Since the desired geometry of each ignition loss test coupon was a square of dimension 25.4 mm (1.0 in) by 25.4 mm (1.0 in) as stated by ASTM D2584, the extra length left on each tensile coupon could be cut off and used as an ignition loss test specimen. This was done using the same band saw and instrumentation described earlier where the fence was set at a distance of 25.4 mm (1.0 in) from the blade and the ends of each tensile specimen were simply cut off, leaving a nearly perfect square from each panel of dimension 25.4 mm (1.0 in) by 25.4 mm (1.0 in). In all, since five tensile specimens were constructed from each panel, 5 ignition loss test specimens were also constructed from each panel. An illustration of finalized ignition loss test specimens can be seen in Figure 4.4-4.

Fig 4.4-4: Finalized Ignition Loss Test Specimens, Dimensions of 1 inch by 1 inch

Once each tensile specimen was cut to a length of approximately 254 mm (10 in), they finally had to be tabbed to finalize their construction. Tabs are adhesively bonded at the coupon ends to protect the tensile specimen from grip induced damage during testing. They are constructed at the same width as the tensile specimen, 25.4 mm (1.0 in), but are cut to a much shorter length to expose the specimen gage area in the middle of each individual tensile coupon. The suggested length of each tensile tab is the grip length from the purposed testing device. Tabs are also prepared with beveled tips to feather the tab down to the specimen which reduces stress concentrations at the tab termination region. To construct these tabs, a specialized fixture was necessary. The fixture must be built at an angle to account for the angle at the tab tip. Also, depending on the cutting method, the tabs must be held firmly in place while cutting is allowed to commence.

In order to construct each tensile tab, the dimensions of the tabs had to be determined. The tab width was to be approximately 25.4 mm (1.0 in) since the width of each tensile coupon was of this dimension. After studying the testing apparatus at WSUV for future tensile testing, the grip length was measured to be 57.2 mm (2.25 in), and therefore each tab length must be cut

to this dimension as well. Once the tab dimensions were understood, construction of each tab was carried out using the guided band saw previously stated. Tabs were made of 1.67 mm (0.065 in) thick, NEMA FR-4 (G10) Glass Cloth Epoxy Laminate Circuit Board purchased from Trident Plastics Inc. This material is strain compatible with each of the purposed material systems, and serves well to protect the specimen ends from grip induced defects. The final preparation of tab construction was to make each tensile tab with a beveled angle. It was determined from previous research that each tab had to be instrumented with a beveled tip angle of approximately 15 degrees. A specialized fixture was designed and implemented for the beveled tab region. This fixture was designed at an angle of 15 degrees to account for the angle needed for each tab and was instrumented with three press clamps to firmly hold three tabs in place at one time. An illustration of this fixture can be seen in Figure 4.4-5.

Fig 4.4-5: Specialized Fixture Designed for Cutting Tensile Tabs with Beveled Angle Region

To cut each tab with the beveled region, a manually operated Birmingham Vertical Mill was instrumented with a 4 fluted, ½ inch diameter, HSS bit and set at a speed of 1000 rpm upon cutting. Each clamp could hold one tensile specimen, and in one pass of the HSS bit, three tabs could be constructed with the desired beveled region. Once the fixture was firmly gripped by the mill's vice, each clamp was set to firmly hold one tensile tab. An illustration of this can be seen in Figure 4.4-6.

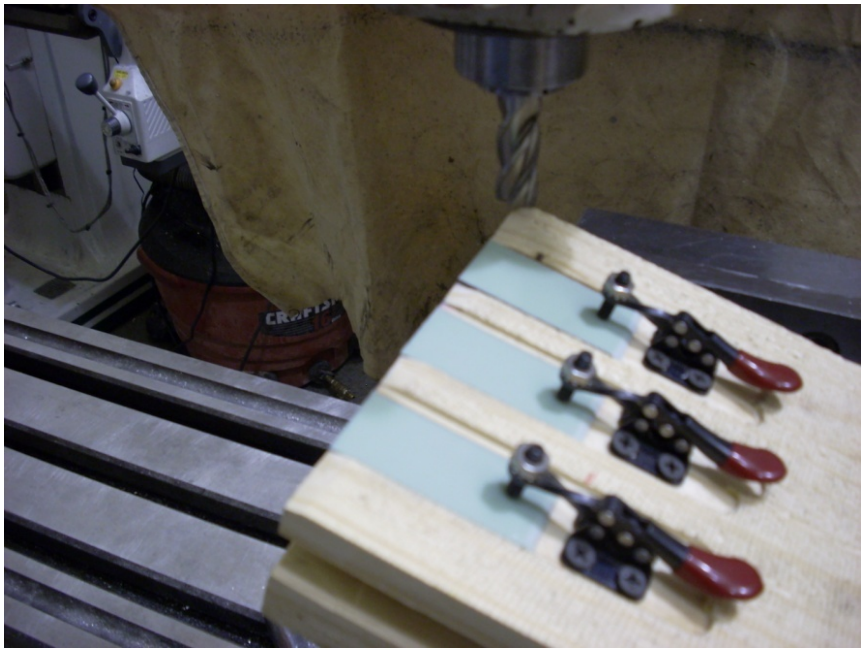

Fig 4.4-6: Tensile Tabs Held in Place by the Cutting Fixture

The mill was set at the desired speed of 1000 rpm and manually fed over the ends of each tab. Since the mill is set to near perfect verticality and only grazed the ends of each tab, the desired beveled angle of 15 degrees was achieved for each tensile tab. A schematic of a finalized tab can be seen in Figure 4.4-7.

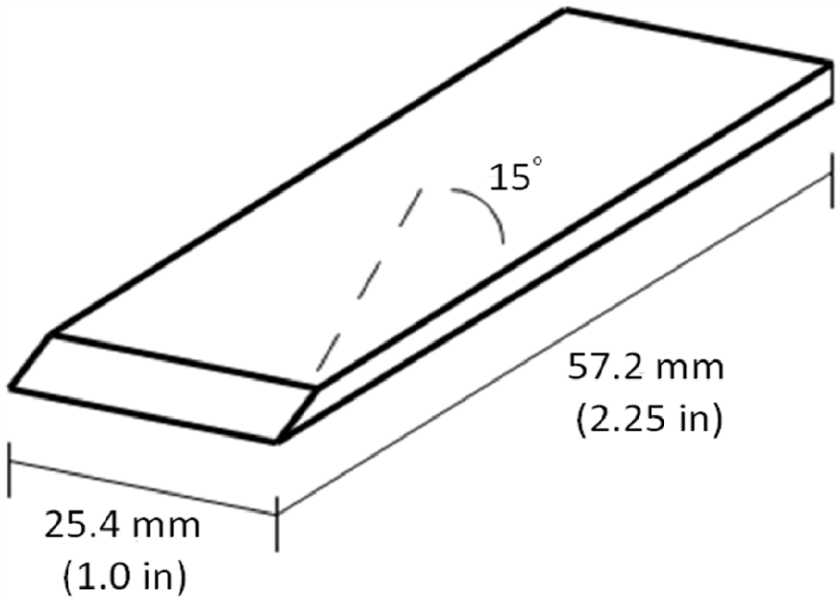

Fig 4.4-7: Schematic of Finalized Tensile Tab Construction with Beveled Angle Region, mm (in)

Now that tabs were properly constructed, they had to be adhesively applied to each tensile coupon. To prepare the coupons and tabs for adhesion, the bonded surfaces were abraded to add surface area for adhesion. It was found using the tip of a steel wood screw to gouge the adhesion surfaces of each tensile specimen end and tab would provide sufficient surface roughness for adhesion. Before and after pictures of this process taking place on a tensile specimen can be seen in Figures 4.4-8 and 4.4-9 respectively.

Fig 4.4-8: Tensile Specimen End Before Surface Preparation for Adhesion

Fig 4.4-9: Tensile Specimen End After Surface Preparation for Adhesion

The same actions were taken to prepare each tab's back surface for adhesion as well; the front surface is where the 15 degree beveled region exists. Once the desired surfaces were properly roughened for adhesion, two-part 3M Scotch-Weld Epoxy, model DP-460 was mixed and applied to each prepared adhesion surface. This epoxy was used for its high shear strength properties and ease of accessibility. An illustration of the materials being prepared for adhesion can be seen in Figure 4.4-10.

Fig 4.4-10: Materials Prepared for Tab Adhesion (Epoxy, Specimen, & Tab)

Four tabs in all were bonded to each tensile coupon, two on either side of each end. Care was taken to ensure that the beveled surface of each tab was not the bonded surface, and that the beveled region was aligned towards the gage section of each coupon. After the tabs where properly bonded to each side of each tensile specimen end, they where clamped and left to cure overnight. An illustration of some finalized tensile coupons can be seen in Figure 4.4-11.

Fig 4.4-11: Finalized Tensile Coupons Bonded with Beveled Tabs

4.4.2 Compression Specimens

Two sets of compression specimens were produced for their respective testing method. The first geometry produced for compression testing was made in accordance with ASTM D695 [3] which had a shape that resembled a dog-bone. The second geometry produced for compression testing was made in accordance with ASTM D695M [4] which was a straight sided specimen that had adhesively bonded tabs at the specimen ends. The following describes the construction of both test specimen geometries.

ASTM D695

To achieve the desired dog-bone geometry outlined by ASTM D695, an aluminum template was first constructed with a 4 axis Haas Mini Mill CNC Machine operated at WSUV. A computer model was established and integrated with G-Code software to accurately cut the desired shape at exact dimensions. The overall length of the dog bone template was 79.5 mm (3.13 in) with a gage section width of 12.7 mm (0.5 in) and an end width of 19.1 mm (0.75 in). A 38.1 mm (1.5 in) radius slowly guided the end width down to the gage section width. An illustration of this aluminum template can be seen in Figure 4.4-12.

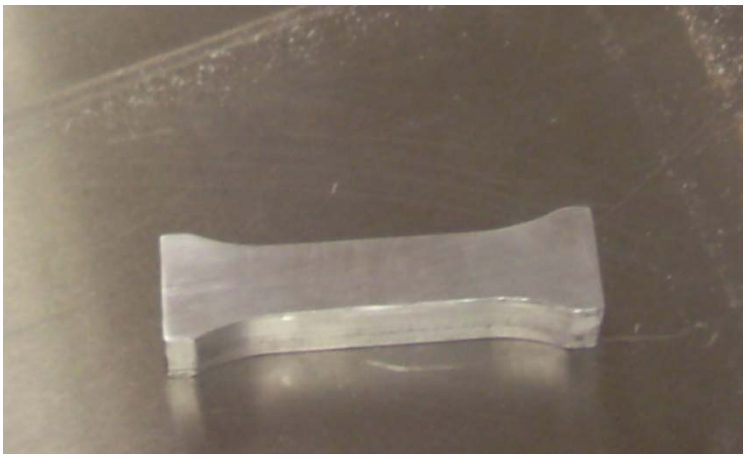

Fig 4.4-12: Dog-Bone Shaped Aluminum Template of Exact Dimension Specified by ASTM D695

This template would serve to cut each compressive coupon. Once the template was made, rectangular strips of each material system were cut using the previously purposed band saw to a width slightly larger than 19.1 mm (0.75 in) and a length slightly larger than 79.5 mm (3.13 in). An illustration of the prepared strip and the template can be seen in Figure 4.4-13.

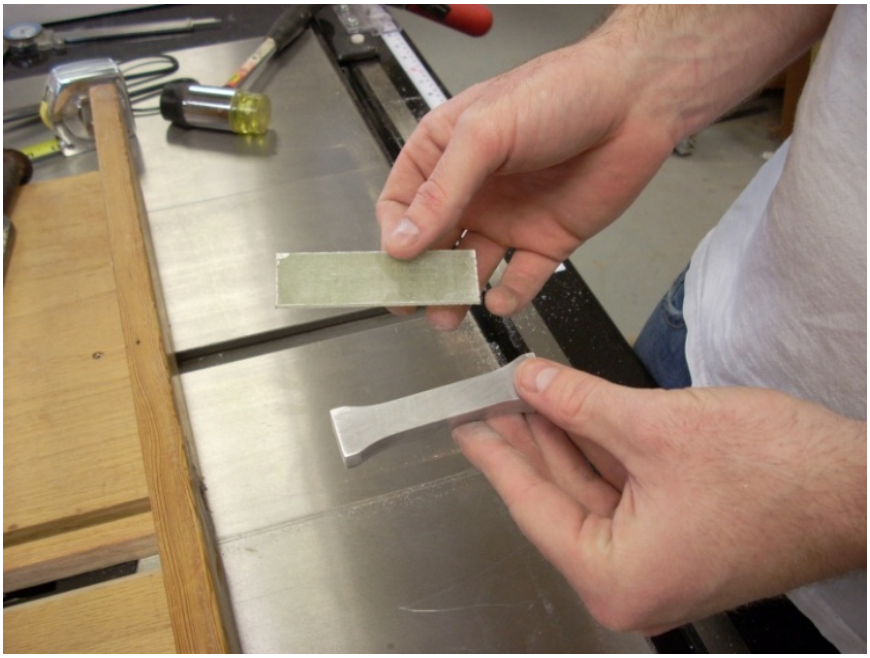

Fig 4.4-13: Prepared Compressive Strip Next to Compressive Template

The next step taken was to momentarily bond the prepared strip onto the aluminum template. This was done using Gerber Double Sided Router Tape that held the template onto the prepared composite strip for as long as needed. Removal could be done at any time. The double sided tape was first administered to the rectangular composite strip and firmly pressed in place. An illustration of this procedure can be seen in Figure 4.4-14.

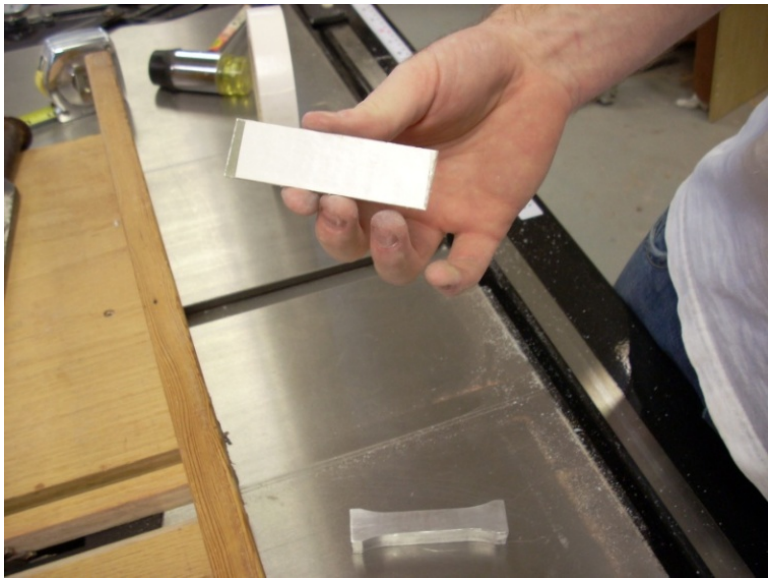

Fig 4.4-14: Double Sided Tape Applied to Prepared Composite Strip

Once the tape was secured to the prepared strip, the aluminum template could be secured to each individual rectangular strip. An illustration of this can be seen in Figure 4.4-15.

Fig 4.4-15: Aluminum Template Taped to a Prepared Composite Strip

Care was taken to overhang the prepared strip on all sides of the aluminum template so that the overall shape of the compression specimen could be eventually achieved. Once the template and the prepared strip were firmly, yet momentarily bonded together, they were taken to the previously purposed router that was configured with a secondary router bit. The bit used for cutting each of the ASTM D695 compressive specimens was a 2 fluted, ¼" carbide router bit instrumented with a guided bearing. The bearing was also ¼" in diameter and served to guide the bit around the aluminum template to eventually cut the rectangular strip into the shape of the template. For safety purposes, it is advised that some fixture be designed to keep the operator's fingers away from the spinning bit during operation. The template's geometry is small and requires close proximity to the operating bit. An illustration of a compressive coupon being constructed can be seen in Figure 4.4-16.

Fig 4.4-16: ASTM D695 Compressive Coupon Being Constructed with a Guided Router Bit

Once the overall shape is accomplished upon routing, the specimen can be removed from the template and stored for future testing. Since the shape of these specimens is relatively complex, the method of routing is a fairly cost effective way to construct each specimen. However, if numerous specimens are to be constructed, it is advised that multiple guided router bits be acquired before construction due to the abrasive nature of cutting composites. From experience, approximately 10 specimens can be prepared with a single 2 fluted, ¼ “ carbide router bit. A light sanding on the routed surfaces followed using 320 grit sandpaper. The final product, once removed from the aluminum template, can be seen in Figure 4.4-17.

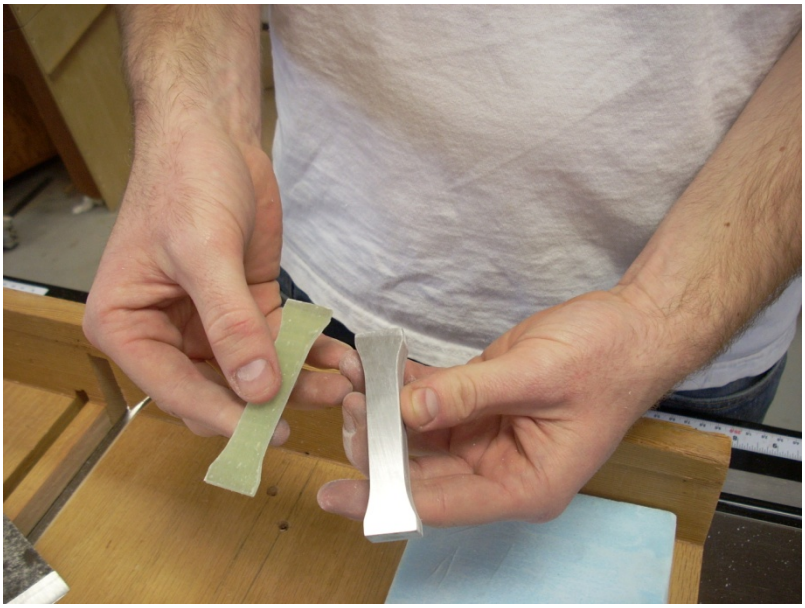

Fig 4.4-17: Final ASTM D695 Compressive Coupon Upon Removal from Aluminum Template

ASTM D695M

Compressive coupons in accordance with ASTM D695M were fabricated in similar fashion to that of the ASTM D695 compressive specimens. However, its geometry is entirely different. The ASTM D695M specimens are straight sided with a constant width of 12.7 mm (0.5 in) and a length of 80.1 mm (3.18 in). The ends of each specimen are tabbed, leaving a 5 mm (0.2 in) gage area. To achieve this sample geometry, a secondary aluminum template was constructed to have a width of 12.7 mm (0.5 in), and a length of 80.1 mm (3.18 in). The previously purposed router configuration with a 2 fluted, carbide ¼" guided router bit was used to take strips of composite material and cut out the desired shape of each specimen. All parameters for cutting the ASTM D695M compressive specimens were the same outlined for cutting the ASTM D695 specimens. Care was again taken to prepare composite strips slightly larger dimensions compared to the final dimensions of the specimen and to overhang the strips from the template on all sides. A light sanding followed on all machined surfaces using 320 grit sandpaper. An illustration of the aluminum template and achieved specimen geometry can be seen in Figure 4.4-18.

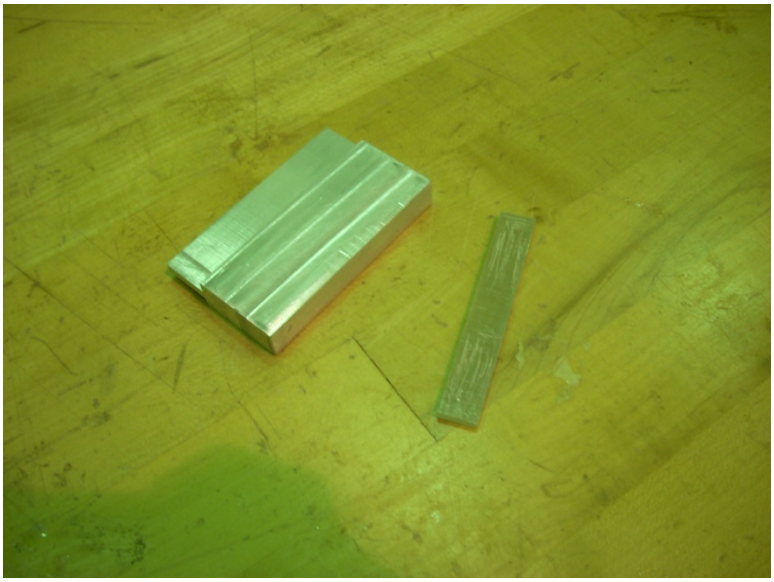

Fig 4.4-18: Aluminum Template and Compressive Specimen in Accordance with ASTM D695M

Once the overall shape was accomplished, each end of every compressive specimen had to be tabbed. The tabbing material was the same outline in the tensile specimen preparation section; however, a different tab geometry had to be achieved. Just like the tensile specimens, the width of each tab had to be the same width of the specimen; this was 12.7 mm (0.5 in). Also, since the untabbed gage section was purposed as 5 mm (0.2 in), each tab was made at a purposed length of 37.9 mm (1.49 in). Tabs were cut using the previously purposed band saw where the fence was set at an initial distance of 12.7 mm (0.5 in) from the blade. Once 12.7 mm (0.5 in) narrow pieces of tabbing material were cut out, the fence was again set at an approximate distance of 37.9 mm (1.49 in) from the blade. This final cut gave the exact dimensions needed for each individual tab. It should be noted that compressive tabs are not in need of a beveled region compared to the tensile tabs. It was determined that all compressive tabs were to be instrumented with square tab tip of 90 degrees. An illustration of the tabs used for compressive coupons and a tab schematic can be seen in Figures 4.4-19 and 4.4-20 respectively.

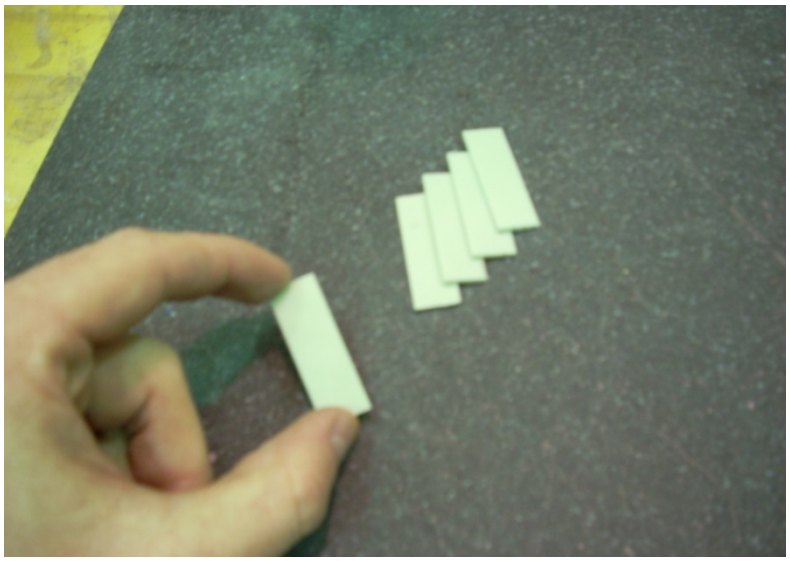

Fig 4.4-19: Constructed Compressive Tabs for ASTM D695M Coupons

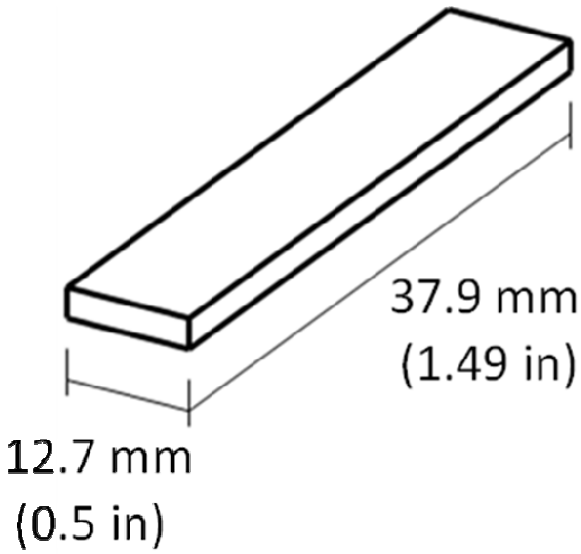

Fig 4.4-20: ASTM D695M Compressive Tab Schematic, mm (in)

Once the tabs were properly constructed, the challenge came to bond them to each compressive specimen while keeping an order of high alignment. In order to do this, a specialized fixture was fabricated. The fixture was made from ABS polymer acquired at WSUV and was cut using the previously purposed vertical mill and ½" HSS mill bit. The entire fixture was designed to have a constant width of 80.1 mm (3.18 in) and was arranged with straight, rectangular cross sectioned channels. Each channel was constructed to have a width of 12.7 mm (0.5 in) and a depth in accordance with the sum of thicknesses between two tabs and the prepared specimen. The channels would serve to orient the tabs and specimen in high alignment. Finally, a center channel approximately 5 mm (0.2 in) in width was cut longitudinally through the center of the fixture. This center channel would be instrumented with narrow pieces of aluminum designed to fit into the channel so that the compressive tabs would not come closer together than the aluminum pieces would allow. An illustration of this designed fixture can be seen in Figure 4.4-21.

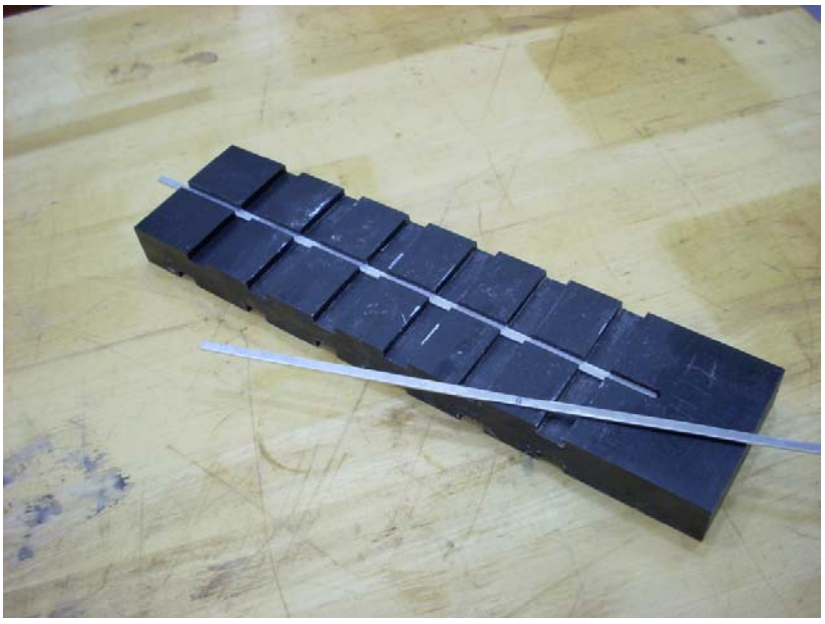

Fig 4.4-21: ASTM D695M Tabbing Fixture with Aluminum Tab Displacers

Before adhesion could take place, each bonding surface of each tab and specimen needed to be abraded in order to create a region of high surface area in which to bond the tabs to the specimen. This was done in the same fashion as the tensile coupons. The tip of a steel wood screw was used to gouge the ends of a specimen and one surface of a compressive tab. The same two part epoxy was again used as the adhesive for bonding the tabs to the specimen. Two tabs were first laid in a channel of the fixture with adhesive spread onto their roughened surfaces. More adhesive was spread on both ends of the compressive specimen and it was placed on top of the two base tabs. Finally, two more tabs were instrumented with epoxy and laid on the top ends of the specimen after being placed within the channel. To ensure a perfect gap between tabs, the two flat aluminum strips were guided down the center channel of the fixture. These aluminum strips were thinner in thickness compared to the tabs and served as a solid displacer for the tab ends to come into contact. This ensured an accurate displacement of 5 mm (0.2 in) between the tab ends, leaving an exposed gage area of each compressive specimen. It is important to note that excess adhesive is likely to bond, not only to the specimen and tabs, but also to the fixture. It is recommended that a finishing wax be spread throughout each channel so that bonding will only occur within the specimen, and not the fixture. The wax used for the construction of the below specimens was Behlen Blue Label Paste Wax. Step by step illustrations of the procedures for preparing the ASTM D695M compressive coupon can be seen in Figures 4.4-22, 4.4-23 and 4.4-24.

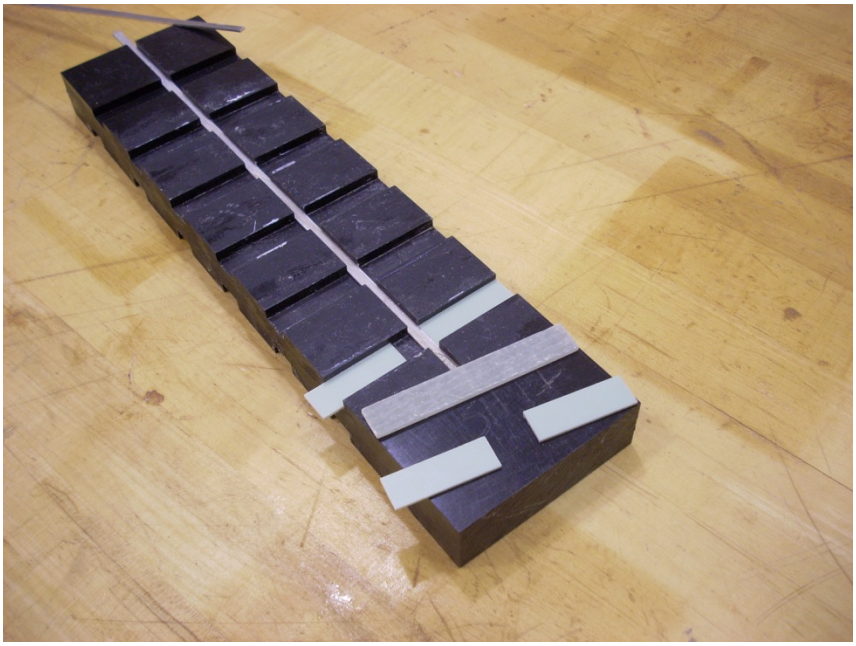

Fig 4.4-22: Insertion of Bottom Compressive Tabs in the Fixture's Channel, Tabs Coming into Contact with Aluminum Displacer

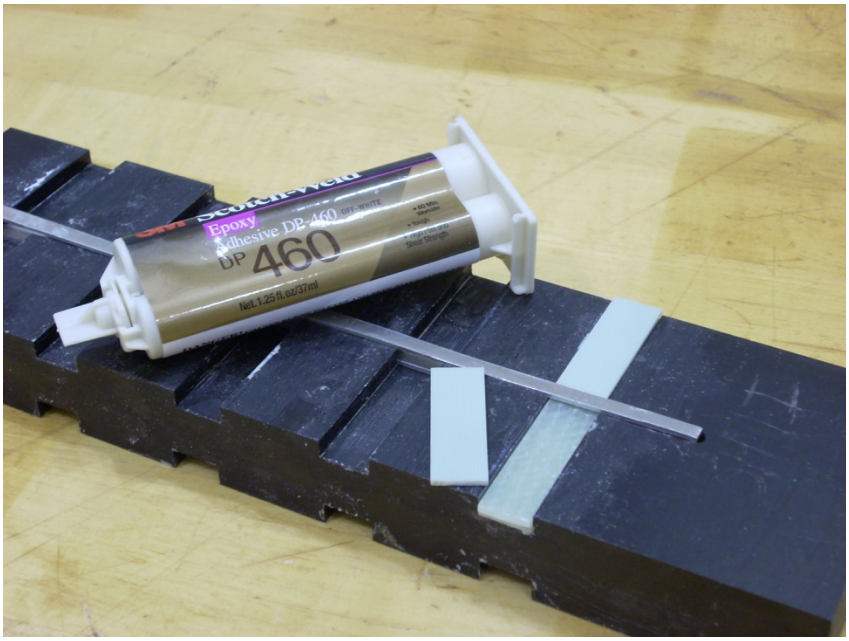

Fig 4.4-23: Specimen then Bonded on Top of Bottom Tabs and Top Tabs Being Inserted into the Fixture. The Secondary Aluminum Strip Acting as the Top Tab Displacer.

Fig 4.4-24: Overall Construction of ASTM D695M Compressive Specimens Bonded Together

Once the specimens were properly bonded with epoxy, they were left to cure overnight at ambient conditions. Examples of finalized compressive specimens for this standardized testing procedure can be seen in Figure 4.4-25.

Fig 4.4-25: Finalized ASTM D695M Compressive Test Specimens

4.5 Mechanical Testing of FRP Composite Materials

4.5.1 Tension Testing

Tensile properties such as tensile modulus, tensile strength, and Poisson's Ratio of flat composite laminates are determined by static tension tests in accordance with ASTM D3039 [2]. This test method determines the in-plane tensile properties of polymer matrix composite materials reinforced by high-modulus fibers. The following are guidelines and procedures that determine the tensile properties of a tested composite material.

Test Setup

Tensile testing of composite materials requires no fixture or jig to support the test coupon. A testing apparatus capable of firmly griping specimens while applying a steady pull rate is essential. Because the test specimens in tension have large gage sections with no interruption, extensometers are very acceptable for capturing strain readings while a load cell captures the force readings. An illustration of the true tensile test setup can be seen in Figure 4.5-1.

Fig 4.5-1: Tensile Test Setup, Extensometer Applied

Strain Rate and Measurement

In all cases, an adequate strain measurement device must be implemented for accurate data accumulation. The use of an extensometer shall satisfy this requirement by accordance with ASTM D3039. The extensometer needs to be free of inertia lag at the specified speed of testing and the weight of the device should not induce bending strains to cause premature failure. Every effort should be made to eliminate excess bending from the test system. The standard strain rate of the cross head during tensile testing should be 2 mm/min (0.05 in/min) [2]. All tension tests were administered at WSUV with an Instron mechanical tester, model 4482. Wedge operated grips were implemented as the holding mechanism.

4.5.2 Compression Testing

Compressive properties such as compressive modulus and compressive strength are determined by static compressive tests in accordance with ASTM D695 and D695M [3, 4]. These test methods determine the mechanical properties of unreinforced and reinforced rigid plastics, including high modulus composites, when loaded in compression at relatively low uniform rates of straining or loading. The following are guidelines and procedures that determine the compressive properties of a tested composite material.

Test Setup

It is well known that compressive properties of composite materials are difficult to measure due to a sidewise buckling effect from the specimen [12]. In order to properly test a composite material in compression, this buckling effect must be eliminated from testing if adequate compressive results are to be obtained. Therefore, the use of both ASTM D695 and ASTM D695M test methods require a supporting jig that enables pure axial loading and eliminates sample buckling. See Figure 4.5-2.

Fig 4.5-2: ASTM D695 & D695M Supporting Jig Test Fixture

The supporting jig is constructed of two “I” beams with machined grooves that sandwich the compressive specimen while being bolted to an “L” bracket to hold the specimen in near perfect verticality. The “I” beams serve as the anti-buckling fixture, while the “L” bracket serves to hold the specimen in a vertical position. Dimensions for the “I’ beam design are located in ASTM D695. The specimen is then end loaded to perform the test. An illustration of the compressive test setup can be seen in Figure 4.5-3.

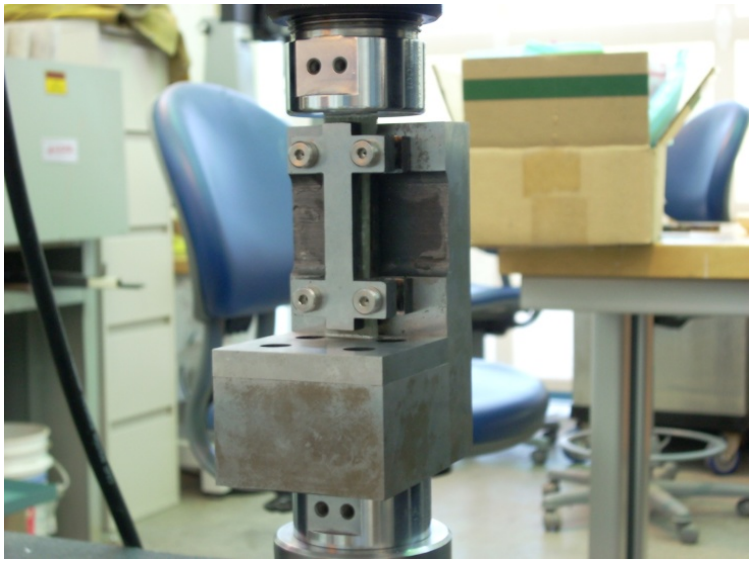

Fig 4.5-3: Compressive Test Setup with Supporting Jig

Strain Rate and Measurement

To accumulate accurate data, adequate strain measurement devices must be implemented in order to correctly measure desired mechanical properties. However, this has been shown to be difficult when measuring properties of composites in compression. A major disadvantage to the ASTM D695(M) testing methods is that their gage sections are very small and promote difficulty for practical uses of a strain measuring devices, even for small strain gages [30]. Also, the testing fixture covers the majority of the specimen during testing, adding to the difficulty. To account for this difficulty, a rectangular groove was cut in the center of one of the compressive fixture's I beams to give room for an applied strain gage. Fixtures that were available for purchase also came equipped with this groove feature and were the reason for its application. Loading of the specimen shall be tested at a standard cross head speed of 1.3 +/- 0.3 mm/min (0.05 +/- 0.01 in/min) [3]. All compression tests were administered at WSUV with an Instron mechanical tester, model 4482. Flat platens were installed as the compressive mechanism for testing.

4.5.3 Ignition Loss Testing (Burn Test)

Material properties such as resin and fiber content within fiber reinforced polymer composites can be determined by ignition loss testing in accordance with ASTM D2584 [5]. The following are the guidelines and procedures necessary to successfully perform this test. Details are also given in order to acquire specific material property values.

Test Setup

The basis for performing this test is to simply burn off the cured resin from the reinforcing fibers. In order to do this, a high temperature furnace capable of maintaining its thermal loading is essential. The prepared specimen must first be weighed to the nearest thousandth of a gram and its dimension must be accurately measured to find its total volume. The specimen will then be placed in a crucible that has been previously heated to evaporate any influence of saturated humidity and has also been weighed to the nearest thousandth of a gram. The combination of the crucible and specimen is then placed in the furnace set at approximately 565 C (1050 F) and left to burn for about an hour. Once the resin is burned from the specimen, the remnants of fiber within the crucible will finally be weighed once more to establish the weight of fiber within the specimen. All ignition loss tests were administered at WSUV with a 1200 C max (2200 F) Lucifer Furnace, model number RD7-H21, set at 565 C (1050 F).

Measured Properties

This testing procedure outlines descriptive material properties within FRP composites. The following are descriptions and equations of specific properties found by using this testing method.

Nomenclature:

F_{wt} : weight of exposed fibers (g)
$F_{wt}\%$: fiber weight percent
$R_{wt}\%$: resin weight percent
T_{wt}: measured total specimen weight (g)
ρ_{fiber} : fiber density (g/cc)
ρ_{resin} : resin density (g/cc)
$F_{vol}\%$: fiber volume percent
$R_{vol}\%$: resin volume percent
T_{vol} : measured total specimen volume (cc)
$V_{vol}\%$: void volume percent
E_c: composite elastic modulus
E_f: elastic modulus of fiber
E_m: elastic modulus of matrix

1) *Rule of Mixture*: Under the iso-strain condition, the elastic modulus of a composite follows the rule of mixtures equation:

$$E_c = f_{vol}\% * E_f + (1 - f_{vol}\%) * E_m$$

2) *Fiber Weight %*: The fiber weight % is the weight percentage of fibers within a composite laminate. It is found by the following equation:

$$F_{wt}\% = \frac{F_{wt}}{T_{wt}} * 100$$

3) *Resin Weight %*: The resin (matrix) weight % is the weight percentage of resin/matrix within a composite laminate. It is found by the following equation:

$$R_{wt}\% = \left[\frac{(T_{wt} - F_{wt})}{T_{wt}}\right] * 100$$

4) *Fiber Volume %*: The fiber volume % is the volume percentage of fibers within a composite laminate. It is found by using the following equation:

$$F_{vol}\% = \left[\frac{\left(\frac{F_{wt}}{\rho_{fiber}}\right)}{T_{vol}}\right] * 100$$

5) *Resin Volume %*: The resin/matrix volume % is the volume percentage of resin/matrix within a composite laminate. It is found by using the following equation:

$$R_{vol}\% = \left[\frac{\left(\frac{T_{wt} - F_{wt}}{\rho_{resin}}\right)}{T_{vol}}\right] * 100$$

6) *Void Volume %*: The void volume % described the void content with a composite laminate. The value of void content can be found by the following equation:

$$V_{vol}\% = \left[1 - \frac{\left(\frac{F_{wt}}{\rho_{fiber}}\right) + \left(\frac{T_{wt} \quad F_{wt}}{\rho_{resin}}\right)}{T_{vol}}\right] * 100$$

CHAPTER FIVE

RESULTS AND DISCUSSION

5.1 Composite Fabrication Process and its Influence on Mechanical Properties

The effect of fabrication procedure on the mechanical properties of composite materials was investigated by several testing methods. Compression, tension and ignition loss tests were carried out on specific composite materials to gage their results. The materials tested for this research were the Inner Laminate Hull Side (ILHS), Vacuum Infusion Medium (VIM), and WSUV Hand Lay-Up (MHL) panels. The reason for choosing these specific materials was their similarity to one another. All three panels were made from the same fiber type, layer count, fiber orientation, and resin type, but were fabricated under different conditions. The MHL panel was manufactured under ambient conditions based on the fabrication procedure for the hand lay-up (HL) method. Then, both the VIM and ILHS panels were manufactured under the same manufacturing method, vacuum infusion (VI), but at separate vacuum pressures. The VIM panel was fabricated under a vacuum pressure of 20 in. Hg, while the ILHS panel was fabricated under a vacuum pressure of 28 in. Hg. Therefore, when comparing the three, all were constructed in the same manor except for their vacuum pressure, with the MHL panel being at 0 in. Hg (ambient pressure), the VIM panel at 20 in. Hg, and the ILHS panel at 28 in. Hg. Mechanical testing was then performed on all three to find resultant trends that relate to the pressure applied during fabrication. It is worthy to note that an increase in mechanical properties of any material is a favorable result. An increase in ultimate strength is beneficial due to a material's ability to withstand more load per unit area until failure. Also, an increase in elastic modulus is also beneficial because it insinuates that a material has a higher resistance to deformation. All supplied error bars for all results are an indication of one standard deviation from the mean. These are the foundations for which to base the acquired results.

5.1.1 Tension Tests

Static tension tests were conducted to investigate the performance of the three reviewed composite panels. Standard tensile stress-strain diagrams for 5 prepared tensile specimens can be seen from each individual panel type. The three most noteworthy variables monitored from tensile testing were the tensile elastic modulus, the ultimate tensile strength, and the maximum percentage strain at failure. Figures 5.1-1 shows the tensile stress-strain diagrams for the MHL panel, while Figures 5.1-2 and 5.1-3 show the tensile stress-strain diagrams for the VIM and ILHS panels respectively. Averages of each property are located adjacent to each diagram.

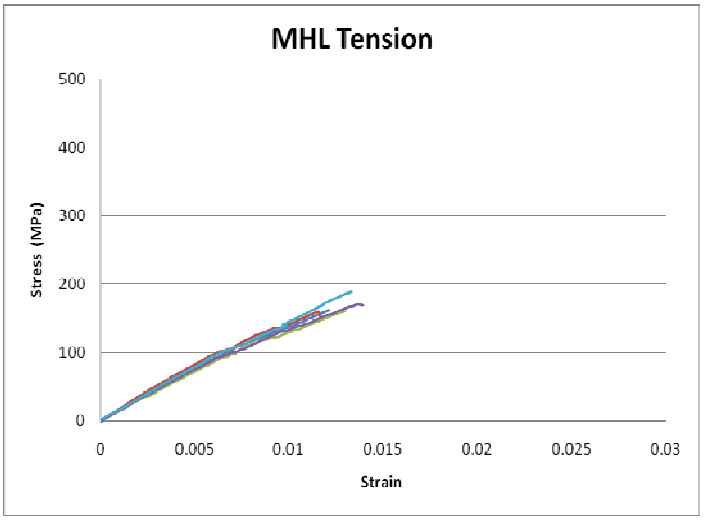

MHL Averages	
UTS (MPa)	168.73
Max % Strain	1.279
Modulus (GPa)	16.03

Fig 5.1-1: Tensile Stress-Strain Diagrams for 5 Tested MHL Specimens

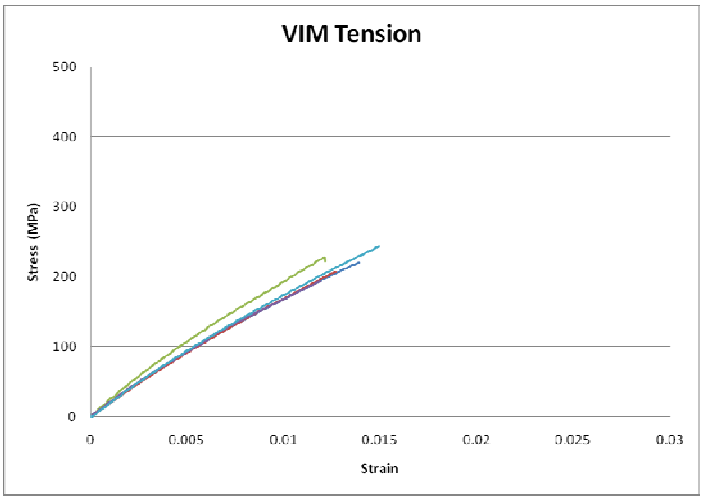

VIM Averages	
UTS (MPa)	218.58
Max % Strain	1.310
Modulus (GPa)	19.89

Fig 5.1-2: Tensile Stress-Strain Diagrams for 5 Tested VIM Specimens

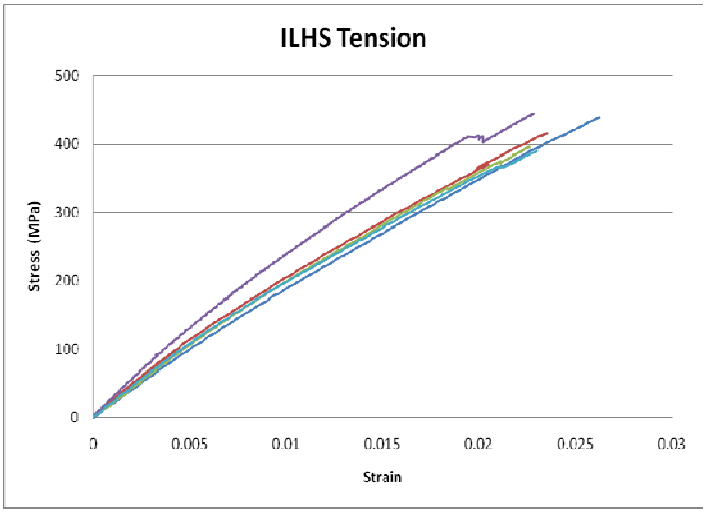

ILHS Averages	
UTS (MPa)	416.79
Max % Strain	2.363
Modulus (GPa)	22.42

Fig 5.1-3: Tensile Stress-Strain Diagrams for 5 Tested ILHS Specimens

5.1.2 Compression Tests

Static compression tests were administered to all reviewed composite panels for this research. Standard compressive stress-strain diagrams were acquired from each individual panel after testing 5 specimens in accordance with ASTM D695. The three most noteworthy variables monitored from compressive testing were the compressive elastic modulus, the ultimate compressive strength, and the maximum percentage strain at failure. 350 Ohm, 5 mm grid strain gages were implemented as a direct way to measure strain from the specimen. Figure 5.1-4 shows the compressive stress-strain diagrams for the MHL panel, while figures 5.1-5 and 5.1-6 show the compressive stress-strain diagrams for the VIM and ILHS panels respectively. Averages of each variable are located adjacent to each diagram.

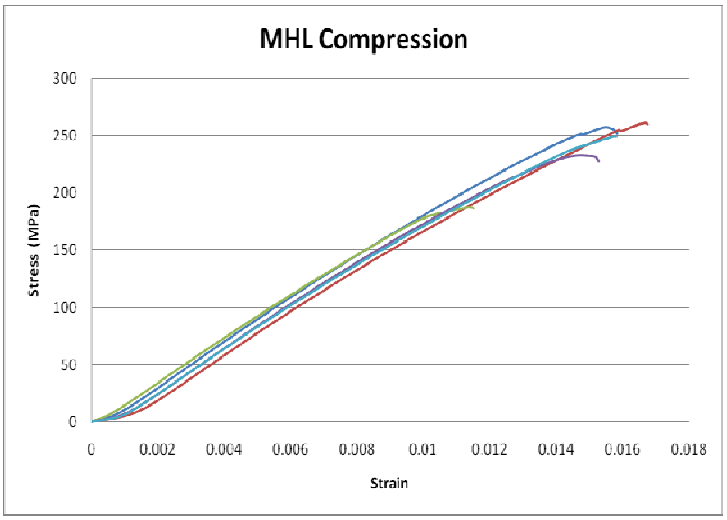

MHL Averages	
UCS (MPa)	237.62
Max % Strain	1.503
Modulus (GPa)	18.03

Fig 5.1-4: Compressive Stress-Strain Diagrams for 5 Tested MHL Specimens

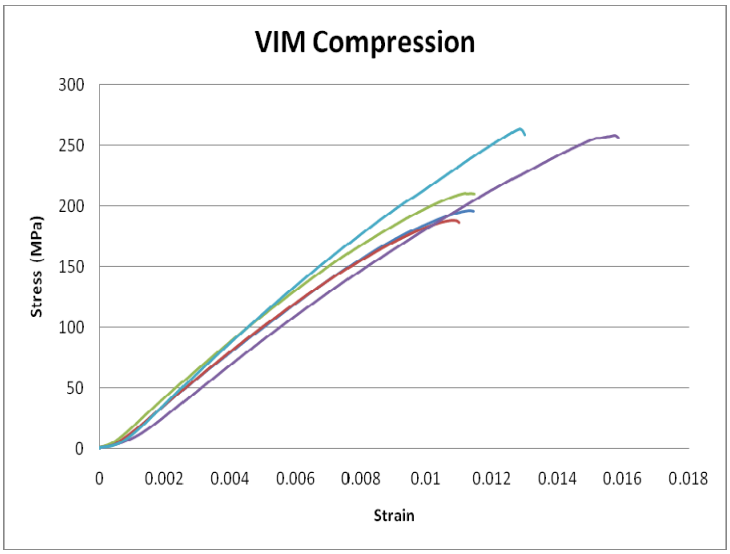

VIM Averages	
UCS (MPa)	223.46
Max % Strain	1.254
Modulus (GPa)	21.62

Fig 5.1-5: Compressive Stress-Strain Diagrams for 5 Tested VIM Specimens

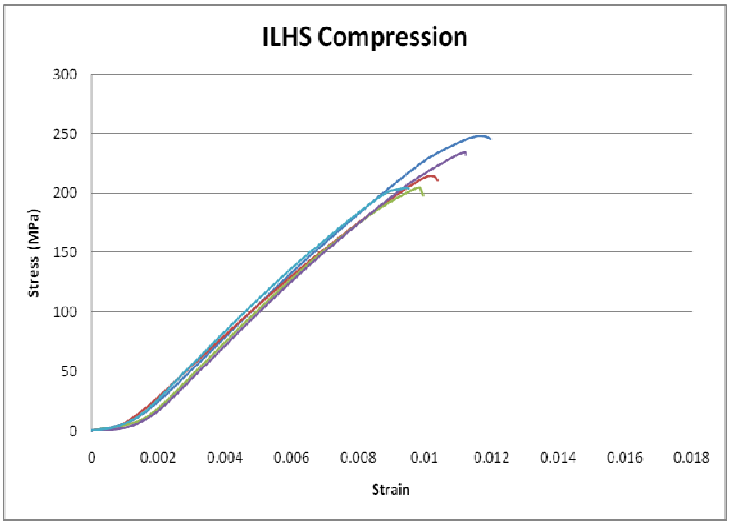

ILHS Averages	
UCS (MPa)	221.23
Max % Strain	1.060
Modulus (GPa)	25.81

Fig 5.1-6: Compressive Stress-Strain Diagrams for 5 Tested ILHS Specimens

5.1.3 Ignition Loss Tests

Ignition loss tests were also performed on all mechanically tested composite specimens for this study. By essentially burning off the resin from the reinforcing glass fibers, important material properties such as fiber weight percent, resin weight percent, sample density, and percentage void content could be established for all reviewed panels. Five specimens were prepared from each panel in this testing procedure. Table 5.1-1 gives the average weight properties found using this test method while Figure 5.1-7 gives the average volume properties.

	MHL	VIM	ILHS
Fiber Wt %	53.65	68.95	70.71
Matrix Wt %	46.35	31.05	29.29
Density (g/cc)	1.529	1.766	1.812

Table 5.1-1: Weight % Comparison of MHL, VIM, and ILHS Panels

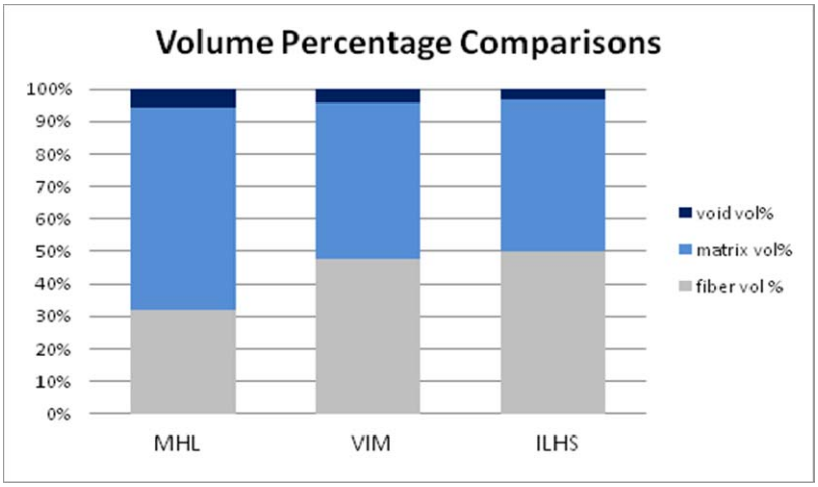

Fig 5.1-7: Volume % Comparisons of MHL, VIM, ILHS Panels

5.1.4 Analysis and Trends

Based on the acquired data, some important relationships can be based from the testing results. It can be seen from figure 5.1-8 that as vacuum pressure during fabrication increases, the amount of voids within each panel decreases. A 42% void reduction was seen from fabrication at ambient conditions compared to using a 28 in. Hg vacuum pressure and progressed at a fairly linear rate. This trend shows that void content is a function of vacuum pressure. However, it is expected that if the vacuum pressure were to continue to increase, this trend would become non-linear, and level off at a lower minimum value. This value is the threshold where voids are essentially minimized and no increase in pressure would do any justice.

This decrease in void content would also lead to an increase in sample density. From this observed extraction, maximum densities could be reached due to the void free material. From Figure 5.1-9, the sample density from the lowest pressure to the highest experienced an 18.5% increase. This trend was found to be non-linear and as vacuum pressure increases, sample densities are maximized.

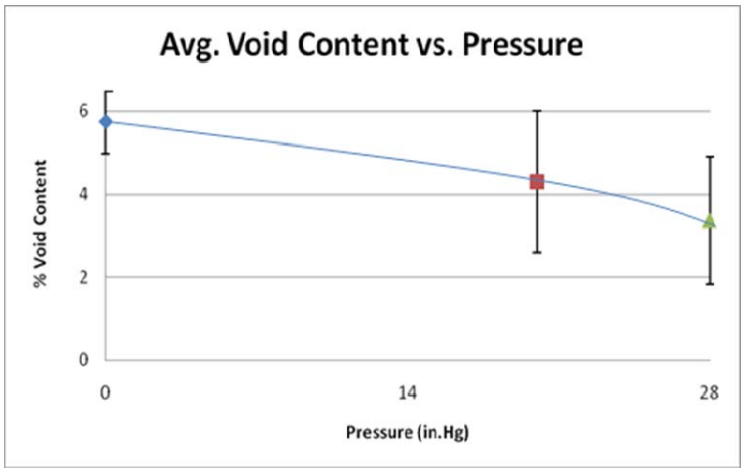

Fig 5.1-8: Average % Void Content vs. Vacuum Pressure

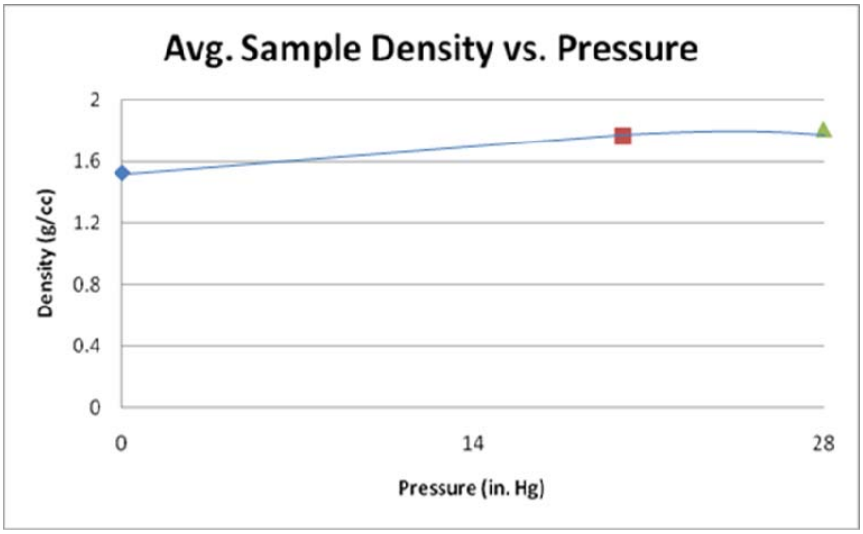

Fig 5.1-9: Average Sample Density vs. Vacuum Pressure

Also, as vacuum pressure increased during fabrication, the fiber weight percentage was also found to increase. This would then lead to a decrease in resin (matrix) weight percentage. This was experienced due to squeezing effect from the negative pressure exerted by the vacuum. As the vacuum compressed against the prepared laminate, the layers of fiber remained intact, but a reduction in resin was experienced, leaving a thinner cured laminate. By keeping the same amount of fibers and reducing the overall laminate volume, this would then lead to an increasing in fiber weight percentage. From the results, a 17% increase in fiber weight percentage was experienced. Figures 5.1-10 and 5.1-11 show the trends of fiber and resin weight percent over increasing vacuum pressure.

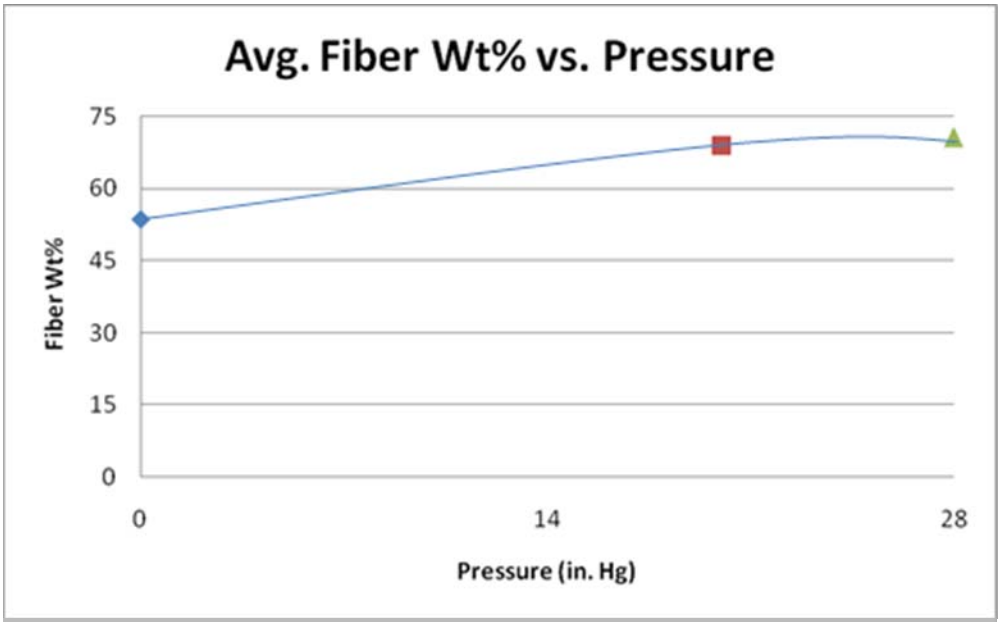

Fig 5.1-10: Average Fiber Weight Percentage vs. Vacuum Pressure

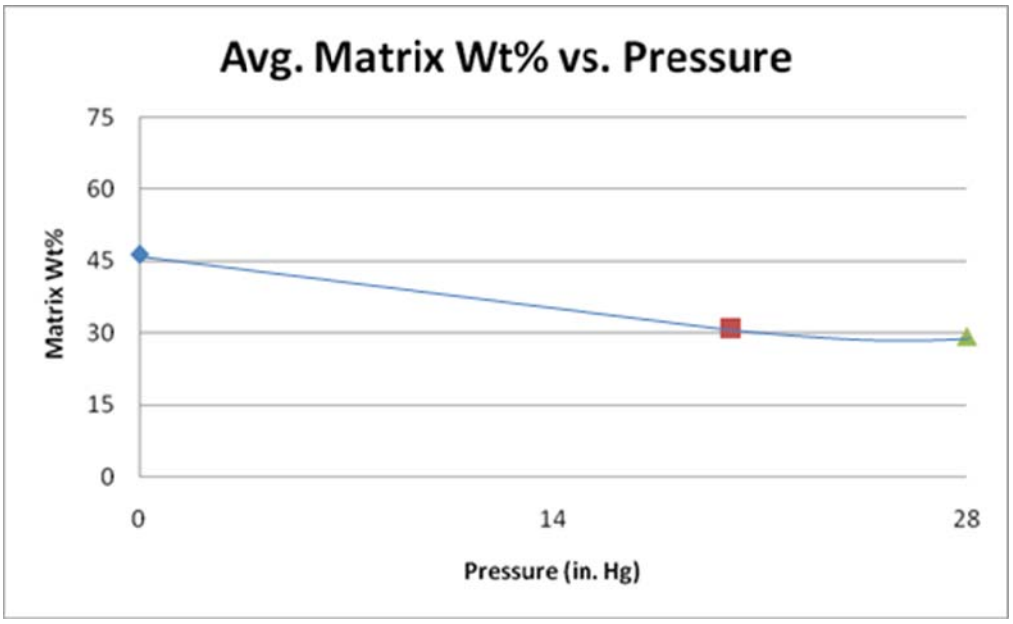

Fig 5.1-11: Average Matrix Weight Percentage vs. Vacuum Pressure

Altering the fabrication pressure also had its effect on the measured tensile and compressive mechanical properties. Over the three samples tested, an increase in tensile modulus and ultimate strength was oberserved with increasing vacuum pressure. A 248.1 MPa or 147% increase ultimate tensile strength was seen from the MHL samples to the ILHS samples. Also, over the range of samples tested, a 6.39 GPa or 39% increase in tensile modulus was observed. Figures 5.1-12 and 5.1-13 show these trends of UTS and tensile modulus with increasing vacuum pressure, respectively.

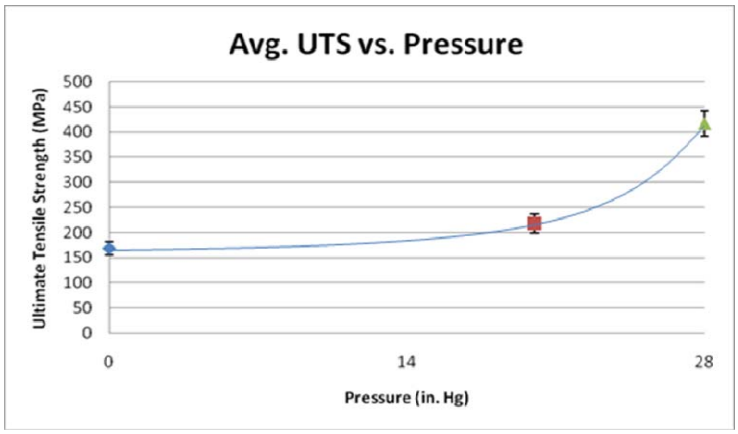

Fig 5.1-12: Average Ultimate Tensile Strength vs. Vacuum Pressure

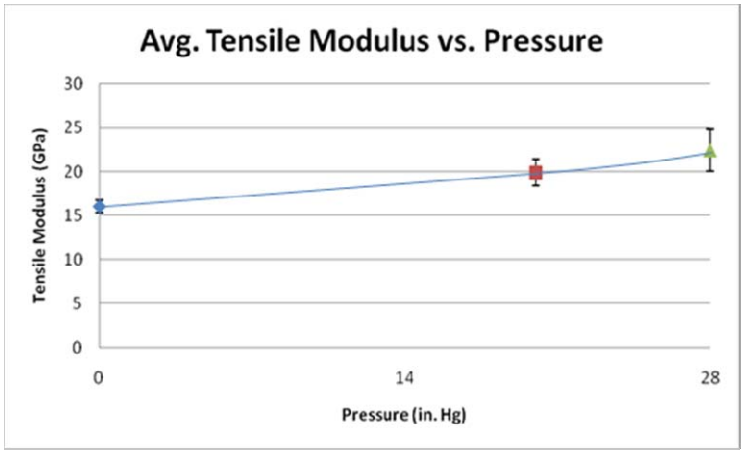

Fig 5.1-13: Average Tensile Modulus vs. Vacuum Pressure

The extraction of voids can attribute to the increasing trends of tensile modulus and strength. This is due to the fact that voids are known to accelerate the failure of composites under tension due to the debonding of broken fibers from the surronding matrix material. If porous cavities are left at the fiber/matrix interface, the shear strength exerted by the surrounding matrix on the fiber is severely diminished. As a result, the effectiveness of the fiber is reduced. Also, voids initiate matrix cracking due to localized stress concentrations. As a result, the matrix material can become separated from the fibers, weakening the entire structure [12]. Figure 5.1-14 shows photographs taken of actual voided regions within the MHL composite panel.

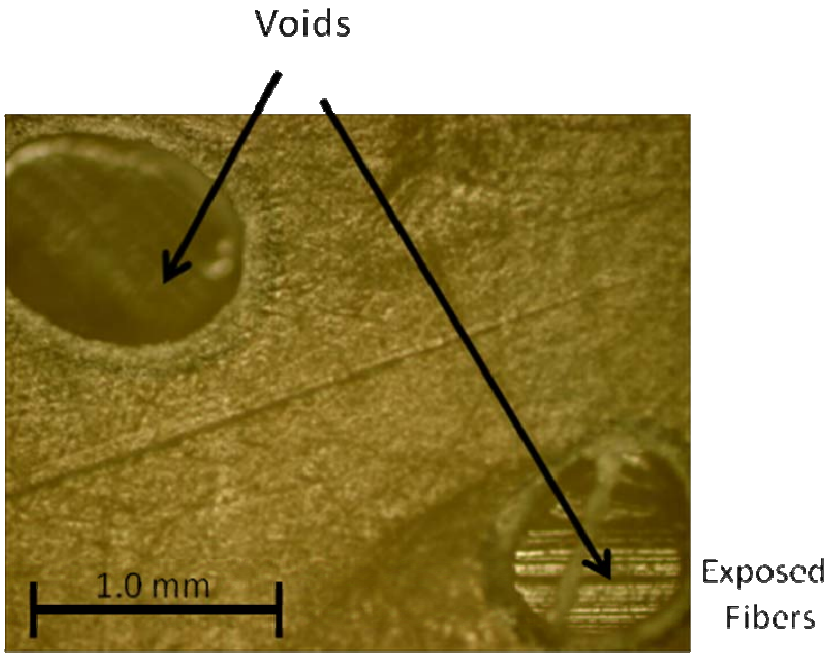

Fig 5.1-14: Voided Regions Within the MHL Panel

It can actually be seen in one of the voided regions that the cavity penetrates to the first layer of fiber. By not having surrounding matrix on this portion of fiber, the interfacial strength between fiber and matrix is essentially non-existant. Hence, this exposure can severly degrade the mechanical ability of a composite material.

The failure modes described above can be seen when taking a look at the failed MHL tensile specimen surface. A failed MHL specimen and enlarge view of the failed edge can be seen in Figure 5.1-15. By looking at the photos taken, it is apparent that micro-cracks have initiated failure within the MHL specimen. The cracking matrix across the width of the specimen weakened the structure of the matrix, with the fibers soon to follow. The fibers are not pulled from the matrix as much as they are broken across the plane of cracking. With the ILHS specimen, fibers were extracted deep within the structure. As seen in Figure 5.1-16, the ILHS specimen appears ruptured, with fibers being extrated deep within the matrix. It is believed that this is where the fibers were at their weakest, and eventually were pulled from that point. Unlike the MHL specimen, which had fibers that mostly failed across the cracked edge.

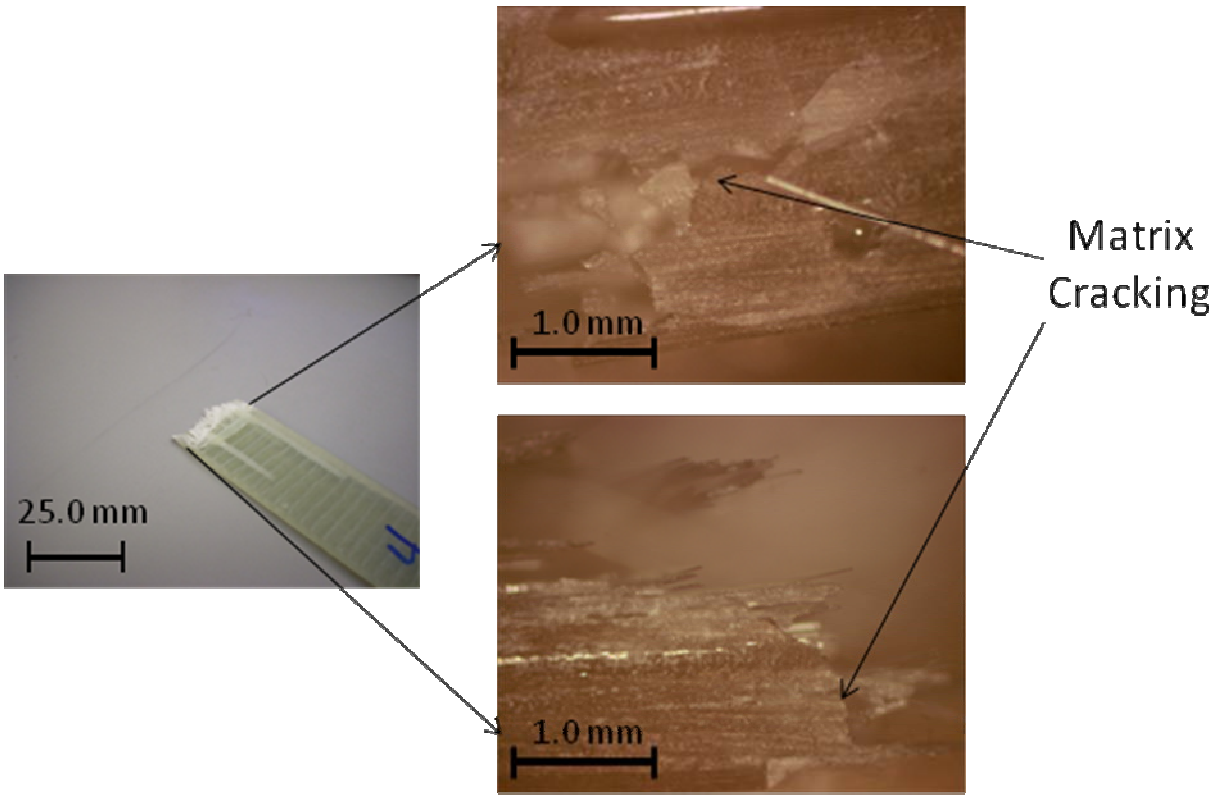

Fig 5.1-15: Failed MHL Specimen and Enlarged Veiws of the Failed Edge

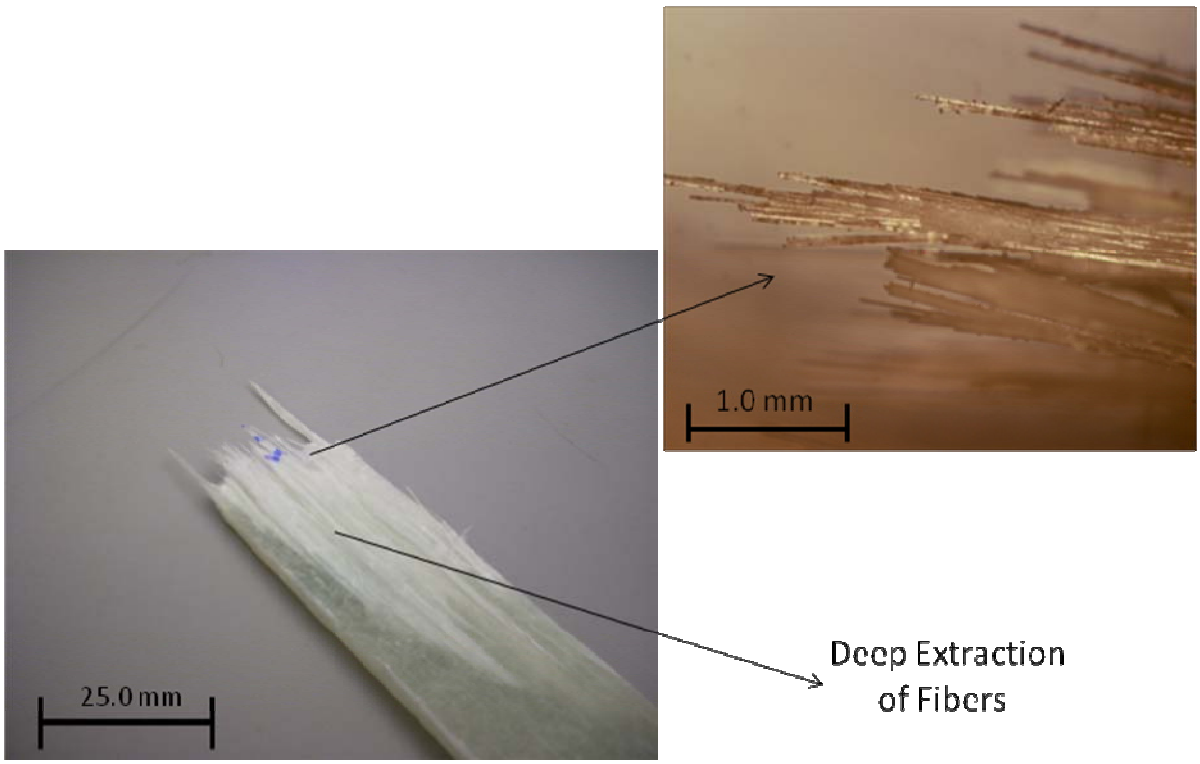

Fig 5.1-16: Failed ILHS Specimen with Enlaged View of Failed Fibers

When taking a deeper look at failed tensile specimens, further evidence of void induced failure can be seen. Weak interfacial strength is a result of excess void concentrations. Figures 5.1-17 and 5.1-18 show two individual strands of fiber from both the MHL and ILHS specimens after tensile failure. It can be seen from the two photographs that matrix material still exists on the ILHS fiber and not on the MHL fiber. The fact that matrix material still clings to individual strands of ILHS fibers even after failure suggests that the interfacial shear strength between fiber and matrix is exceptionally high. Higher interfacial bonding between fiber and matrix will improve the ability of a composite material to undergo loading. Hence giving it superior mechanical properties. The opposite is seen with the MHL specimen. By having relatively no matrix material left behind compared to the ILHS specimen indicates lower interfacial strength between fiber and matrix. When there is lower interfacial strength, a broken fiber will simply slip

away from the surrounding matrix. Hence, extra load will not be carried by the fiber/matrix interface and failure will happen at lower load intervals. Overly voided regions within the material are the purposed cause of this, again showing the relationship that an increase in void volume percentage leads to a decrease in mechanical properties.

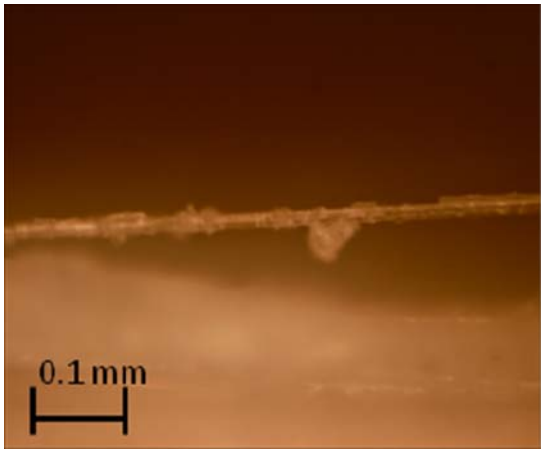

Fig 5.1-17: Failed Tensile Fiber, ILHS

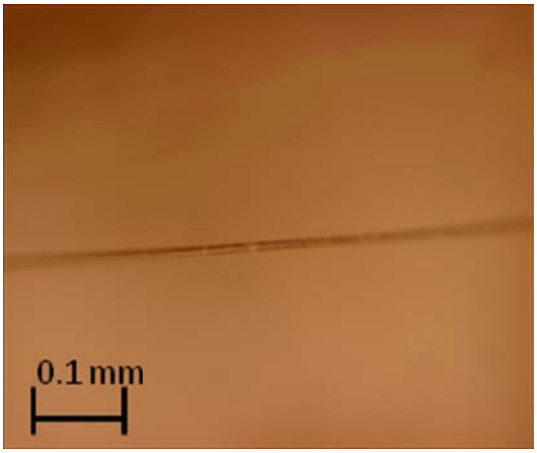

Fig 5.1-18: Failed Tensile Fiber, MHL

As vacuum pressure during fabrication was allowed to increase, an increase in measured compressive modulus was experienced. Over the range of tested vacuum pressures, a 7.78 GPa or 43% increase in compressive modulus was observed. This increasing relationship was seen in both tension and compression. However, the same trend was not experienced when comparing the ultimate strengths in compression. Ultimate compressive strengths were found level off with applied vacuum pressure. No substantial change was experienced over the range of tested pressures, which was dissimilar to the results taken under tension. Figures 5.1-19 and 5.1-20 show the trending results for compressive strength and compressive modulus vs. vacuum pressure, respectively.

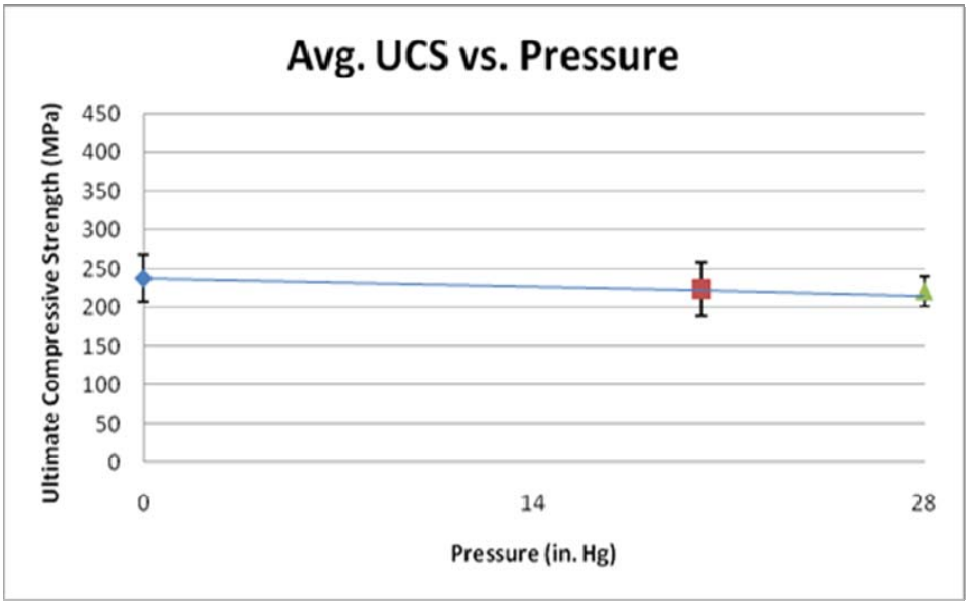

Fig 5.1-19: Average Ultimate Compressive Strength vs. Vacuum Pressure

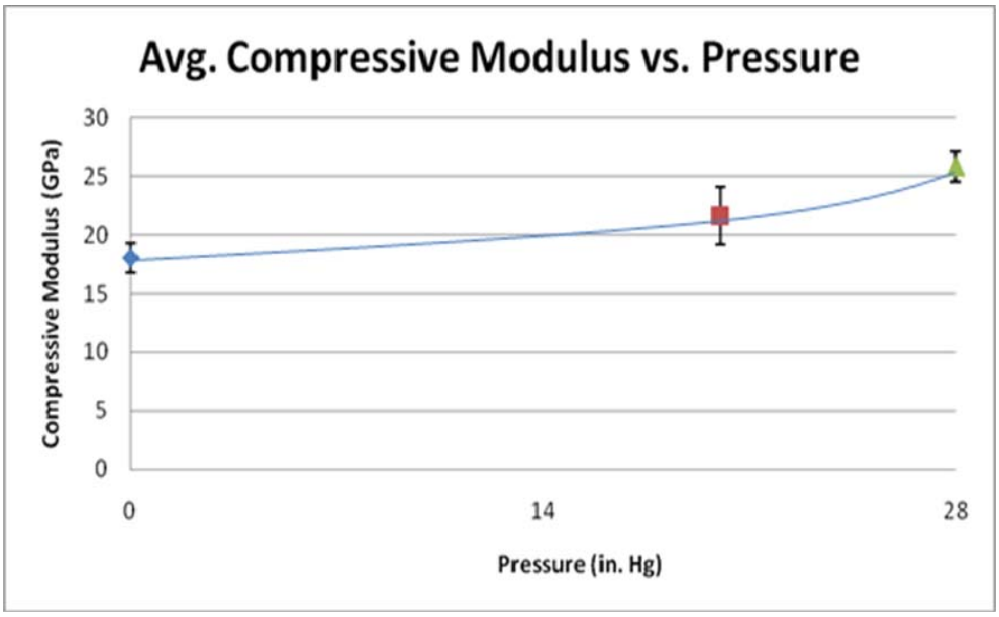

Fig 5.1-20: Average Compressive Modulus vs. Vacuum Pressure

The flat trend of ultimate compressive strength indicates that vacuum pressure and void content seem to have no significant affect on the compressive load bearing capabilities of each composite panel. This was not expected out of the measured results. A possibility for this occurrence is the fact that since there was no vacuum pressure applied to the MHL panel, the squeezing effect from the vacuum never took place, creating a thicker sample. This increase in thickness may have distributed the load better across the top end surface of the compressive specimen compared to the vacuum infused samples, and allowed more load to be carried before failure. This conclusion is very odd due to the nature in which the MHL material failed under compression and basically insists that compressive strength may be a function of top end surface area. This is not covered in this study and may need to be investigated further. However, this increase is vacuum pressure does increase the capability of a material to withstand deformation, hence the increase in compressive modulus values. This is likely from a decrease in void percentage which will strengthen the fiber/matrix interface. A weaker interface, however, initiates delamination, which is the separation of layers within a laminate [14]. As a result, premature failure modes may be seen, which cause mechanical property values to diminish. Proper failure within the gage region will likely be seen from modes such as fiber kinking and micro-buckling [12], where not only the matrix material is seen to fracture, but so do the fibers. When taking a look at the MHL and ILHS compressive specimens after failure, these phenomena are seen to exist. Figures 5.1-21 and 5.1-22 show failed compressive MHL and ILHS specimens, respectively.

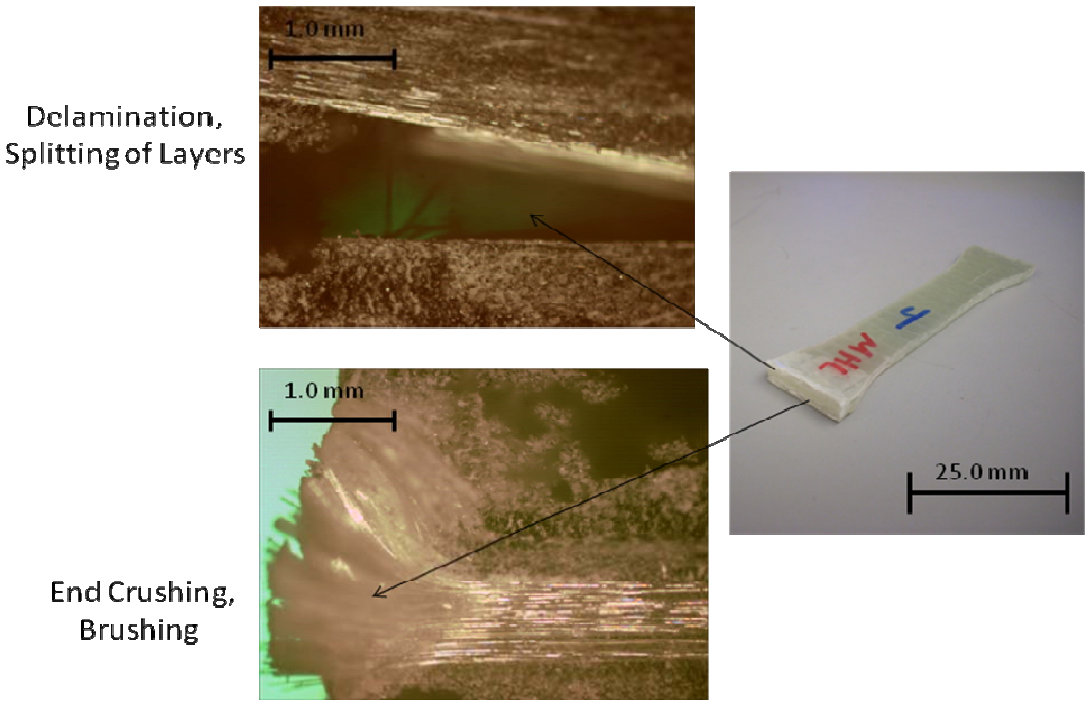

Fig 5.1-21: Failed MHL Compressive Specimen with Enlarged Views of End Failure

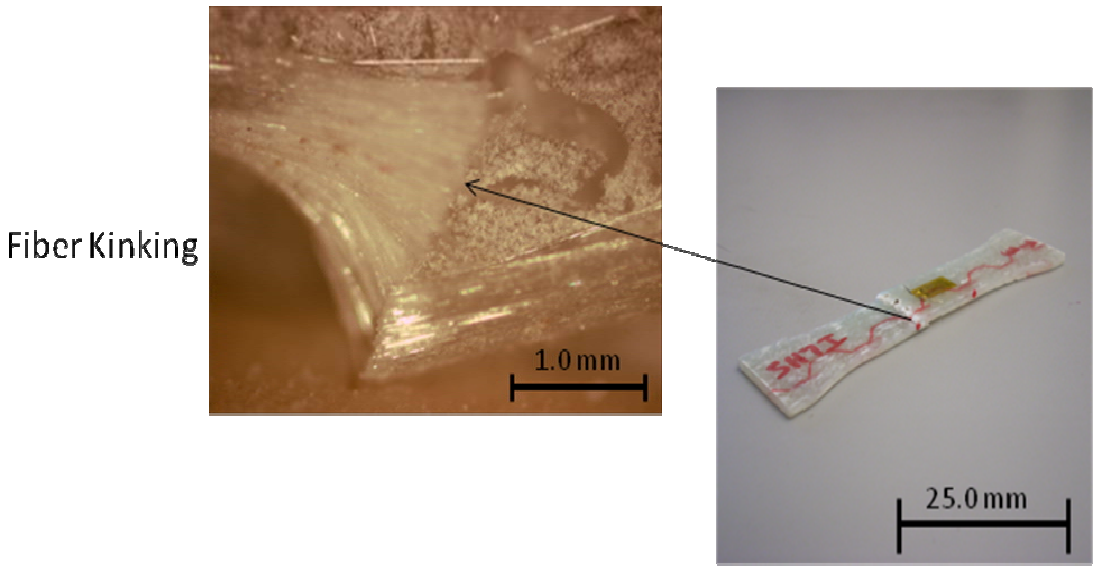

Fig 5.1-22: Failed ILHS Compressive Specimen with Enlarged View of Gage Failure

Failure within the ILHS specimens under compression is seen to take place in the gage section, where failure is supposed to occur. This was not seen within the MHL samples. All the MHL specimens failed at the top end surface where loading was applied. As can be seen in the above figure, the MHL gage section is completely unharmed and the top surface is crushed. This type of failure has been seen by previous researchers [22, 28, 30] which is referred to as end crushing, or brushing. When a deeper look was taken at the failed MHL specimen end, the phenomenon of delamination was confirmed. Layers of fiber were separated from the matrix material, and fiber tows were not fractured. Instead fiber tows were frayed, leaving them intact but separated. This is likely where the term brushing was established. In the ILHS specimen, fiber tows were seen to kink at the point of failure. This mode of failure does not leave the fibers intact, but rather fractures them at an angle. This was not caused by a delaminating specimen and suggests that the fiber/matrix interface was strong at the point of failure. The fact that these failure modes distinguish the two samples suggests further that void content will diminish the mechanical properties of a composite material.

5.2 Laminate Type and Lay-Up Sequence

To study the effect of laminate type and lay-up sequence, panels CHL, ILHS, ILHB, ILHB2, OLHS and OLHB were chosen to compare results. First, to study the effect of lay-up sequence, panels ILHS, ILHB, and ILHB2 were chosen as the comparative laminates due to the fact that all were made from common materials and under the same manufacturing conditions, but with different amounts of fiber sheet layers. The ILHS panel was constructed with 2 sheets of 1.5 oz. mat/0/90 fiber, the ILHB panel was constructed with 3 sheets of 1.5 oz. mat/0/90 fiber, and finally, the ILHB2 panel was constructed with 4 sheets of 1.5 oz. mat/0/90 fiber. The vacuum infusion (VI) process was applied to all three laminates under the same fabrication pressure. Resin type, fiber type, and fiber orientation was the same through all the respective panels. Mechanical testing was then performed on all three to find resultant trends that relate lay-up sequence to the measured mechanical properties.

Secondly, to study the effect of laminate type on mechanical properties, panels CHL, OLHS, OLHB, and ILHB2 were chosen to base comparisons due to the manner in which they are constructed. The CHL panel is purely a hand lay-up (HL) manufactured laminate having been constructed with four sheets of reinforcing E-glass fiber. The ILHB2 panel is purely a vacuum infusion (VI) manufactured laminate having also been constructed with four sheets of reinforcing E-glass fiber. The interesting aspect about this comparison comes from the OLHS and OLHB panels. Both are manufactured by two separate fabrication methods. Half of each laminate is manufactured by the HL method while the other half is manufactured by the VI method. It has been reported from the composite manufacturer that while the VI portion of each panel is noticeably stronger, the HL portion has proven to be more resistant to impact damage. Hence, the combination of the two provides a hybrid material that is very strong and impact resistant. Mechanical testing was performed on all four panels to relate the laminate type to the proceeding mechanical properties.

5.2.1 Tension Tests

Static tension tests were conducted to investigate the performance of the six reviewed composite panels. Standard tensile stress-strain diagrams for 5 prepared tensile specimens can be seen from each individual panel type. The three most noteworthy variables monitored from tensile testing were the tensile elastic modulus, the ultimate tensile strength, and the maximum percentage strain at failure. Figures 5.2-1, 5.1-3, 5.2-2, 5.2-3, 5.2-4, and 5.2-5 shows the tensile stress-strain diagrams for the CHL, ILHS, ILHB, ILHB2, OLHS, and OLHB panels, respectively.

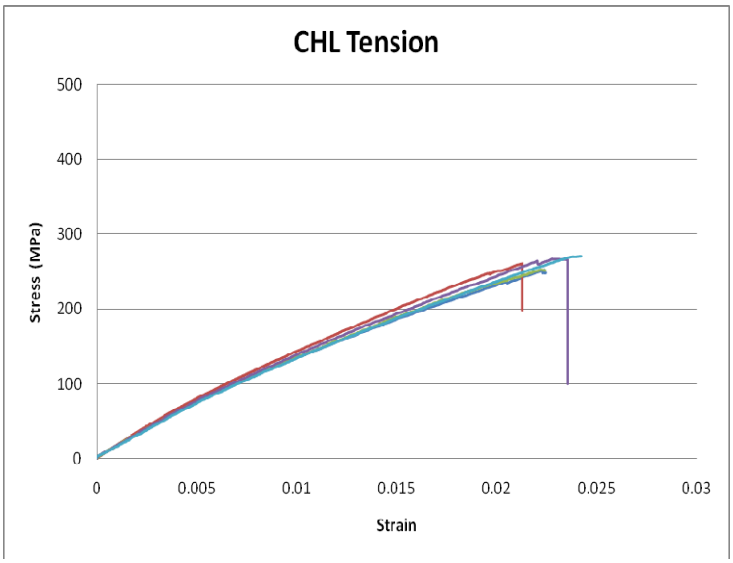

CHL Averages	
UTS (MPa)	260.56
Max % Strain	2.279
Modulus (GPa)	15.32

Fig 5.2-1: Tensile Stress-Strain Diagrams for 5 Tested CHL Specimens

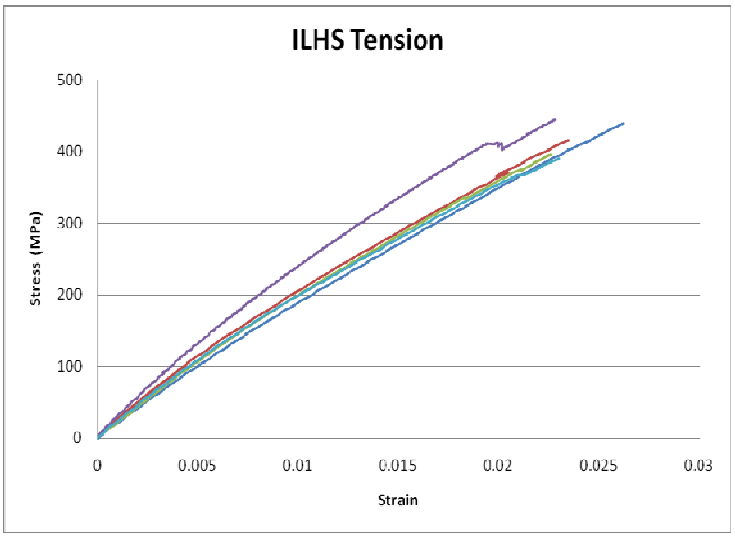

ILHS Averages	
UTS (MPa)	416.79
Max % Strain	2.363
Modulus (GPa)	22.42

Fig 5.1-3: Tensile Stress-Strain Diagrams for 5 Tested ILHS Specimens

ILHB Averages	
UTS (MPa)	430.50
Max % Strain	2.288
Modulus (GPa)	25.71

Fig 5.2-2: Tensile Stress-Strain Diagrams for 5 Tested ILHB Specimens

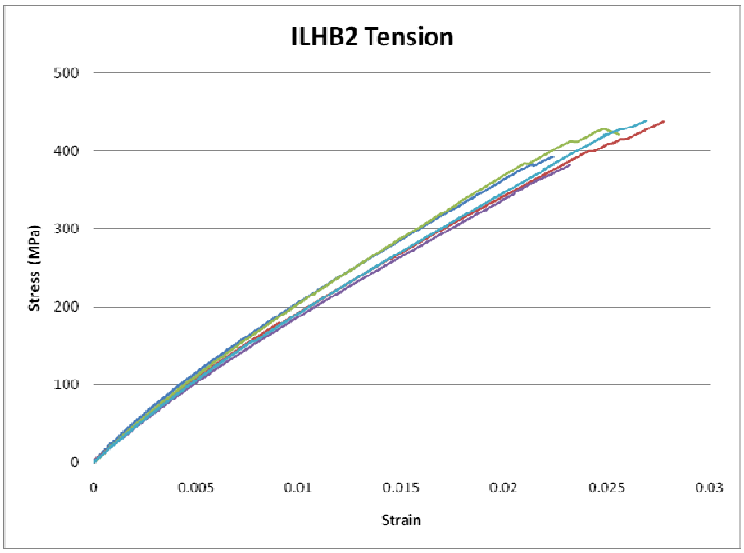

ILHB2 Averages	
UTS (MPa)	416.07
Max % Strain	2.51
Modulus (GPa)	22.81

Fig 5.2-3: Tensile Stress-Strain Diagrams for 5 Tested ILHB2 Specimens

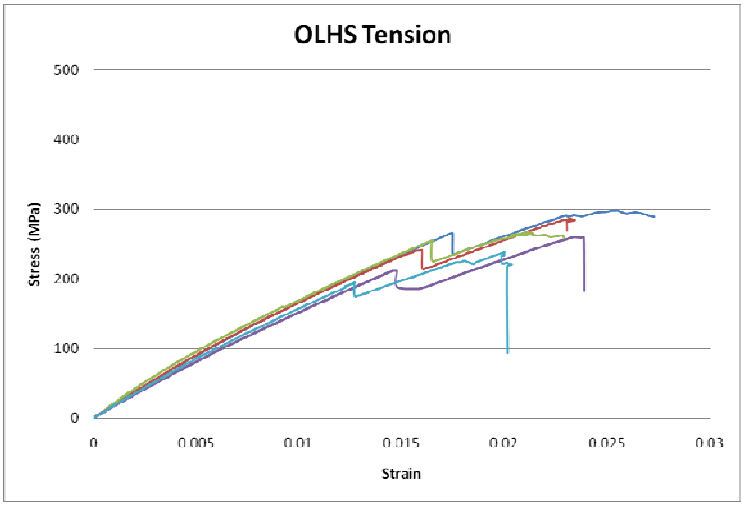

OLHS Averages	
UTS (MPa)	269.97
Max % Strain	2.358
Modulus (GPa)	17.87

Fig 5.2-4: Tensile Stress-Strain Diagrams for 5 Tested OLHS Specimens

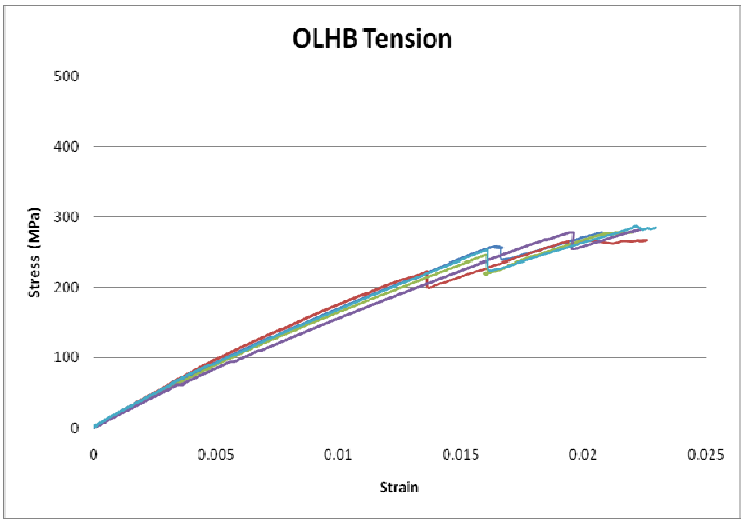

OLHB Averages	
UTS (MPa)	278.45
Max % Strain	2.219
Modulus (GPa)	18.55

Fig 5.1-5: Tensile Stress-Strain Diagrams for 5 Tested OLHB Specimens

5.2.2 Compression Tests

Static compression tests were administered to all reviewed composite panels for this research. Standard compressive stress-strain diagrams were acquired from each individual panel after testing 5 specimens in accordance with ASTM D695. The three most noteworthy variables monitored from compressive testing were the compressive elastic modulus, the ultimate compressive strength, and the maximum percentage strain at failure. 350 Ohm, 5 mm grid strain gages were implemented as a direct way to measure strain from the specimen. Figures 5.2-6, 5.1-6, 5.2-7, 5.2-8, 5.2-9, and 5.2-10 shows the compressive stress-strain diagrams for the CHL, ILHS, ILHB, ILHB2, OLHS, and OLHB panels, respectively.

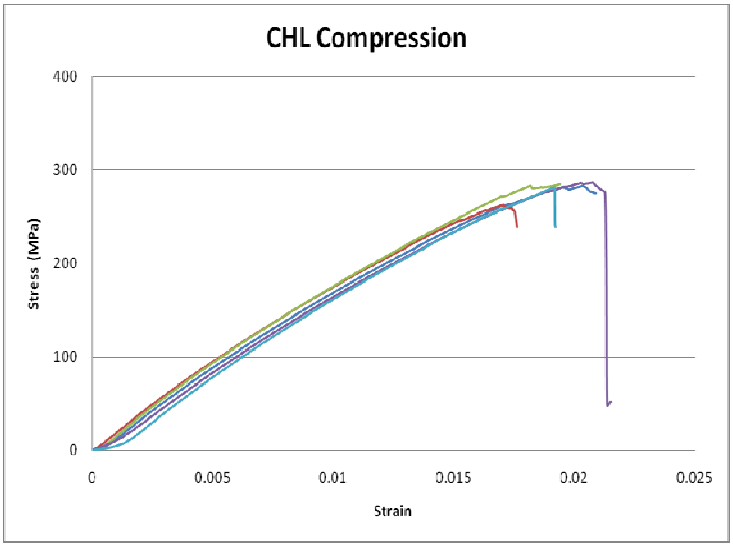

CHL Averages	
UCS (MPa)	279.95
Max % Strain	1.973
Modulus (GPa)	17.32

Fig 5.2-6: Compressive Stress-Strain Diagrams for 5 Tested CHL Specimens

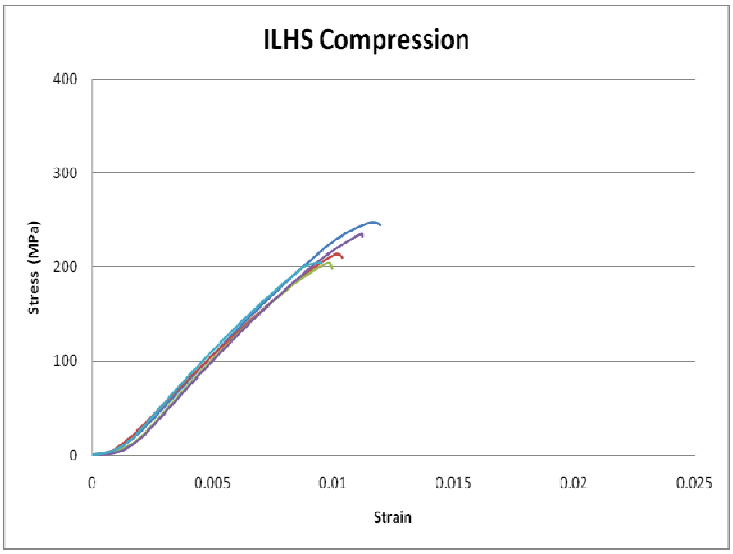

ILHS Averages	
UCS (MPa)	221.23
Max % Strain	1.060
Modulus (GPa)	25.81

Fig 5.1-6: Compressive Stress-Strain Diagrams for 5 Tested ILHS Specimens

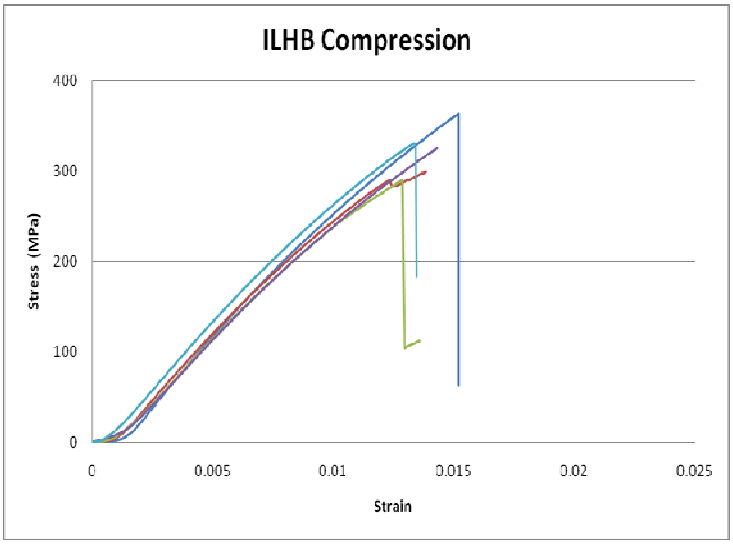

ILHB Averages	
UCS (MPa)	322.02
Max % Strain	1.408
Modulus (GPa)	27.90

Fig 5.2-7: Compressive Stress-Strain Diagrams for 5 Tested ILHB Specimens

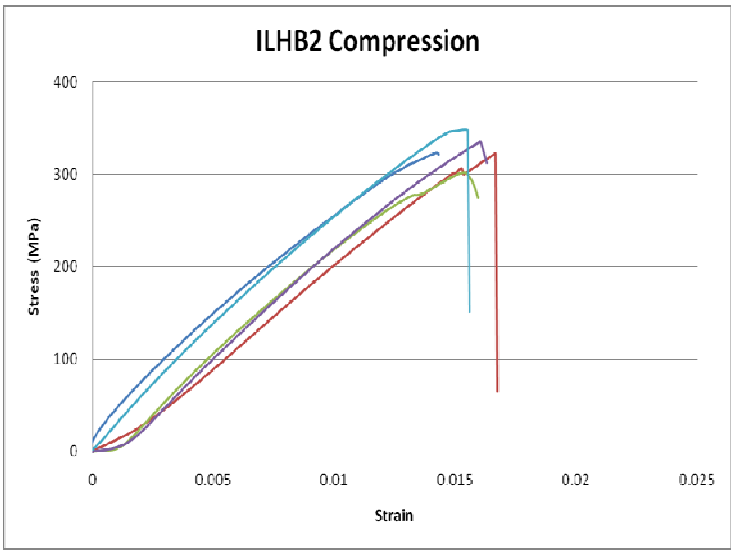

ILHB2 Averages	
UCS (MPa)	326.41
Max % Strain	1.578
Modulus (GPa)	24.04

Fig 5.2-8: Compressive Stress-Strain Diagrams for 5 Tested ILHB2 Specimens

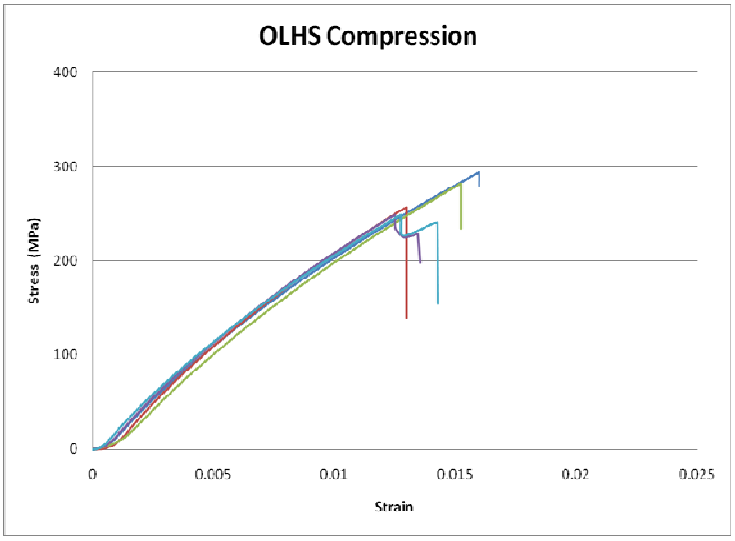

OLHS Averages	
UCS (MPa)	266.25
Max % Strain	1.442
Modulus (GPa)	23.62

Fig 5.2-9: Compressive Stress-Strain Diagrams for 5 Tested OLHS Specimens

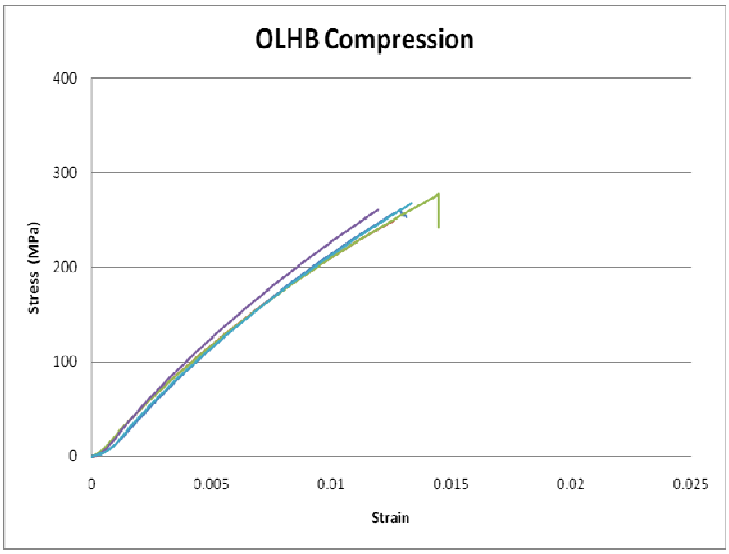

OLHB Averages	
UCS (MPa)	263.31
Max % Strain	1.309
Modulus (GPa)	25.37

Fig 5.2-10: Compressive Stress-Strain Diagrams for 5 Tested OLHB Specimens

5.2.3 Analysis and Trends

Relating the number of fiber sheet layers to the resultant tensile material properties of the ILHS (2 sheets), the ILHB (3 sheets), and the ILHB2 (4 sheets) showed no trend in mechanical properties. As can be seen from Figures 5.2-11 and 5.2-12, the average UTS and tensile modulus found between the three panels seems to insist no improvement, nor degradation.

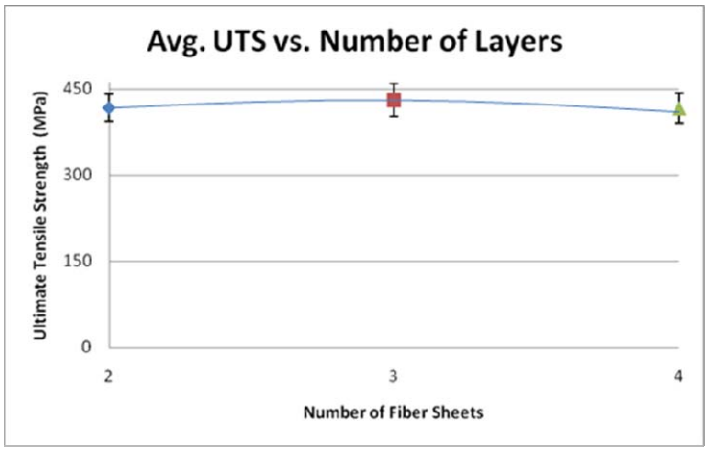

Fig 5.2-11: Average Ultimate Tensile Strength vs. Increasing Fiber Layers

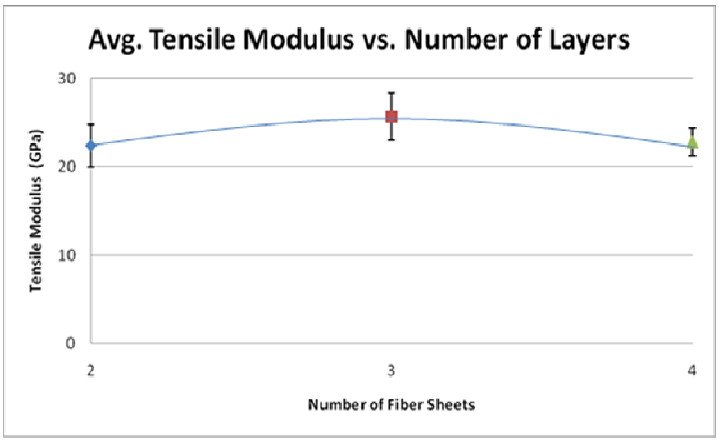

Fig 5.2-12: Average Tensile Modulus vs. Increasing Fiber Layers

The recorded tensile modulus had a slight increase from the two to three sheet samples, but then reversed its trend and came back down for the four layer samples. For the ultimate tensile strength, the trend appeared to be very flat, and no positive or negative feedback can be established. This is primarily due to the fact by increasing the layers of fiber within a composite panel also increases its thickness. More load can be exerted on a specimen as the layers of fiber increase, but the area is also increased. When relating these properties to the increasing cross-sectional area, they remain the same, and are illustrated in the above figures. This establishes that by increasing the layers of fiber within a composite panel, no substantial effect will be seen in tensile performance.

Relating the number of fiber sheets to the resultant compressive material properties of the can be seen from Figures 5.2-13 and 5.2-14.

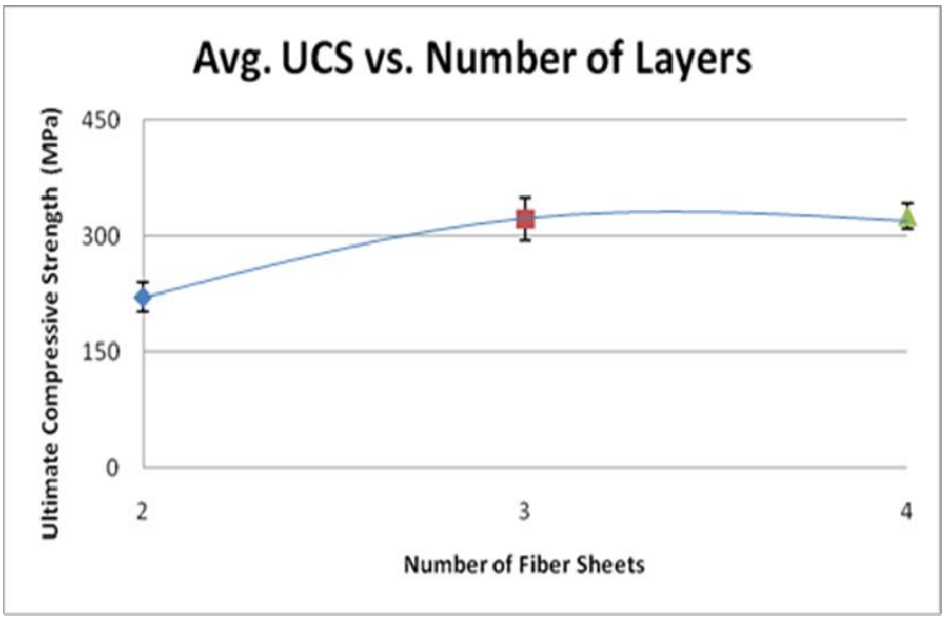

Fig 5.2-13: Average Ultimate Compressive Strength vs. Increasing Fiber Layers

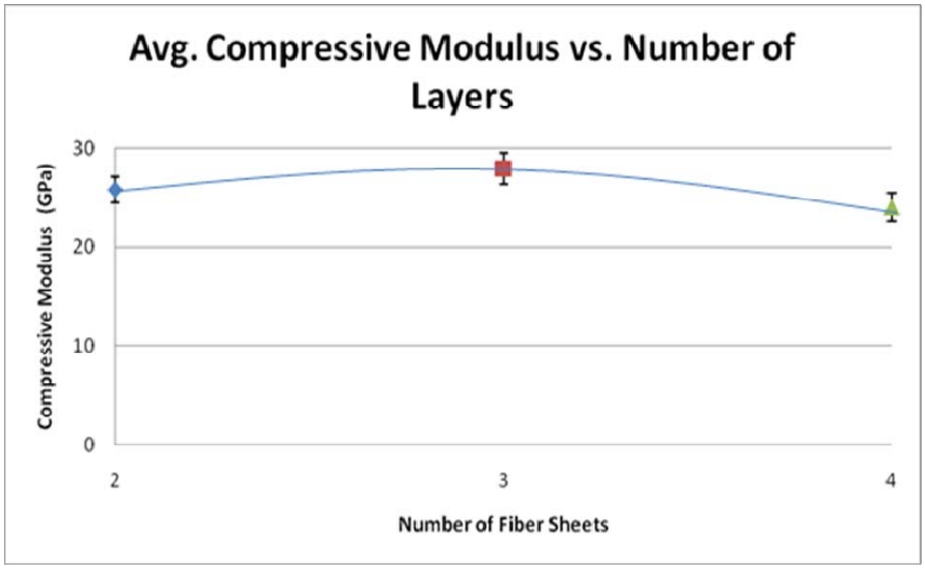

Fig 5.2-14: Average Compressive Modulus vs. Increasing Fiber Layers

It was seen as layers of fiber increased that the compressive strength increased. Over the course of the tested samples, a strength increase of 105.2 MPa or 47% was experienced. However, as layers of fiber sheet increased, there seemed to be no conclusive trend in compressive modulus. Similar to the tensile data, as the layer count increased from two to three layers, an increase in modulus was seen, only to be redirected downwards when comparing it to the four layer samples. The same justification can be made as in the tensile data for the compressive modulus. As the fiber layers increase, the sample volume does also. This leads to an increase in sample area, which creates similarities in compressive moduli. The increase in compressive strength suggests that an increasing in fiber sheet layers and the cross-sectional area does have positively influences on mechanical properties. This was the only conclusive trend observed for this study.

Relating the panel type to the measured mechanical properties did show some interesting results. By comparing panels made from purely hand lay-up (CHL), mixed hand lay-up and vacuum infusion (OLHS and OLHB), and purely vacuum infusion (ILHB2), conclusions can be made based on whether single manufactured or bi-manufactured panels provide better outcomes

in performance. Figures 5.2-15 and 5.2-16 show the relative tensile properties as they compared to tested panel type.

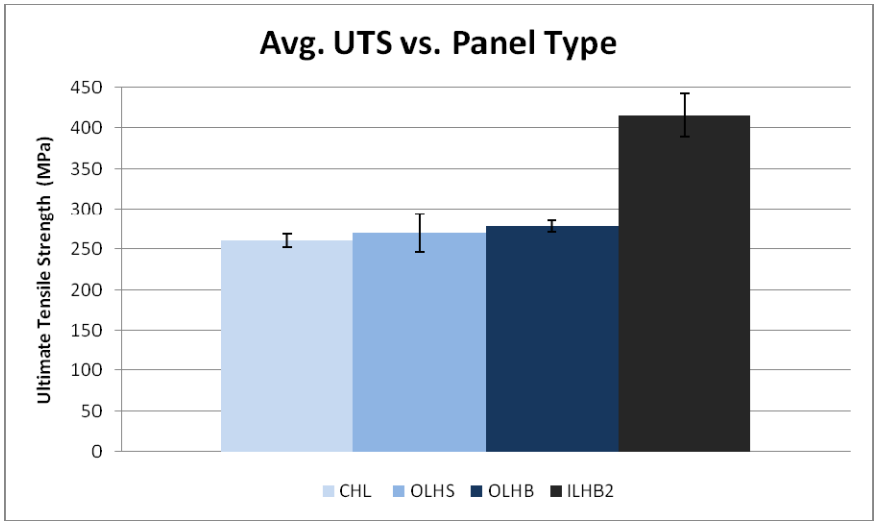

Fig 5.2-15: Bar Chart indicating UTS as it Relates to Type of Panel

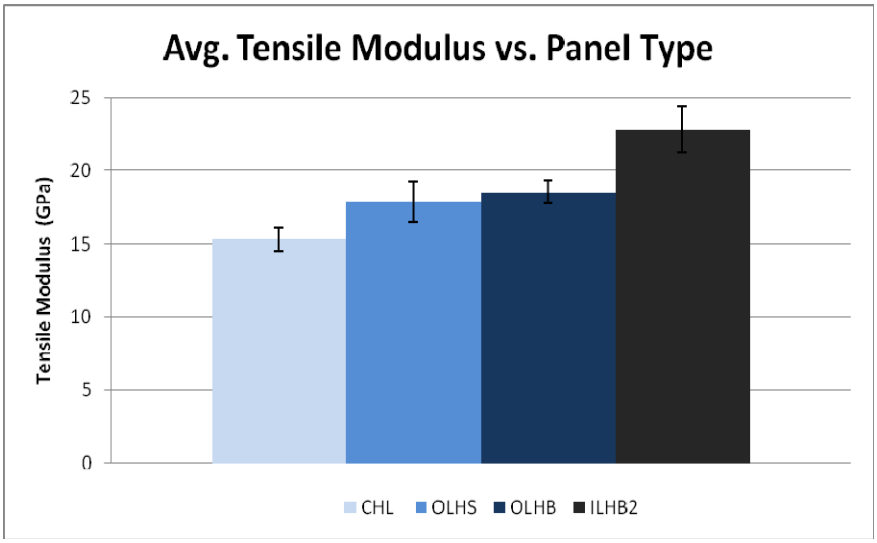

Fig 5.2-16: Bar Chart Indicating Tensile Modulus as it Relates to Type of Panel

It was seen that as the panel type progressed towards the purely vacuum infusion panel, the tensile properties experienced a steady improvement in performance. This trend was also seen in section 5.1, due to the decreasing trend of void content in HL to VI panels. There is no difference here with the progression towards pure VI manufactured panels. Over the range of panels tested, a 7.5 GPa increase in modulus was seen, which accounted for a 49 % increase. However, the increase in tensile strength wasn't substantial until the vacuum infusion panel was reached. A 155.5 MPa increase in strength was seen over the range of panels tested which accounted for a 40% increase. For the HL and bi-manufactured panels, ultimate tensile strengths had little improvement. It has been documented in this research that HL composites are inferior to VI composites due to a higher void content. However, the hybrid materials are made from both processes and even though a portion of the material is made from the HL process, it still carries that strong characteristic VI portion to give it added strength. To understand why no substantial increase was made, the resulting tensile stress-strain graphs should be understood. A typical stress-strain curve for the hybrid panels can be seen in Figure 5.2-17.

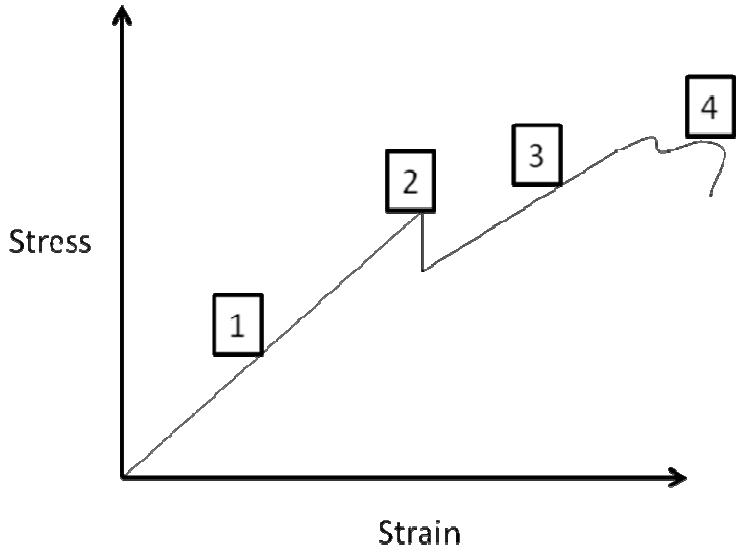

Fig 5.2-17: Schematic of Typical Hybrid Stress-Strain Curve

As can be seen from the above schematic, four characteristic segments of the curve are indicated. As loading is initiated, the coupon being tested begins as a thick, two part material system that is loaded at a steady rate; this is illustrated by segment number 1 in the above schematic. This occurs until there is a sizeable drop in load somewhere during the middle of testing; segment number 2. This drop in loading is where the HL portion of the specimen fails, which leaves only the VI portion to be under the remaining load; segment number 3. The VI portion is then pulled until ultimate failure when the entire specimen breaks; segment number 4. A schematic of each portion from the typical stress-strain curve can be seen in Figure 5.2-18.

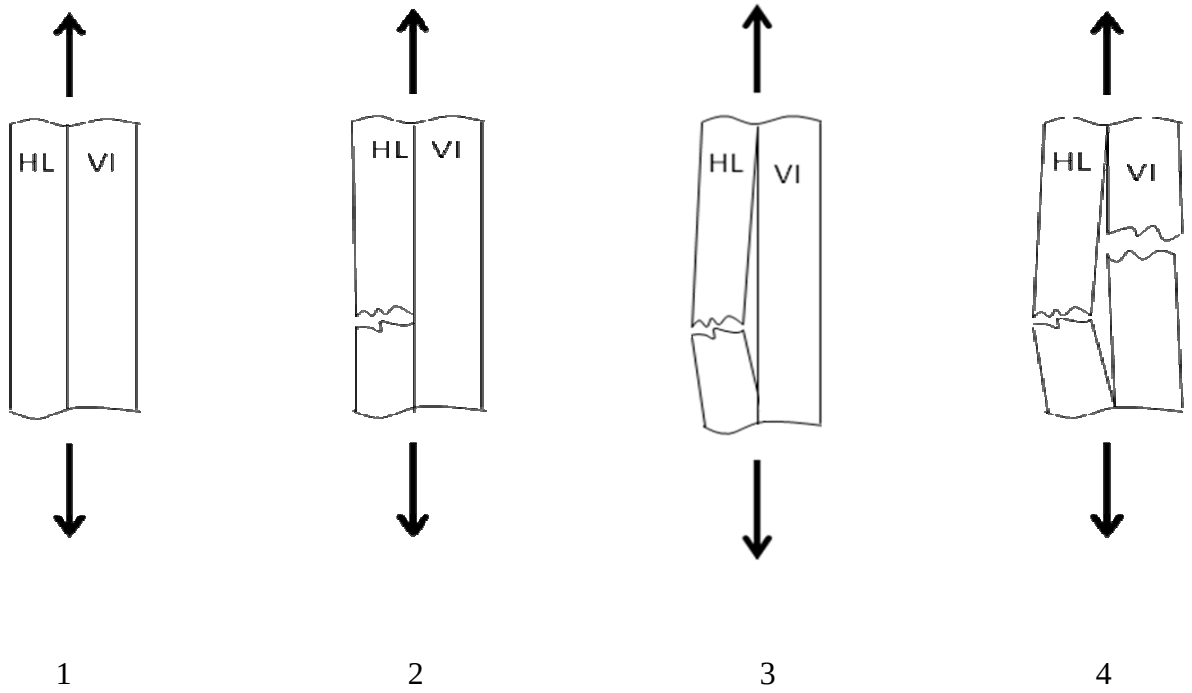

Fig 5.2-18: Illustrations of Segments 1 Through 4 from Hybrid Stress-Strain Diagram

As can be seen from the progressing segments, once the HL portion is unable to carry anymore load, it fractures, and eventually detaches itself from the VI portion. This detachment severely decreases the cross-sectional area that was used for testing. By decreasing this area

during testing, more stress was exerted on the VI portion of each specimen. However, the recorded area before testing was used as the initial area measurement in which to calculate stress. This is primarily why there is no substantial improvement in ultimate strength in panel type until the pure VI panel is reached. Figure 5.2-19 shows a hybrid specimen after tensile testing was complete.

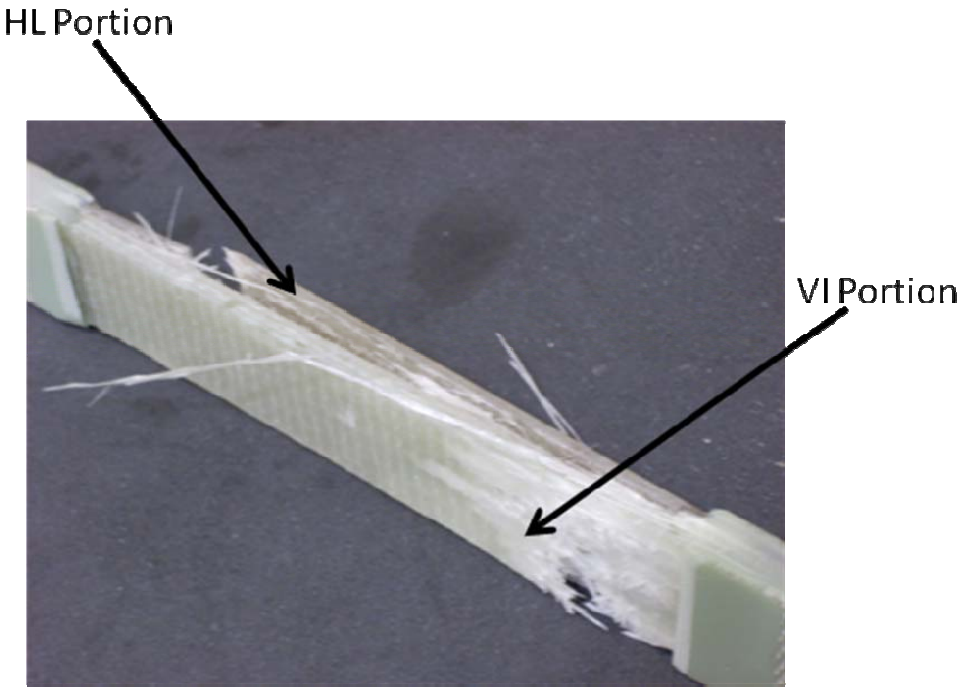

Fig 5.2-19: Failed Hybrid Tensile Specimen

Results under compressive testing yielded comparative results for compressive and tensile ultimate strengths, but dissimilar results when comparing compressive and tensile modulus. Figures 5.2-20 and 5.2-21 illustrate the relative compressive properties as they compared to tested panel type.

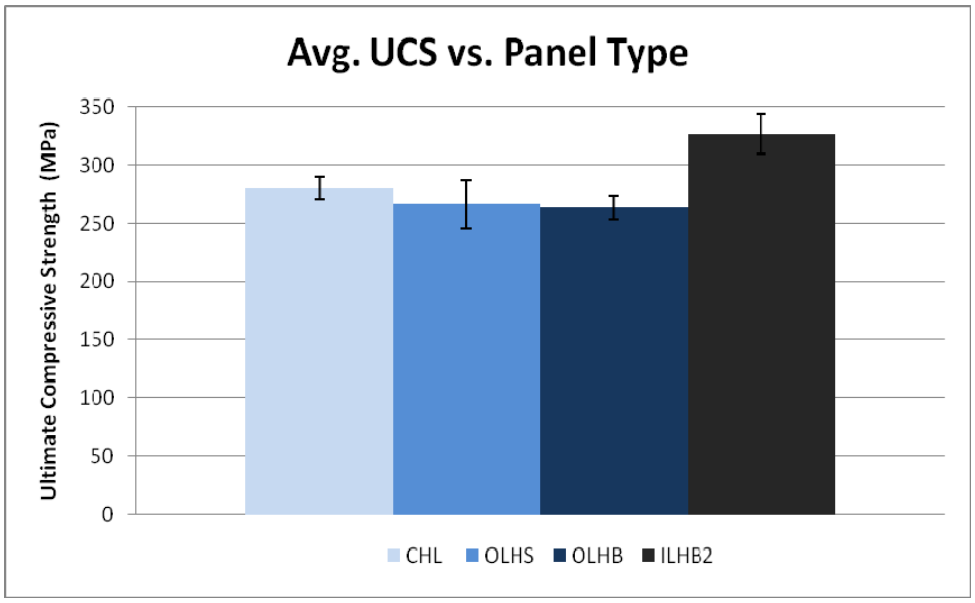

Fig 5.2-20: Bar Chart indicating UCS as it Relates to Type of Panel

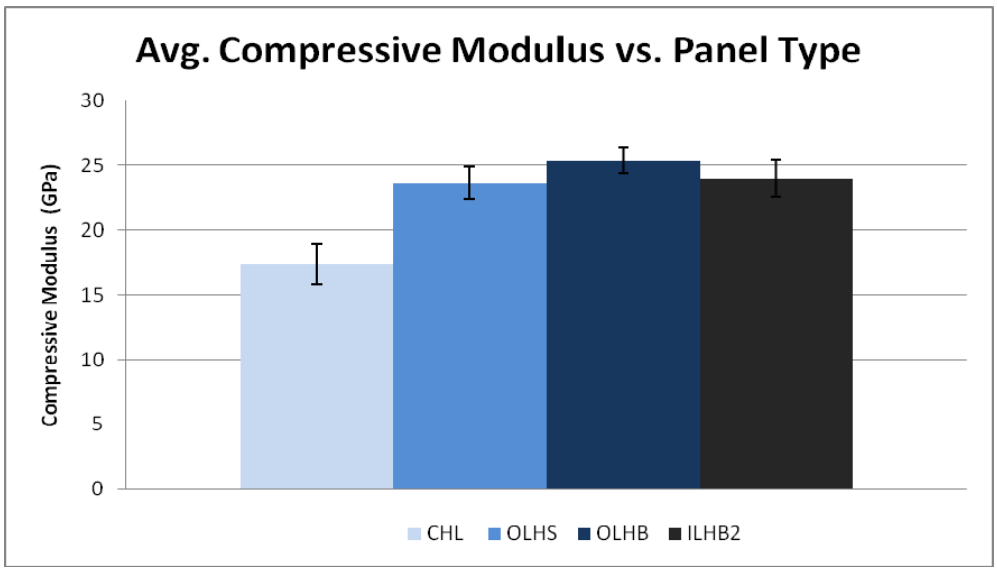

Fig 5.2-21: Bar Chart Indicating Compressive Modulus as it Relates to Type of Panel

As seen with the ultimate strengths in tension, the same scenario was experienced in compression. Neither significant improvement, nor deterioration in strength was seen with the HL and hybrid panels. Once the VI panel was reached, the maximum increase in strength was 63.1 MPa, which accounted for a 24% increase. When comparing the tested compressive modulus, a sizeable increase was experienced from the HL to hybrid panels. However, no substantial improvement was seen in relation from the hybrid panels to the VI panel. From minimum to maximum modulus, an increase of 8.0 GPa was seen, which accounted for a 46% increase. However, even though this increase was experienced, it did not follow the steady trend seen for the tensile samples. This is again due to the manner in which the hybrid specimens failed. As the sample was being compressed, the HL and VI portions of the specimen remained intact until failure. Typical failures were seen as a rupture from the gage section of each specimen. By failing in this manner, the overall area of each hybrid specimen remained intact until ultimate failure. This is unlike the manner in which these samples failed in tension because it was seen that the HL portion failed before the VI portion. This left a smaller cross-sectional area which was under higher stresses, which were not accounted for by initial area measurements. In compression, however, this separation was not seen and both HL and VI portions of each specimen failed in unison, therefore allowing the entire initial area to be under stress throughout the duration of the test. It is believed that throughout the duration of the tensile test, both HL and VI portions were not straining at the same rate. The HL side of the sample was deforming much faster than the VI portion which could account for the reason behind lower modulus values. For the compression samples, since the VI portion was much stiffer, each test specimen was at the mercy of this portion. Because this manufacturing method allows for less deformation rate, the HL side did not deform faster than the VI side and the results depicted a stiffer material. Figure 5.2-22 depicts actual pictures of failed hybrid compression specimens.

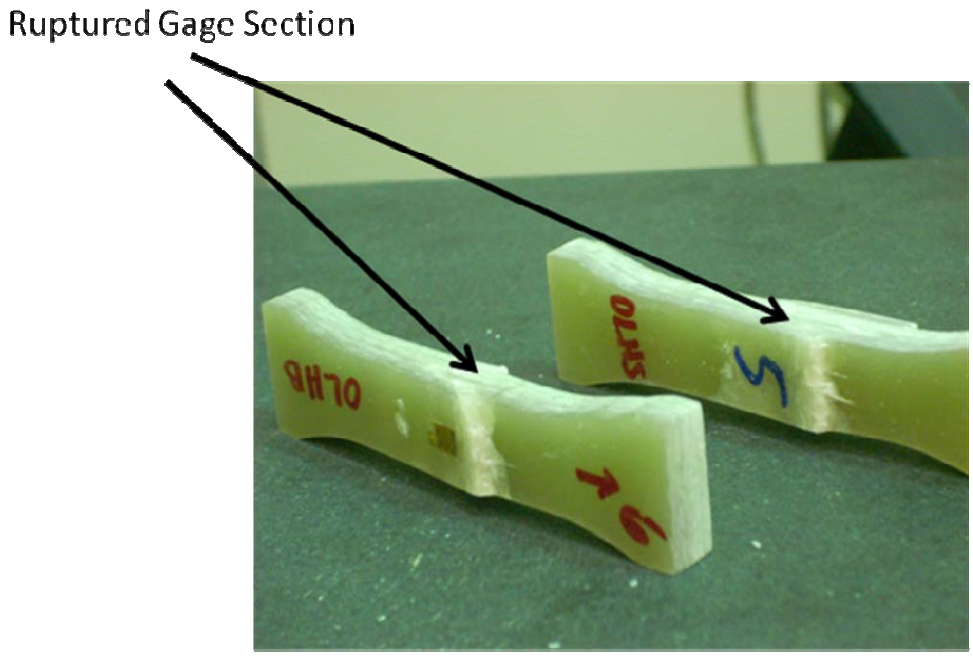

Fig 5.2-22: Failed Hybrid Compressive Specimen

5.3 Separate Compressive Testing Methods

Two common methods to test FRP composite materials in compression are the ASTM D695 method and the ASTM D695M method. Both methods use the same strategy and testing fixture to establish their compressive properties, but the difference lies within the fabrication of their test specimen. The ASTM D695 method requires a compressive coupon that is cut to a dog-bone shape. The cross-section is not constant throughout the specimen due to standards that require the ends to be wider than the gage section. A large radius guides the wider specimen ends down to the gage region so that internal stresses do not create premature failure in this radial region. The ASTM D695M test method requires a completely different type of coupon. The most distinguishing difference between the two is the use of tabs for the ASTM D695M test coupon. The specimen is created with a constant width giving it a constant cross-section. Each end of the specimen is then adhesively tabbed with a similar material, leaving only a 5 mm gap in the center that is described as the gage region. By testing the same materials under both testing methods, recommendations can be concluded from the outcomes of compressive properties.

5.3.1 Compressive Testing

Static compressive testing was administered to all specimens regarding this study. Standard compressive stress-strain diagrams were acquired from 5 compression specimens of each compressive testing method. The three most noteworthy variables monitored from compressive testing were the compressive elastic modulus, the ultimate compressive strength, and the maximum percentage strain at failure. 120 Ohm, 1.5 mm grid strain gages were implemented as a direct way to measure strain from the specimen. Figures 5.1-4, 5.1-6, 5.3-1 and 5.3-2 shows the compressive stress-strain diagrams for the MHL and ILHS specimens tested under ASTM D695, and then tested under ASTM D695M.

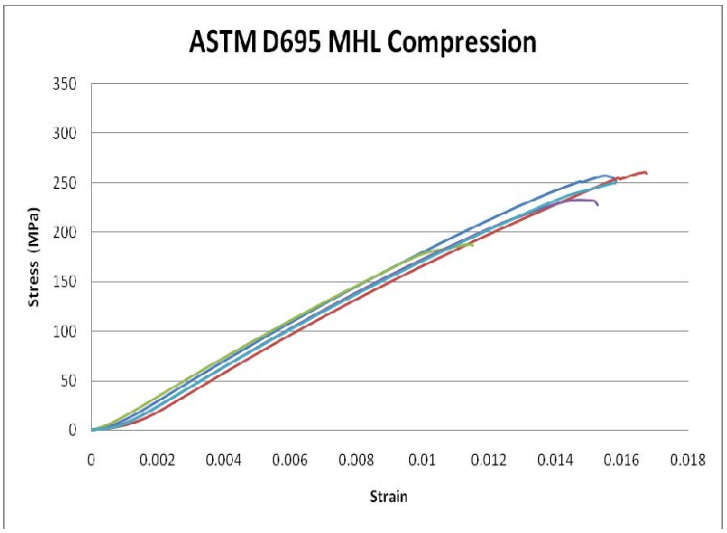

ASTM D695 MHL	
Avg. UCS (MPa)	237.63
Avg. Modulus (GPa)	18.03
Std Dev UCS	29.91
Std Dev Modulus	1.29

Fig 5.1-4: Compressive Stress-Strain Diagrams for 5 MHL Specimens Tested Under ASTM D695

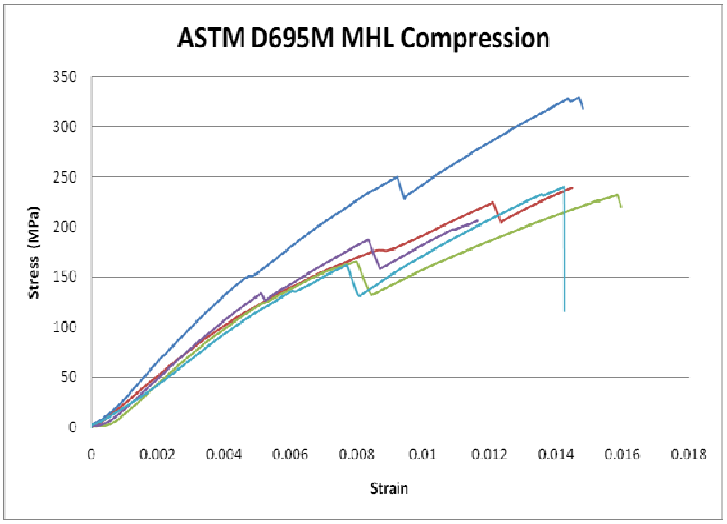

ASTM D695M MHL	
Avg. UCS (MPa)	249.42
Avg. Modulus (GPa)	17.31
Std Dev UCS	46.58
Std Dev Modulus	1.78

Fig 5.3-1: Compressive Stress-Strain Diagrams for 5 MHL Specimens Tested Under ASTM D695M

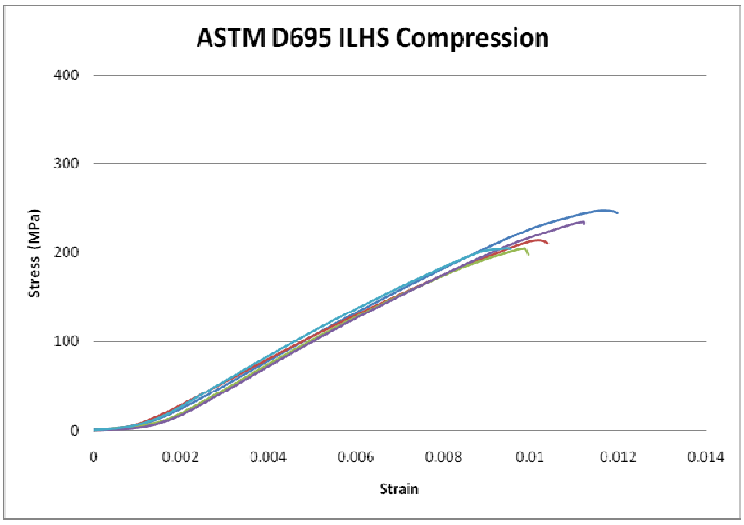

ASTM D695 ILHS	
Avg. UCS (MPa)	221.23
Avg. Modulus (GPa)	25.81
Std Dev UCS	19.28
Std Dev Modulus	1.32

Fig 5.1-6: Compressive Stress-Strain Diagrams for 5 ILHS Specimens Tested Under ASTM D695

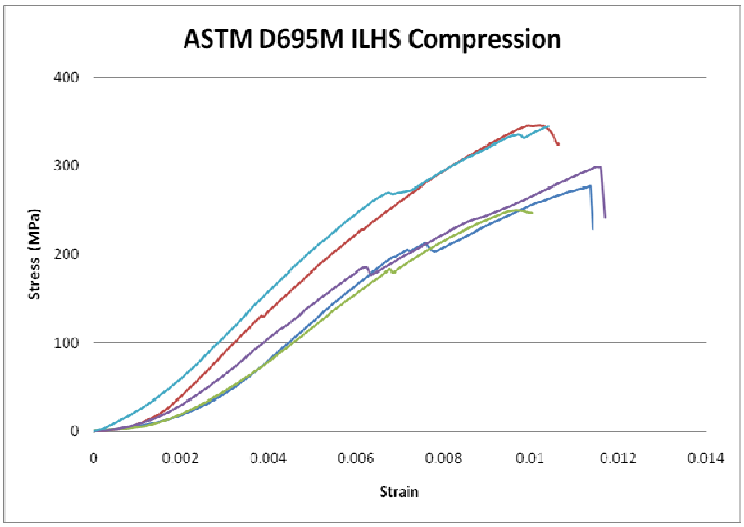

ASTM D695M ILHS	
Avg. UCS (MPa)	303.57
Avg. Modulus (GPa)	20.56
Std Dev UCS	42.22
Std Dev Modulus	1.89

Fig 5.3-2: Compressive Stress-Strain Diagrams for 5 ILHS Specimens Tested Under ASTM D695M

5.3.2 Analysis and Trends

With both materials, the ASTM D695M testing method offered different stress-strain diagrams that appeared very different from the ASTM D695 diagrams. The most noticeable difference is slight drops in loading, before a recovery until ultimate failure. These drops were previously seen in section 5.2 with hybrid specimens under tension. However, these results are formed from compressive diagrams, suggesting a different cause. Figure 5.3-3 depicts a schematic of a typical ASTM D695M stress-strain diagram.

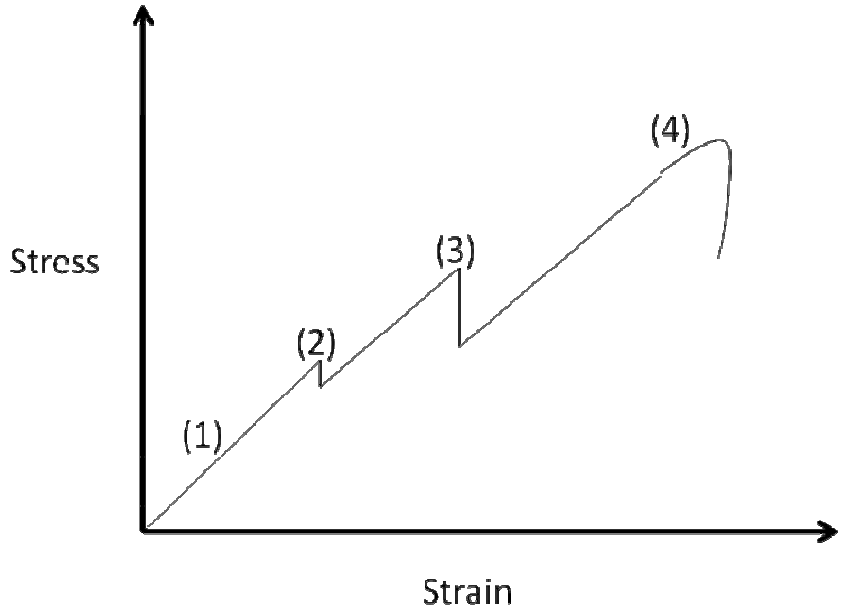

Fig 5.3-3: Typical ASTM D695M Stress-Strain Diagram

The above figure has been broken into four separate stages. All of which are certain occurrences during loading that a typical ASTM D695M specimen experiences. During the first portion of the diagram (1), the tabbed specimen in loaded at a constant rate until portion (2) is reached. In this second portion of the diagram, initial tab debonding from the specimen is

experienced. This always took place at the base of the tab, near the gage section, and led to portion (3). In the third portion, a majority of the tabs separated from the specimen near the gage region. When this occurred, the specimen was not supported as it was initially, and measured loads were seen to drop. This did not have an effect on the location of failure as it was seen to happen within the specified gage region every time, however, this did add variance to the measured data that was not seen with the specimens tested under ASTM D695. Figure 5.3-4 below shows a compressed ASTM D695M specimen with tab debonding. Enlarged views of the separated area and failure are also indicated. As can be seen from the mode of failure, fiber kinking and eventual fiber breakage was the primary mode of failure. Showing that even though the data varied, the failure was acceptable.

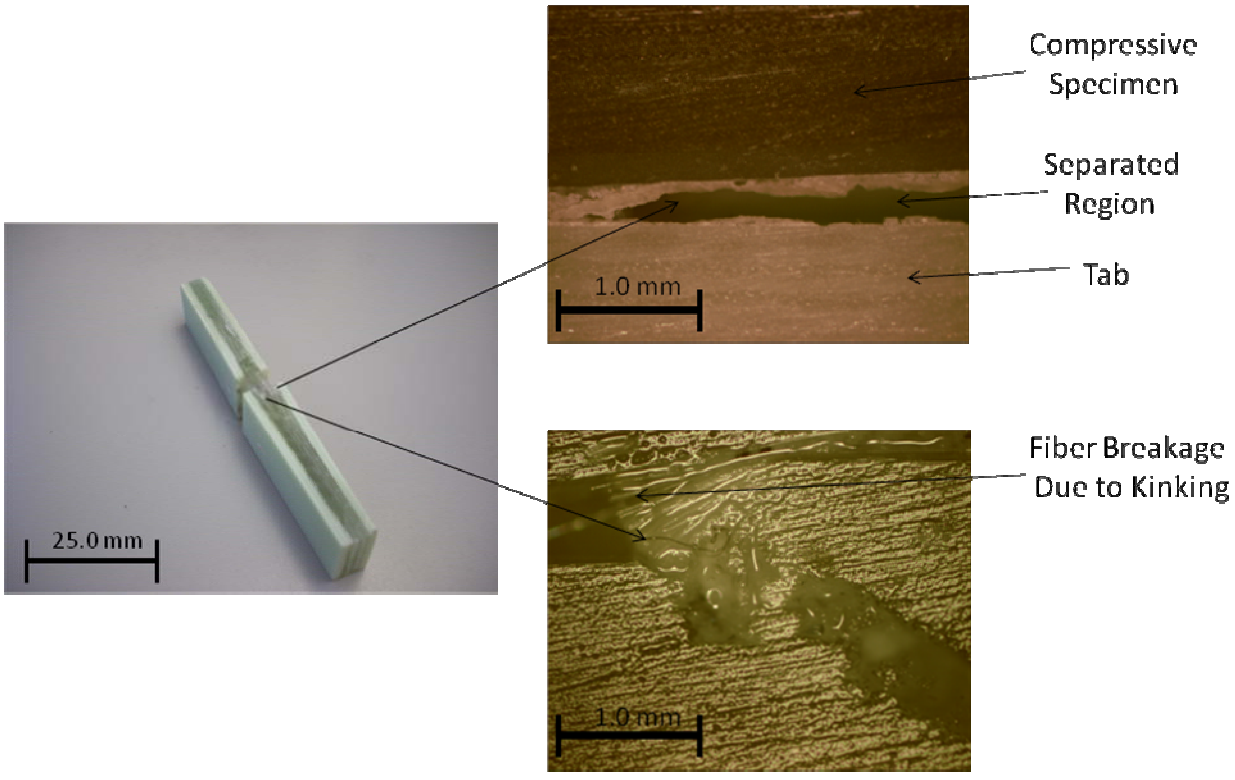

Fig 5.3-4: Compressive Specimen Tested Under ASTM D695M with Enlarged Views

Once the diagrams were understood, comparing the two compressive testing methods with the same materials established some notable results. Below, figures 5.3-5 through 5.3-8 show the average UCS and modulus results for both materials tested (D695 in light, D695M in dark). Errors bars are also shown to indicate a single standard deviation from the overall mean of each obtained property.

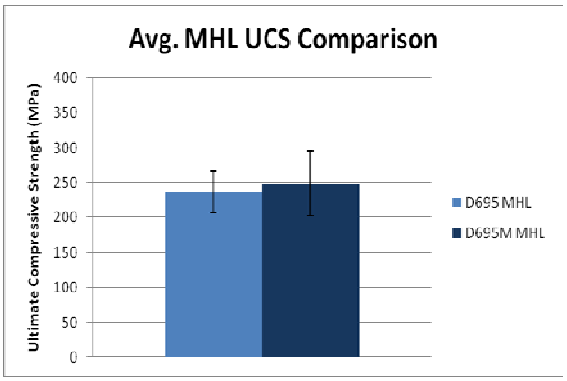

Fig 5.3-5: UCS Comparison of MHL

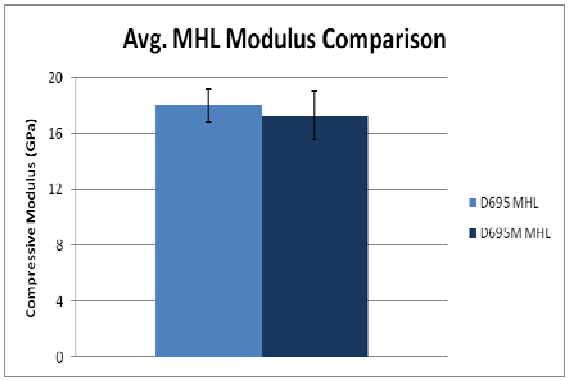

Fig 5.3-6: Modulus Comparison of MHL

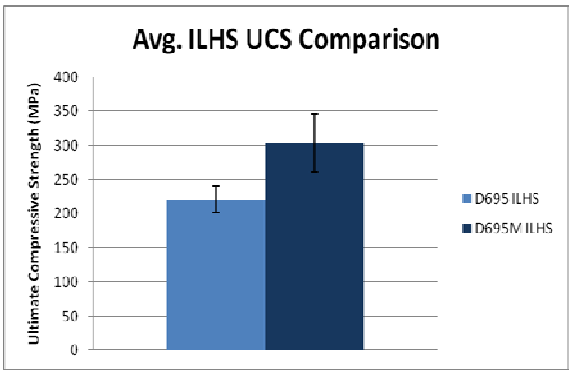

Fig 5.3-7: UCS Comparison of ILHS

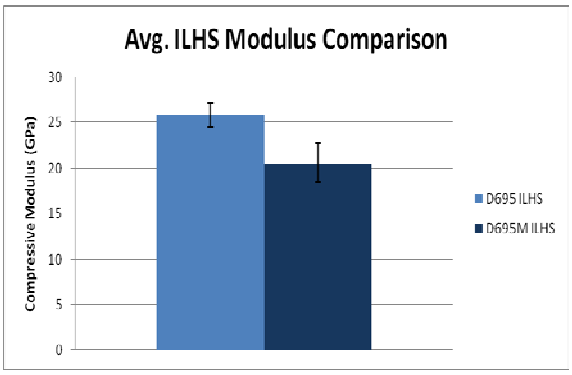

Fig 5.3-8: Modulus Comparison of ILHS

The above figures indicate interesting trends from the measured properties. In both cases, it was observed that using the D695 method yielded higher modulus values compared to the D695M method. However, in both cases, it was observed that using the D695M method yielded higher ultimate strength values compared to the D695 method. These results are interesting and offer a difficult trade off in superiority. On one hand, one test method indicates that a composite material can hold more load until ultimate failure, but has a lesser resistance to deformation. On the other hand, the other indicates that the same material is actually better at resisting deformation, but will not carry a higher load. This leads to further belief that the determined compressive properties of composite materials in a function of specimen end surface area. When the ASTM D695M compressive method is used, the bonded tabs increase the surface area in which the compressive platen contacts the specimen end. When this happens, the load is distributed over a larger area and strengths are seen to increase. It should be noted that in all ASTM D695M specimens tested, not a single specimen experienced premature failure. The same cannot be said for the ASTM D695 test method. From the materials tested, some specimens experienced premature end failure from the ASTM D695 method, as seen in section 5.1. This premature failure may reduce the maximum load limit in which a sample can hold, hence, ultimate compressive strengths are reduced. This is due to increased stress concentrations at the specimen end [11].

Another interesting result that noticeably trends in all cases is the previously acknowledged scatter of data when comparing the two test methods. For all tested properties, the standard deviation from the mean was always higher for the ASTM D695M method. As seen from the error bars on each figure above, one standard deviation from the overall mean of each property was significantly larger for the D695M method compared to the D695 method. This verifies that there is more variance in the data obtained by the D695M method and data is gathered within a wider range.

Based on the results from this study, it is believed by the researcher that the more adequate way to measure material property values from composite materials in to use the ASTM

D695 compressive test method over the ASTM D695M method. Even though the dog-bone specimens have a larger chance at experiencing premature end failure, not all specimens experienced this and the data was much more uniform, indicating that it is much more reliable. Also, specimen fabrication time and strain gage application was far easier for the ASTM D695 specimens. The added tabs from the ASTM D695M method required a specialized fixture for installation and the gage area was incredibly small, making it difficult to apply a strain gage. Even though the ASTM D695 specimens were more complex in geometry, the method of routing used to achieve their shape proved to be time efficient. All of these circumstances add to the recommendation that the ASTM D695 method is the better composite compressive testing method.

5.4 Specimen Preparation and its Influence on Compressive Testing

To study the effect of specimen preparation and its influence of compressive performance, compressive specimen end surfaces from the same material were prepared with progressively increasing surface flatness values. Under the standards set by ASTM D695, each prepared compressive coupon should have a measured surface flatness no larger than 0.025 mm (0.001 in). Since the specimen is under direct end loading, one of the compressive platens used during testing directly contacts the top surface of each compressive coupon. This increase in surface flatness may submit poor results after testing is complete. However, it is not well understood the degree to which this may or may not substantially affect the compressive performance of an altered compressive coupon. Therefore, this study will establish results based on how increasing the surface flatness on a compressive specimen end influences its compressive performance. An illustration of the altered specimen surface, as well as an illustration that defines the flatness parameter can be seen in Figures 5.4-1 and 5.4-2 below.

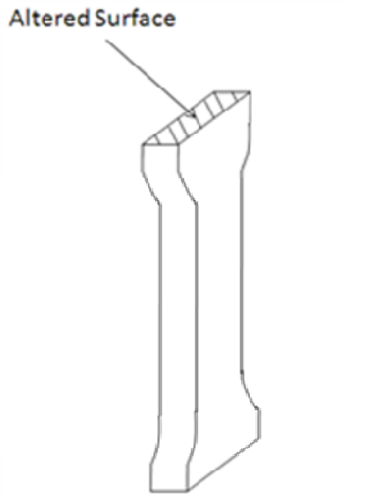

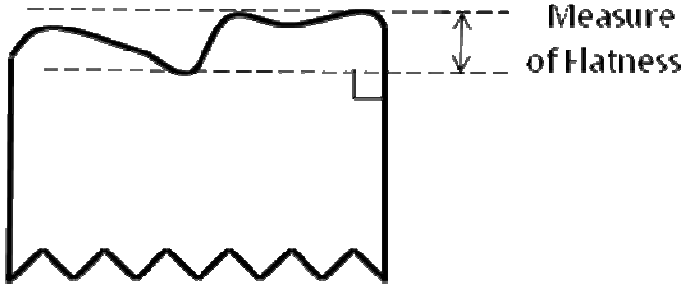

Fig 5.4-1: (Left) Illustration of Compressive Specimen and the Purposely Deviated Surface

Fig 5.4-2: (Right) Definition of the Flatness Parameter

5.4.1 Surface Preparation and Measurement

To perform this analysis, the VIM panel was chosen as the composite material in which to test. It was chosen for immediate availability and excess supply. Fifteen compressive coupons were then manufactured in compliance with the ASTM D695 testing procedure, and prepared for testing. However, five of these coupons were made to be as flat as possible, meeting the standards set by ASTM D695. Then, the remaining ten coupons were slightly set at an angle and milled at one of their ends. Five coupons were cut at approximately 2 degrees off-angle, and the other five were cut at approximately 4 degrees off-angle. A schematic showing the result of this surface finish can be seen in figure 5.4-3.

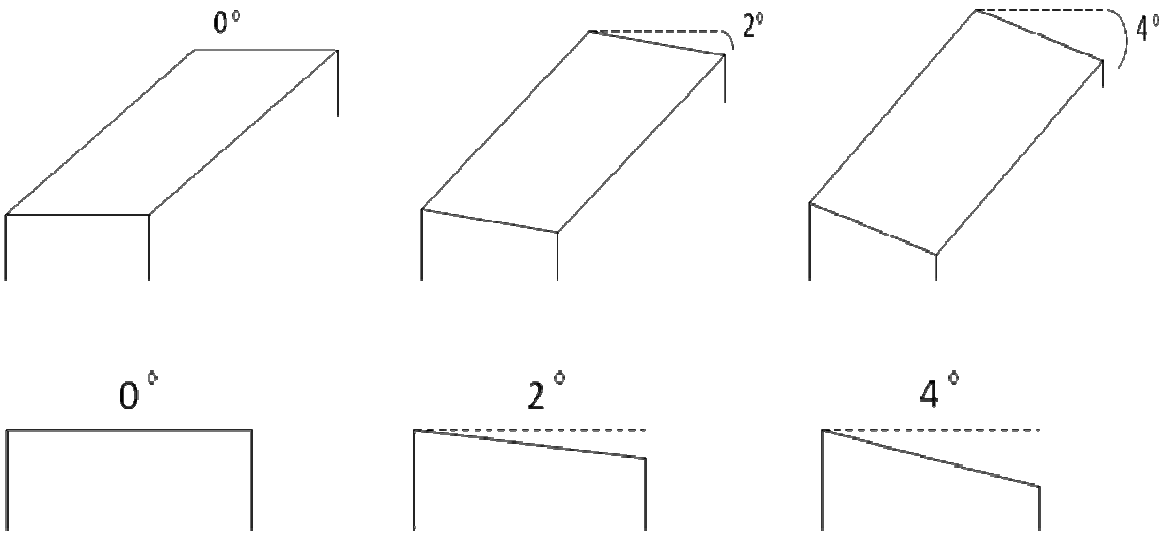

Fig 5.4-3: Surface Flatness Schematic of Compressive Coupon Ends, Top and Side Views

This led to a larger deviation from high point to low point as the angle increased on all prepared compressive coupons. This deviation was then measured using a Brown and Sharp, Gage 2000 CMM (Coordinate Measuring Machine). All measurement data can be seen in Table 5.4-1.

Vacuum Infusion Medium Compression Specimens 0 degrees		
Sample Number	**Surface 1 Flatness (mm)**	**Surface 2 Flatness (mm)**
1	0.021	0.022
2	0.027	0.029
3	0.028	0.020
4	0.025	0.014
5	0.020	0.020
Avg. Surface Flatness	**0.024**	**0.021**
Vacuum Infusion Medium Compression Specimens 2 degrees		
Sample Number	**Surface 1 Flatness (mm)**	**Surface 2 Flatness (mm)**
1	0.028	0.107
2	0.021	0.133
3	0.017	0.103
4	0.024	0.126
5	0.028	0.141
Avg. Surface Flatness	**0.024**	**0.122**
Vacuum Infusion Medium Compression Specimens 4 degrees		
Sample Number	**Surface 1 Flatness (mm)**	**Surface 2 Flatness (mm)**
1	0.023	0.214
2	0.030	0.206
3	0.016	0.192
4	0.022	0.205
5	0.021	0.217
Avg. Surface Flatness	**0.022**	**0.207**

Table 5.4-1: Surface Flatness Measurements (mm)

Every base surface fabricated for this study was finished to be as flat as possible (surface #1). All top surfaces (surface #2) were altered, depending on sample type. As can be seen from the above table, the 0 degree specimens maintained the surface parameter set to standard on both prepared end surfaces. The same cannot be said for the 2 and 4 degree specimens. All base surfaces maintained the defined flatness parameter, but the top surfaces were altered past the

allowed threshold of flatness. All 2 degree specimens averaged a flatness of 0.122 mm, and all 4 degree specimens averaged a flatness of 0.207 mm. Therefore, the 2 degree samples averaged surface flatness values 4.9 times greater than the standard allows, and the 4 degree samples averaged surface flatness values 8.3 times greater than the standard allows. This is substantially larger in specified flatness by ASTM D695 and is the measurement of deviation from highest, to lowest point on all compressive specimen end surfaces.

5.4.2 Compression Testing

Static compressive testing was administered to all specimens regarding this study. Standard compressive stress-strain diagrams were acquired from 5 compression specimens of each deviated surface type in accordance with ASTM D695. The three most noteworthy variables monitored from compressive testing were the compressive elastic modulus, the ultimate compressive strength, and the maximum percentage strain at failure. 350 Ohm, 5 mm grid strain gages were implemented as a direct way to measure strain from the specimen. Figures 5.1-5, 5.4-4, and 5.4-5 show the compressive stress-strain diagrams for the VIM-0deg, VIM-2deg, and VIM-4deg samples, respectively.

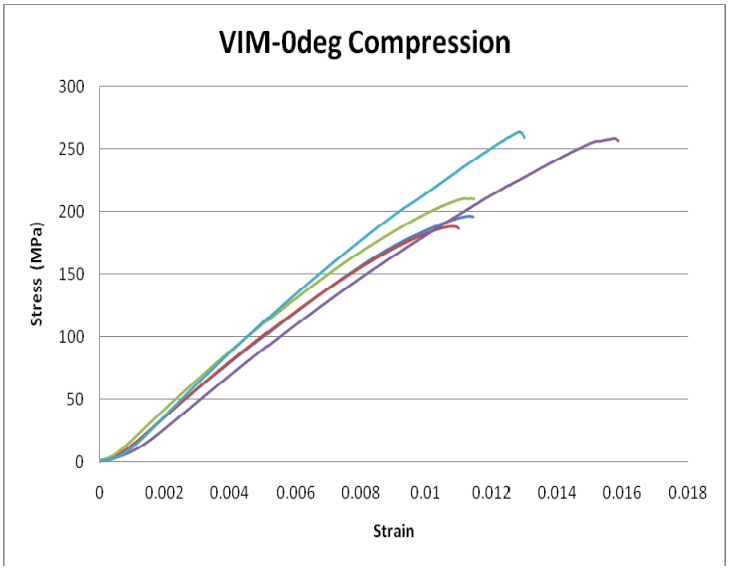

VIM-0deg Averages	
UCS (MPa)	223.46
Max % Strain	1.254
Modulus (GPa)	21.62

Fig 5.1-5: Compressive Stress-Strain Diagrams for 5 Tested VIM-0deg Specimens

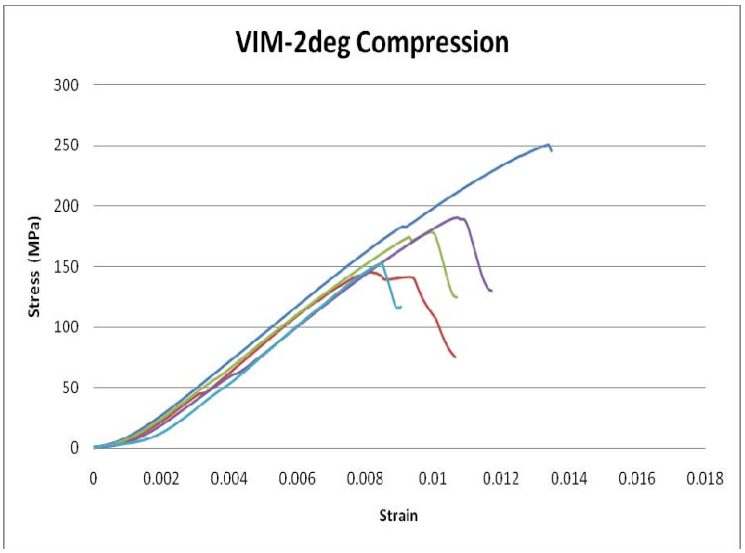

VIM-2deg Averages	
UCS (MPa)	183.69
Max % Strain	1.111
Modulus (GPa)	21.12

Fig 5.4-4: Compressive Stress-Strain Diagrams for 5 Tested VIM-2deg Specimens

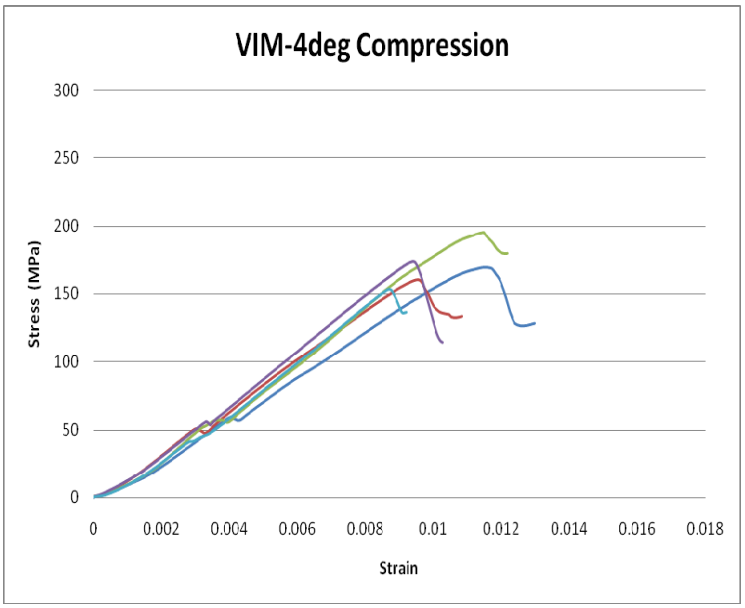

VIM 4-deg Averages	
UCS (MPa)	170.43
Max % Strain	1.110
Modulus (GPa)	19.27

Fig 5.4-5: Compressive Stress-Strain Diagrams for 5 Tested VIM-4deg Specimens

5.4.3 Analysis and Trends

Based on the testing results, relationships between the compressive properties and the increase in off-set angle were established. From Figures 5.4-6 and 5.4-7, the ultimate compressive strength and compressive modulus are plotted with respect to increasing off-set angle, hence increasing surface flatness.

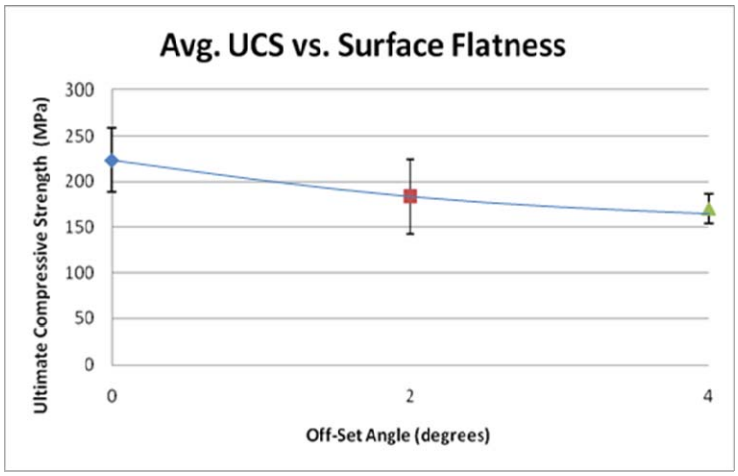

Fig 5.4-6: Average Ultimate Compressive Strength vs. Off-Set Angle

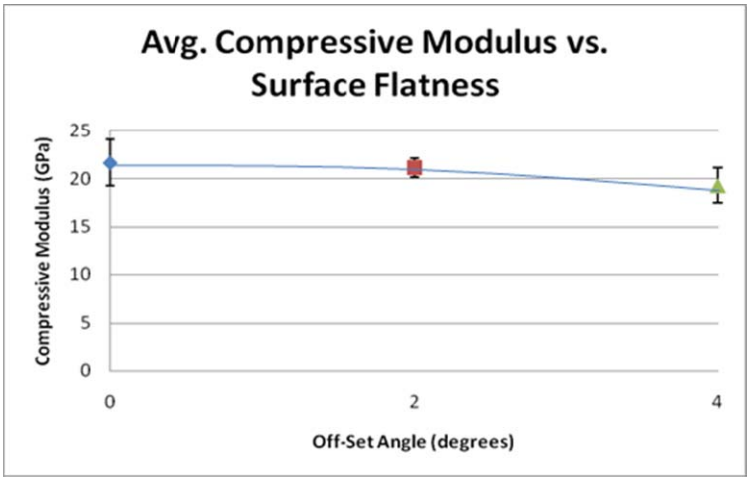

Fig 5.4-7: Average Compressive Modulus Strength vs. Off-Set Angle

It can be seen from the results that a decreasing trend was experienced between all three samples for both compressive modulus and strength. Over the range of samples tested, a 53.0 MPa reduction in ultimate strength and a 2.35 GPa reduction in modulus was experienced. This accounted for a 24% decrease in strength, and a 11% decrease in modulus. This verifies that having ill prepared specimen surfaces will lead to a noticeable reduction in compressive properties. More importantly, this trend is steady, indicating that if flatness values were to continue to increase, compressive properties may further diminish.

To understand why this decrease is happening, the location and mode of failure must be examined. For the 0 degree samples, the most common location of failure was within the specified gage region. Failure within the region indicates proper sample preparation and geometry. This, however, was not the case for the other samples. By increasing the surface flatness on the 2 and 4 degree specimens, the most common location of failure was at the specimen ends. When failure took place at the top coupon surface, localized stresses were maximized causing premature failure to initiate. Figure 5.4-8 through 5.4-10 show failed compressive specimens from all prepared samples with enlarged views of the failed areas.

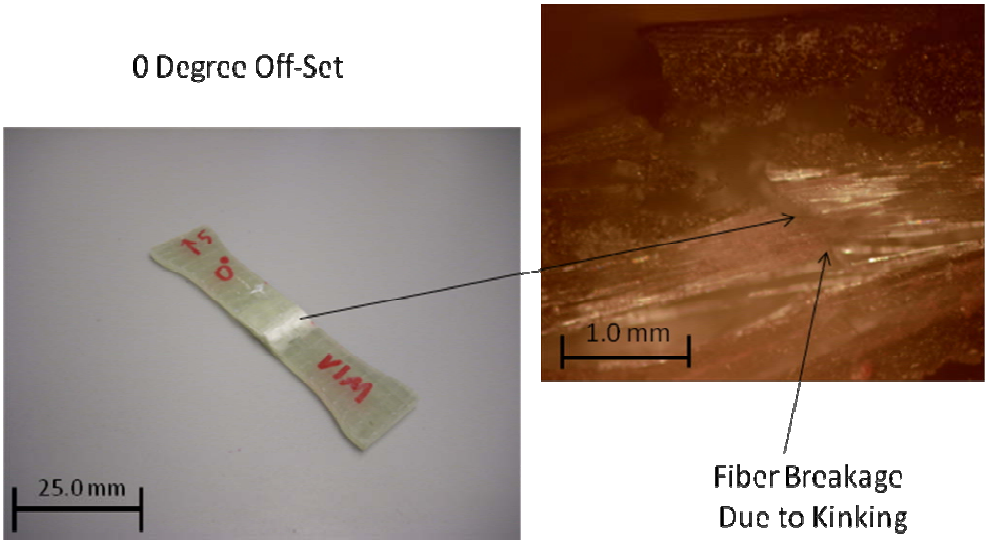

Fig 5.4-8: Failed VIM 0 Degree Off-Set Specimen with Enlarged View of Failed Region

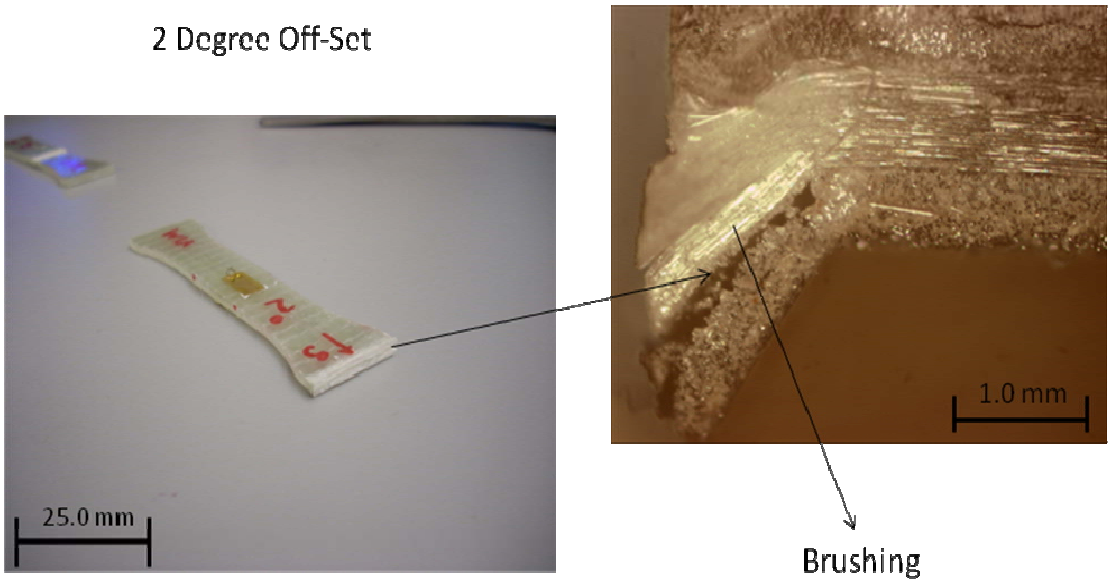

Fig 5.4-9: Failed VIM 2 Degree Off-Set Specimen with Enlarged View of Failed End

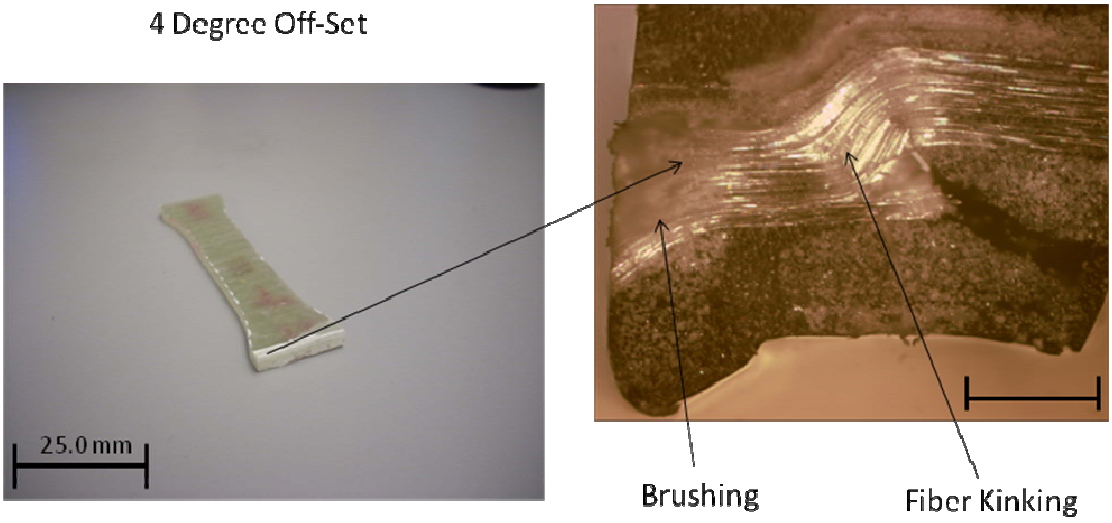

Fig 5.4-10: Failed VIM 4 Degree Off-Set Specimen with Enlarged View of Failed End

In the 0 degree specimens, failure occurred in the gage region. The mode of failure as seen in previous sections was fiber breakage due to kinking. This mode is acceptable and has been experienced in previous sections of this report. However, as surface flatness increased over the 2 and 4 degree specimens, the failure occurred at the specimen end surface where the flatness was altered. From the above pictures of the 2 and 4 degree specimens, failure modes were end crushing, or brushing. However, as the surface flatness increased from the 2 degree to the 4 degree specimen, multiple failure modes were revealed. When the flatness values reached their highest values, a combination of brushing and fiber kinking was seen. This would seem to indicate that when surface flatness values become very large, the fiber tows that add structural integrity to the specimen are not held in place by the matrix. Therefore, not only do the fiber ends become frayed from brushing, but the imbedded sections of fiber fail as well. This would explain why there was a noticeable drop in properties even when the failure between the 2 and 4 degree specimens appeared to occur in the same fashion. It is believed from looking at these photos that if surface flatness were to continue to increase, that mechanical property values would diminish to a minimum level where no further non-improvement would be seen.

CHAPTER SIX

CONCLUSIONS

In order to understand the factors that affect the mechanical properties of marine composites, studies were carried out that tested the influence of vacuum pressure, layer sequence and panel type, compressive testing procedure, and sample flatness. Based on the measured mechanical properties, some conclusions can be made.

1) As vacuum pressure increased, mechanical properties progressively improved. By increasing the vacuum pressure used during composite fabrication, the void content was found to decrease. Voids within a composite are locations were failure is likely to initiate, weakening the overall structure. Since increasing vacuum pressure was found to extract more voids, mechanical properties were also found to increase.

2) Increasing the layers of fiber within a composite panel was not found to have a significant effect on mechanical properties. Even though the more load was experienced by the larger layered panels, the relationship to the cross-sectional area was essentially the same throughout.

3) As panel type progressed from HL towards VI, the tensile properties were found to progressively improve in modulus, but only significant improvements were made in ultimate strength with the VI panel. The steady improvement in modulus suggests that panels made from two dissimilar fabrication procedures yield stiffness values in between the two extremes of manufacturing method. However, since the hybrid panels were made from both the HL and VI process, they failed in a sequential manor. By doing this the rate of strain was affected due to uneven portions of the

material. As a result, the modulus of these panels was weak in comparison the VI panel.

4) As panel type progressed from HL towards VI, the compressive strength was found to significantly improve only for the VI specimen, and modulus measurements were found to improve for both the hybrid and VI specimens, and level off at similar values. This also is due to the manner in which these specimens failed. Unlike the tensile specimens, compressive hybrid samples ruptured at both portions at the same time. Since the VI portion was much stiffer, each test specimen was at the mercy of the VI portion. Because this manufacturing method allows for less deformation rate, the HL side did not deform faster than the VI side and the results depict a stiffer material; hence, giving larger modulus values.

5) Comparing the ASTM D695 method and the ASTM D695M (Modified) method led to results that favored the ASTM D695 method. The Modified method offered more variance in the measured data and more complications during testing. Also, this method proved to be time inefficient with added procedures to fabricate individual specimens. All leading to the recommendation of the ASTM D695 method by the researcher.

6) When surface flatness was purposely increased, the compressive results steadily decreased. At a closer look, the material with an acceptable flatness yielded proper failure modes and locations. For the altered specimens, the failure mode occurred at the specimen end, resulting in brushing. However, the most extreme altered surface tested showed a combination of failures. Concluding that the matrix did not support the reinforcing fiber as well. This explained the lower property values even though

failure was occurring in the same manner and leads to the estimation that if surface flatness values were to continue to increase, the measured properties would eventually hit a minimum value where no further deterioration of properties would be seen.

BIBLIOGRAPHY

[1] A.P. Mouritz, E. Gellert, P. Burchill, K Challis, Review of Advanced Composite Structures for Naval Ships and Submarines. Composite Structures 53 (2001) 21-41.

[2] ASTM D3039, Standard Test Method for Tensile Properties of Polymer Matrix Composite Materials. http://www.astm.org.

[3] ASTM D695, Standard Test Method for Compressive Properties of Rigid Plastics. http://www.astm.org.

[4] R.L. Westberg, M.G. Abdallah, An Experimental and Analytical Evaluation of Three Compressive Test Methods for Unidirectional Graphite/Epoxy Composites. Rep. RI-86B12100, Hercules Inc. (1987) 350-361.

[5] ASTM D2584, Standard Test Method for Ignition Loss of Cured Reinforced Resins. http://www.astm.org.

[6] G. Belingardi, M. P. Cavatorta, D. S. Paolino, Repeated Impact Response of Hand Lay-Up and Vacuum Infusion Thick Glass Reinforced Laminates. International Journal of Impact Engineering 35 (2008) 609-619.

[7] J.A. Schey, Introduction to Manufacturing Processes. The McGraw-Hill Companies. ISBN 0-07-116911-3, 3rd Edition (2000).

[8] D. Modi, M. Johnson, A. Long, C. Rudd, Investigation of Pressure Profile and Flow Progression in Vacuum Infusion Process. Plastics, Rubber and Composites 36, No. 3 (2007) 101-110.

[9] D. Modi, N. Correia, M. Johnson, A. Long, C. Rudd, F. Robitaille, Active Control of the Vacuum Infusion Process. Composites: Part A 38 (2007) 1271-1287.

[10] N.C. Correia, F. Robitaille, A.C. Long, C.D. Rudd, P. Simacek, S.G. Advani, Analysis of the Vacuum Infusion Moulding Process: I. Analytical Formulation. Composites: Part A 36 (2005) 1645-1656.

[11] A.G. Evans, F.W. Zok, Review: The Physics and Mechanics of Fiber-Reinforced Brittle Matrix Composites. Journal of Material Science 29 (1994) 3857-3896.

[12] P.K. Mallick, Fiber Reinforce Composites: Materials, Manufacturing, and Design. CRC Press, Taylor and Francis Group. (2007), 3rd Edition.

[13] S.H. Lee, A.M. Waas, Compressive Response and Failure of Fiber Reinforced Unidirectional Composites. International Journal of Fracture 100 (1999) 275-306.

[14] C.R. Schultheisz, A.M. Waas, Compressive Failure of Composites, Part 1: Testing and Micro-Mechanical Theories. Prog. Aerospace Science 32 (1996) 1-42.

[15] D.C. Lagoudas, A.M. Saleh, Compressive Failure Due to Kinking of Fibrous Composites. Journal of Composite Materials 27 (1993) 83-106.

[16] I.M. Daniel, H-M. Hsiao, S-C. Wooh, Failure Mechanisms in Thick Composites Under Compressive Loading. Composites: Part B 27B (1996) 543-552.

[17] J.S. Berg, D.F. Adams, An Evaluation of Composite Material Compression Test Methods. Journal of Composites Technology & Research. 11, No. 2 (1989) 41-46.

[18] A.P. Mouritz, K.H. Leong, I. Herszberg, A Review of the Effect of Stitching on the In-Plane Mechanical Properties of Fibre-Reinforced Polymer Composites. Composites: Part A 28A (1997) 979-991.

[19] H.M. Hsiao, I.M. Daniel, Effect of Fiber Waviness on Stiffness and Strength Reduction of Unidirectional Composites under Compressive Loading. Composites Science and Technology 56 (1996) 581-593.

[20] M. Khatibzadeh, M.R. Piggott, The Effect of Fiber Alignment on Composite Strength: I. Single Fiber Studies. Composites Science and Technology 56 (1996) 1435-1442.

[21] K.H. Lo, E. S-W. Chim, Compressive Strength of Unidirectional Composites. Journal of Reinforced Plastics and Composites 11 (1992) 838-893.

[22] C.A. Squires, K.H. Netting, A.R. Chambers, Understanding the Factors Affecting Compressive Testing of Unidirectional Carbon Fiber Composites. Composites: Part B 38 (2007) 481-487.

[23] C. Baley, Y. Perrot, P. Davis, A. Bourmaud, Y. Grohens, Mechanical Properties of Composites Based on Low Styrene Emission Polyester Resins for Marine Applications. Applied Composite Materials 13 (2006) 1-22.

[24] J.L. Thomason, The Interface Region in Glass Fiber Reinforced Epoxy Resin Composites: 1. Sample Preparation, Void Content and Interfacial Strength. Composites 26 (1995) 467-475.

[25] P.O. Hagstrand, F. Bonjour, J.-A.E. Manson, The Influence of Void Content on the Structural Flexural Performance of Unidirectional Glass Fiber Reinforced Polypropylene Composites. Composites: Part A 36 (2005) 705-714.

[26] S.L. Bazhenov, A.M. Kuperman, E.S. Zelenskii, A.A. Berlin, Compression Failure of Unidirectional Glass Fiber Reinforced Plastics. Composites Science and Technology 45 (1992) 201-208.

[27] C.S. Yerramalli, A.M. Waas, The Effect of Fiber Diameter on the Compressive Strength of Composites – A 3D Finite Element Based Study. CMES 6 (2004) 1-16.

[28] J. Lee, C. Soutis, Thickness effect on the Compressive Strength of T800/924C Carbon Fiber-Epoxy Laminates. Composites: Part A 36 (2005) 213-227.

[29] O. Anthoine, J.C. Grandidier, L. Daridon, Pure Compression Testing of Advanced Fiber Composites. Composites Science and Technology, 58 (1998) 735-740.

[30] D.F. Adams, E.Q. Lewis, Influence of Specimen Gage Length and Loading Method on the Axial Compressive Strength of a Unidirectional Composite Material. Experimental Mechanics (1990) 14-21.

[31] K. N. Shivakumar, G. Swaminathan, M. Sharpe, Carbon/Vinyl Ester Composites for Enhanced Performance in Marine Applications. Journal of Reinforced Plastics and Composites 25 (2006) 1101-1116.

[32] V.M. Karbhari, E-Glass/Vinylester Composites in Aqueous Environments: Effects on Short-Beam Shear Strength. Journal of Composites for Construction 8 (2004) 148-156.

[33] A.P. Mouritz, Z. Mathys, Post-Fire Properties of Marine Polymer Composites. Composite Structures 47(1999) 643-653.

[34] D.O. Adams, D.F. Adams, Tabbing Guide for Composite Test Specimens. US Dept of Transportation: Federal Aviation Administration. (2002) 1-64.